The Yield and Post-Yield Behavior of High-Density Polyethylene

by

M.A. Semeliss, Research Assistant
R. Wong, Research Assistant
M.E. Tuttle, Assistant Professor

Department of Mechanical Engineering, FU-10

University of Washington

Seattle, Washington 98195

Prepared for:

NASA-Langley Research Center

Grant No. NAG-1-974

Dr. W.S. Johnson, Program Monitor

May 1990

TABLE OF CONTENTS

ACKNOWLEDGEMENTS

This research was supported through grant NAG-1-974 from the NASA-Langley Research Center. The authors wish to thank the Program Monitor Dr. W. S. Johnson for his support and enthusiam. The many helpful discussions and suggestions of Drs. J. H. Crews and C. E. Harris of NASA-Langely are also gratefully acknowledged.

CHAPTER 1: INTRODUCTION

There has been a rapid growth in the use of polymers and polymeric-based materials in recent years, and there is every indication that this trend will continue. Of particular interest has been the use of polymers as the matrix component in structural composite materials. Polymers may be roughly categorized as being either thermosets or themoplastics. Both thermosets and thermoplastics are comprised of long molecular chains. However, the molecular chains of thermosets are highly cross-linked, forming an extensive three-dimensional molecular structure. Conversely, thermoplastics do not form cross-links. One of the ramifications of this difference in molecular structure is that once a thermoset polymer has been polymerized (i.e., once the cross-links have been formed) the thermoset cannot be melted. On the other hand thermoplastics can be readily melted and remolded by the application of heat and pressure. Most thermoplastics have glass-transition and melting temperatures much lower than the glass-transition temperature of thermosets, and thus thermoset resins have been used most often in structural composite materials. However, recent advances in polymer materials technology have resulted in a new generation of high-temperature thermoplastic polymers which are better suited for engineering applications. Examples of these new-generation thermoplastics include poly-ether-ether-ketone ("PEEK", with a melting temperature of roughly 340°C) or a variety of polyimide resins (with a melting temperature ranging from 230-350°C). Because of these thermal properties as well as the inherent toughness and relative ease with which thermoplastics can be fabricated, recent research and developmental efforts in structural composite materials have turned to thermoplastic-based matrices.

The expanding role of thermoplastic polymers in load-bearing structural applications has prompted a need to develop a design methodology to predict the mechanical response of these materials under complex loading conditions. In particular, prediction of yield and post-yield

behavior is of current technical interest. At present most of the design tools and concepts used in the analysis of polymeric-based materials are based on the same principles used for metals and metallic alloys. However, the atomic/molecular structure of polymers is entirely different from that of metals. Metals are characterized by a highly crystalline atomic structure whereas polymers are characterized by long molecular chains that may be amorphous or semi-crystalline at the molecular level. Since the macroscopic yield and post-yield behavior of any material is fundamentally governed by its atomic/molecular microstructure, it is unlikely that a design methodology used for metals will apply equally well to polymers. Therefore, it may be necessary to develop new design methodologies for polymers, or to modify existing design tools that had been developed for use with metals.

Purpose

The purpose of this research is to study the yield and post-yield behavior of a thermoplastic polymer subjected to biaxial stress states. In particular, experimental results will be compared with theoretical predictions based on classical plasticity theories previously applied to metals. Of particular interest is whether the yield or post-yield behavior of thermoplastic polymers is influenced by the hydrostatic stress component.

The material chosen for study was high-density polyethylene. High-density polyethylene has a melting temperature of roughly 130°C, and is not considered to be a potential matrix material for use in structural composites. Polyethylene was selected because (1) it is a semi-crystalline thermoplastic, and hence its post-yield behavior may be representative of the general class of thermoplastic polymers, (2) it is readily available in the form of thin-walled tubes, and (3) it is very inexpensive as compared to new-generation thermoplastics such as PEEK or polyimides, and

hence a large number of tests could be conducted at modest cost

The study involved plane stress problems where thin-walled tubes of high-density polyethylene were tested under combined tensile axial loads and internal pressures at room temperatures. A rather specialized testing apparatus was developed during the study in order to perform these tests. This testing system is now fully calibrated and operational, and will be used to study the inelastic behavior of other new-generation thermoplastic resins of greater structural interest during the coming year.

CHAPTER 2: BACKGROUND INFORMATION

THE PREDICTION OF YIELDING

Definition of the Yield Stress

Conceptually, the yield point of a material defines the transition from purely elastic to elastic/plastic behavior. For some materials, the yield point is indicated by a sharp drop in stress in a uniaxial stress-strain curve, followed by slowly increasing stress with increasing strain. In these cases the near-discontinuity in stress makes identification of the yield stress very easy. For other materials no such stress drop occurs, but instead the slope of the stress-strain curve gradually decreases from an initial "elastic" value, which defines Young's modulus, to a lower value. In these cases the identification of yielding becomes more problematic. A common method of defining yield in this case is to use a permanent strain offset. For metals, this strain offset is usually defined as 0.2% strain.

Defining yield in polymers involves complexities not normally encountered with metals. Polymers are viscoelastic and therefore the measured yield stress is sensitive to the stress- or strain-rate imposed. Researchers have attempted to define the yield stress of polymers in a variety of ways. One method [Bowden and Jukes, 1972; Freire and Riley, 1980; Mears et al, 1969; Whitfield and Smith, 1972] is identification of the point of load drop, as described above. Another method [Carapellucci and Yee, 1986] is to perform a constant stress creep test, and to define yield based upon the intersection of tangents drawn to the initial and final portions of the resulting strain versus time curve. Probably the most common method is to apply a monotonically increasing axial load at a constant rate, and to define yielding on the basis of a strain offset. However, no standard loading rate or strain offset has been established. Offset strains ranging from 0.3% strain [Caddell

and Woodliff, 1977; Raghava et al, 1973] to as high as 2% strain [Ely, 1967; Pae, 1977] have been used.

Obviously, the different methods to determine yield result in distinctly different values of measured "yield strength" for a given polymer. Figure 2.1 compares various methods used to determine the yield strength of a polymer, and indicates that distinctly different values of the "yield point" can be deduced from the same experimental data. The inconsistency in the definition of "yielding" makes comparison of results obtained during different studies difficult. A standard definition, such as exists for metals, needs to be adopted for use with polymers.

The method used to define yielding during the present study will be discussed in detail in a following section. At this point it is appropriate to note that yielding was defined on the basis of a 0.3% offset in the *octahedral shear stress vs octahedral shear strain curve* of polyethylene. A value of 0.3% was selected because it is a widely used value of strain offset, at least within the polymers technical community. Yielding was defined in terms of octahedral shear stress and octahedral shear strain because this approach automatically accounts for biaxial loading effects. Also, all tests were conducted under a constant rate in order to minimize rate effects . Specifically, the yield and post-yield response of the polyethylene specimens was measured under a condition of constant octahedral shear stress loading.

Yield Criteria

The yield criteria which have been developed for metals typically make the following assumptions: (1) the initial compressive and tensile yield strengths are equal, (2) the hydrostatic stress component does not contribute towards yielding (i.e., the deviatoric stress component

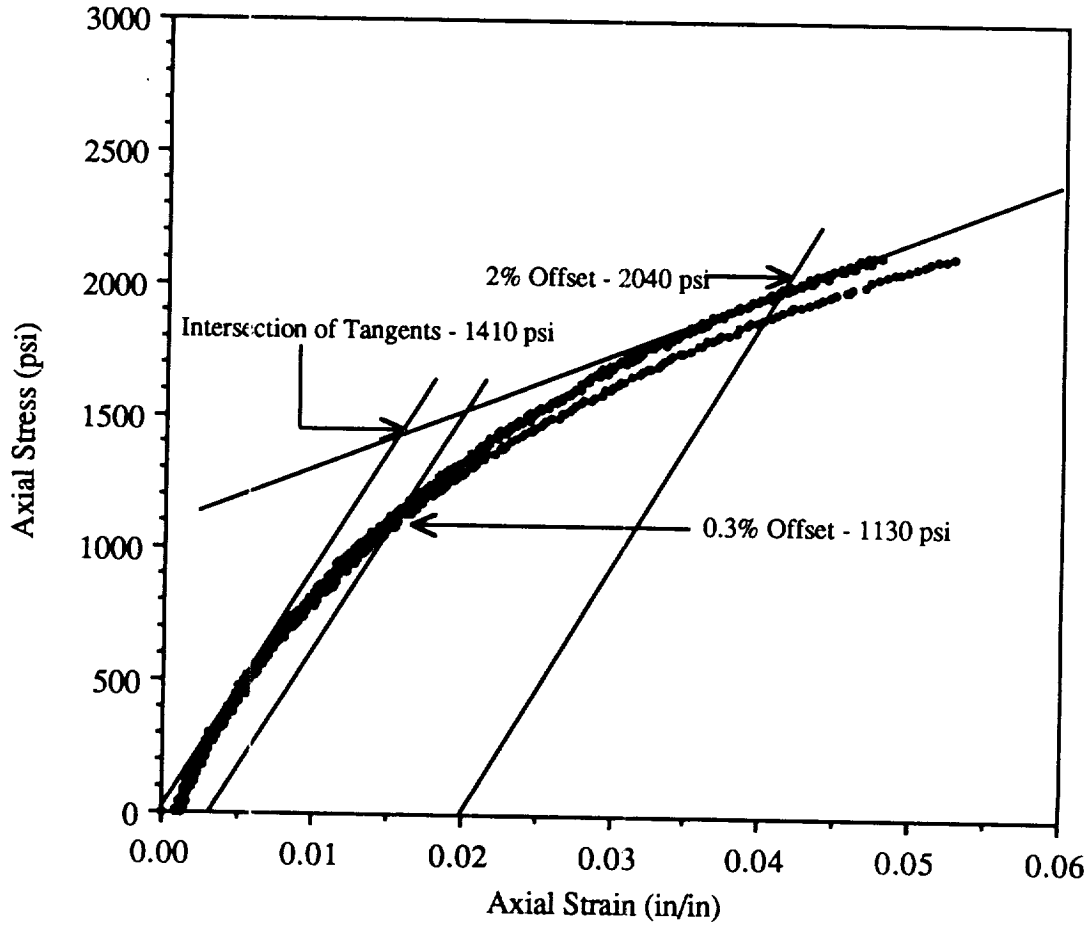

Figure 2.1 - Comparison of Various Methods of Determining the Yield Point (Data Taken from Load Path 1)

governs yielding), and (3) the material is isotropic and homogeneous. If the third assumption is relaxed the resulting yield criterion is suitable for use with anisotropic materials. The most commonly used isotropic and anisotropic yield criterion will be briefly reviewed in seperate sections below. Both "types" of yield criterion involve the hydrostatic and octahedral shear stress levels. Hydrostatic stress (or "mean" stress) may be written in terms of the three principal stresses as:

$$\sigma_{hyd} = \frac{(\sigma_1 + \sigma_2 + \sigma_3)}{3} \tag{2.1}$$

The deviatoric stress level associated with some given stress state is characterized by the octahedral shear stress. The octahedral shear stress may be written in terms of the principal stresses as:

$$\tau_{oct} = \frac{1}{3}\sqrt{(\sigma_1-\sigma_2)^2+(\sigma_2-\sigma_3)^2+(\sigma_3-\sigma_1)^2} \tag{2.2}$$

Isotropic Yield Criteria: The isotropic yield criterion most widely used for ductile metals and polymers is probably the Von Mises criterion. According to the Von Mises criterion, yielding occurs when the octahedral shear stress in the material reaches a critical value:

$$(\sigma_1 - \sigma_2)^2 + (\sigma_2 - \sigma_3)^2 + (\sigma_3 - \sigma_1)^2 = 2T^2 \tag{2.3}$$

where $\sigma_1 > \sigma_2 > \sigma_3$ and T is the uniaxial tensile yield strength of the material.

The Von Mises yield criterion is based on the assumptions that the hydrostatic stress component does not contribute to yielding and that the compressive and tensile yield strengths are equal. Experimental evidence indicates that many polymers violate both of these assumptions.

That is, polymers do in general have distinctly different compressive and tensile yield strengths and furthermore their yield behavior is significantly influenced by the hydrostatic stress level. For example, Christiansen, Baer, and Radcliffe [1971] found that the yield strength of polycarbonate, polyethylene terephthalate, polychloro-trifluoroethylene, and polytetrafluoroethylene all increased with increasing hydrostatic pressure. Mears, Pae and Sauer [1969] have reported similar pressure-dependent yield behaviors for polyethylene and polypropylene. The same conclusions have been reached for a variety of other polymers during studies by Ainbinder et al [1965], Pae and Mears [1968], Sardar et al ([1968], and Spitzig [1979]. This experimental evidence indicates that yield criteria which assume that the hydrostatic stress component does not influence the yield behavior, and/or which assume that the initial compressive and tensile yield strengths are equal are not applicable for use with polymers.

A modified version of the Von Mises criterion, in which these two assumptions are relaxed, was first presented by Stassi-D'Alia [1967] and subsequently presented in a different form by Raghava, Caddell, and Yeh [1973]. Raghava et al modified the Von Mises criterion in the following manner:

$$(\sigma_1 - \sigma_2)^2 + (\sigma_2 - \sigma_3)^2 + (\sigma_3 - \sigma_1)^2 + 2(C - T)(\sigma_1 + \sigma_2 + \sigma_3) = 2CT \qquad (2.4)$$

where C and T are the uniaxial compressive and tensile yield strengths respectively. This criterion, known as the Pressure-modified Von Mises criterion, is based on the assumption that yielding is a function of both the hydrostatic and deviatoric stress states. The first three terms are equivalent to the octahedral shear stress term of the original Von Mises criterion, while the last term is associated with the hydrostatic stress component .

Note that effects of hydrostatic stress and differences in compressive/tensile strength are not independent in the Pressure-modified Von Mises criterion. That is, if the compressive and tensile yield strengths of a material are equal then the hydrostatic stress term disappears and the Pressure-modified Von Mises criterion reduces to the original Von Mises criterion. It is interesting to note that a similar interdependence between tensile/compressive yield strengths and hydrostatic effects has been demonstrated for some metals. Spitzig, Sober, and Richmond [1976] have shown that some sintered powder materials (e.g., sintered iron) exhibit significant differences in compressive and tensile yield strength, and also that the yield behavior of these metals is influenced by the hydrostatic stress component. Similar conclusions were reached by Betten, Frosch, and Borrmann [1982] for the case of quenched and tempered steels.

The yield behavior of polymers has been compared to both the Von Mises and Pressure-modified Von Mises Criterion. Polymers which have been studied include acrylics [Ely ; 1967], polyester mixtures [Freire and Riley ;1980], and polycarbonate, polyvinylchloride, and polyethylene [Raghava and Caddell, 1973; Raghava et al, 1973]. In all cases the Pressure-modified Von Mises criterion was a better predictor of yield than the original Von Mises criterion, indicating that the yield response of these polymers is sensitive to the hydrostatic stress level.

Anisotropic Yield Criteria: Anisotropic materials possess different material properties in different directions. Until recently, most research on the yield behavior of materials has focused on isotropic models. However, many materials are anisotropic. In addition, when shaped by manufacturing processes such as rolling or extrusion even materials which are initially isotropic may become oriented at the atomic/molecular level and therefore become anisotropic at the macroscale. This is particularly true of polymers since they are composed of long molecular chains

which can easily become oriented in one direction, resulting in a polymer with distinctly different stiffnesses and strengths in different directions.

The criterion used most often to model the behavior of anisotropic materials is the Tsai-Hill yield criterion . Hill [1950] developed this criterion by selecting a form which would reduce to the Von Mises criterion if the yield strengths were the same in all directions. Tsai has subsequently applied this theory to composite materials, and the resulting theory is now known as the Tsai-Hill yield criterion. It can be written in the following manner in terms of the principal stresses σ_1, σ_2, and σ_3:

$$H(\sigma_1 - \sigma_2)^2 + F(\sigma_2 - \sigma_3)^2 + G(\sigma_3 - \sigma_1)^2 = 1 \qquad (2.5)$$

with: $H + G = \frac{1}{T_1^2}$ $\qquad H + F = \frac{1}{T_2^2}$ $\qquad G + F = \frac{1}{T_3^2}$

Since the material is anisotropic, the coefficients in the equation are functions of the tensile yield strengths in the 1-, 2- and 3- directions, T_1, T_2 and T_3 respectively. If the material is transversely isotropic, then T_2 and T_3 are equal and consequently G is equal to H. The Tsai-Hill yield criterion is related to the maximum shear which exists in each principal plane; it includes no linear terms which would represent the hydrostatic stress level, and also ignores any differences in initial compressive and tensile yield strengths. Stassi-D'Alia [1969] modified the Tsai-Hill criterion to include these factors, and Caddell, Raghava, and Atkins [1973] proposed a similar yield criterion at a later date. The Pressure-modified Tsai-Hill criterion, as it is sometimes known, is defined as follows:

$$H(\sigma_1 - \sigma_2)^2 + F(\sigma_2 - \sigma_3)^2 + G(\sigma_3 - \sigma_1)^2 + K_1\sigma_1 + K_2\sigma_2 + K_3\sigma_3 = 1 \qquad (2.6)$$

with $H + G = \frac{1}{C_1 T_1}$ $H + F = \frac{1}{C_2 T_2}$ $G + F = \frac{1}{C_3 T_3}$

$K_1 = \frac{C_1 - T_1}{C_1 T_1}$ $K_2 = \frac{C_2 - T_2}{C_2 T_2}$ $K_3 = \frac{C_3 - T_3}{C_3 T_3}$

The compressive and tensile yield strengths in the 1-, 2-, and 3- directions are denoted by C_1, T_1, C_2, T_2, C_3, and T_3. If the material is transversely isotropic then C_2 and T_2 are equal to C_3 and T_3, and therefore, G = H. If the compressive and tensile strengths are equal, Eq (2.6) reduces to the original Tsai-Hill criterion, and if material properties are the same in all directions, it further reduces to the original Von Mises criterion.

The few experimental studies which have been undertaken to investigate the yield behavior of anisotropic polymers seem to validate the Pressure-modified Tsai-Hill yield criterion. Studies by Rider and Hargreaves [1969] and Shinozaki and Groves [1973] followed methods suggested by Hill in which the change in the tensile and compressive yield strengths of oriented polymer sheets was measured as a function of the angle of orientation θ. Caddell and Woodliff [1977] conducted a series of tests using highly anisotropic specimens of polycarbonate, polyethylene, and polypropylene. The test specimens were oriented by applying a tensile load to a specimen until a stable neck had formed. The final test specimens were then machined out of these necked regions. A good correlation between experiment and theory was reported. Carapellucci and Yee [1986] also conducted tests on anisotropic polycarbonate specimens and reported good agreement. Hence, it appears that the yield behavior of anisotropic polymers is significantly affected by the hydrostatic stress level.

THE PREDICTION OF POST-YIELD BEHAVIOR

Post-yield behavior typically involves large deformations, such that the familiar definitions of conventional "engineering" stress and strain no longer apply. Conventional engineering stress σ and engineering strain ε may be converted to true stresses s and true strains e as follows:

$$s = \sigma(\varepsilon+1) \tag{2.7}$$

$$e = \ln(\varepsilon+1) \tag{2.8}$$

A true stress-true strain curve is often called a plastic "flow" curve because it gives the stress which causes the material to flow plastically for any given strain. Post-yield theories are typically developed in terms of the true stress and true strain, and in this report true stress and true strain will be used to describe the post-yield behavior of polyethylene.

The post-yield theories considered during this study will be briefly reviewed below. Both isotropic and anisotropic materials will be discussed. It is appropriate to note that, in contrast to the yield criterion reviewed above, all existing post-yield criteria assume material incompressibility during plastic flow. The possibility that the flow behavior of polymers is influenced by the hydrostatic stress level has apparently not yet been addressed within the technical community.

Post Yield Behavior of Isotropic Materials

The assumption that plastic deformations are independent of the hydrostatic stress level leads to the conclusion that the volume of a solid remains constant during plastic flow. Therefore, during plastic flow the true strains are related by:

$$e_1 + e_2 + e_3 = 0 \tag{2.9}$$

Equation (2.9) represents the "constancy of volume" assumption. Note that if $\nu = 1/2$, then a similar relationship holds for engineering strains:

$$\varepsilon_1 + \varepsilon_2 + \varepsilon_3 = (1-2\nu)(\sigma_1 + \sigma_2 + \sigma_3)/E = 0 \qquad (\text{when } \nu = 1/2) \tag{2.10}$$

For many metals undergoing plastic deformation induced by a uniaxial stress, the flow curve can be expressed by the simple power law relation, also known as the Ludwik expression:

$$s = s_{yield} + Me^n \tag{2.11}$$

where s_{yield} is the true stress at yield, M is the strength coefficient and n is the strain hardening exponent. This equation is only valid for isotropic materials and is defined from the onset of plastic flow to the maximum load at which the specimen begins to neck. Equation (2.11) provides a simple mathematical expression to describe the post-yield flow curves of a material if constants M and n are known.

Equation (2.11) is appropriate for use under uniaxial loading conditions. In a complex state of stress and strain it is more useful to relate invariant functions of true stress and true strain. The invariant functions most frequently used to describe plastic deformation of metals are the effective true stress and effective true strain [Dieter, 1986]. The effective true stress is defined as a function of the principal true stresses:

$$\bar{s} = \frac{1}{\sqrt{2}}[(s_1-s_2)^2 + (s_2-s_3)^2 + (s_3-s_1)^2]^{\frac{1}{2}} \tag{2.12}$$

The effective true strain is defined as a function of the principal true strains:

$$\bar{e} = \frac{\sqrt{2}}{3}[(e_1-e_2)^2 + (e_2-e_3)^2 + (e_3-e_1)^2]^{\frac{1}{2}} \tag{2.13}$$

The power law relation can now be expressed in the form of effective true stress and effective true strains:

$$\bar{s} = \bar{s}_{yield} + M\bar{e}^n \tag{2.14}$$

An assumption implied by Equation (2.14) is that the flow curve is independent of the hydrostatic or mean stress component. That is, the post-yield behavior is assumed to be governed exclusively by the deviatoric stress tensor.

The power law expressions (i.e., either Eqs. 2.11 or 2.14) provide a simple mathematical expression to describe the flow curves of a material, and the power law formulation has been

widely applied because of this simplicity. However, these relations are entirely empirical and deviations from the power law are frequently observed.

More rigorous expressions to describe the post-yield behavior of a material have been developed. Two such systems of equations are the Levy-Mises and Prandtl-Reuss equations. In either case two fundamental assumptions are made: it is assumed that the material is elastic-perfectly plastic, and further, it is assumed that the incremental change in plastic true strain induced by an increase in true stress is proportional to the total stress deviator, rather than the incremental change in the stress deviator. The elastic strains are neglected in the Levy-Mises equation, and thus the Levy-Mises equations are only applicable when large plastic deformations occur such that the elastic deformations can be entirely neglected. The Prandlt-Reuss equations include both elastic and plastic deformations. In the present study the elastic deformations could not be neglected and hence the Prandtl-Reuss equations were applied, as further described below.

Reuss assumed that the plastic true strain-increment, at any instant of loading, is proportional to the instantaneous stress deviation such that:

$$\frac{de_1^p}{s'_1} = \frac{de_2^p}{s'_2} = \frac{de_3^p}{s'_3} = d\lambda \qquad (2.15)$$

where de_i^p are the plastic principal true strain increments, s'_i are the deviatoric true stress components, and $d\lambda$ is a non-negative constant of proportionality which is *not a material constant* but rather varies throughout the stress/strain history.

Equation (2.15) implies that the incremental plastic strains depend on the total current deviatoric stresses and not on the incremental change in deviatoric stresses. It is also implied that the principal axes of stress and plastic strain increments coincide. Again, the hydrostatic stress component assumes no role in the plastic deformation of the material.

For a given direction the total strain increment de^t is defined as the sum of the plastic de^p and elastic de^e strain increments:

$$de_i^t = de_i^p + de_i^e \tag{2.16}$$

The plastic strain increment de^p is given by Equation (2.15), and hence [Slater, 1977]:

$$de_i^p = s_i' \, d\lambda = \frac{3}{2} \frac{s_i' \, d\bar{s}}{\bar{s} H} \tag{2.17}$$

where $\bar{s}$ is the effective true stress defined in Equation (2.12) and H (also known as the "plasticity modulus") is the slope of the effective true stress-plastic strain curve. The elastic strain increment de_i^e is dependent on both the deviatoric and hydrostatic stress components:

$$de_i^e = \frac{ds_i'}{2G} + \frac{(1-2\nu)}{E} ds_{hyd} \tag{2.18}$$

where E is the Young's modulus, ν is the Poissons ratio, and G is the shear modulus. The shear modulus is related to Young's modulus and Poissons ratio:

$$G = \frac{E}{2(1+\nu)} \tag{2.19}$$

Combining Equations (2.17) and (2.18) gives the total strain increments for a given direction i:

$$de_i^t = \frac{3}{2}\frac{s_i' \, d\bar{s}}{\bar{s}H} + \frac{ds_i'}{2G} + \frac{(1-2\nu)}{E} ds_{hy} \tag{2.20}$$

Equation (2.20) is the Prandtl-Reuss relation applicable for initially isotropic materials to describe post-yield stress-strain behavior.

A method of experimentally verifying whether it is appropriate to apply the Prandtl-Reuss system of equations to a given material was developed by Lode (1926). Lode introduced two parameters, μ and ν, known as the Lode stress and plastic strain parameters respectively:

$$\mu = \frac{2s_2 - s_1 - s_3}{s_1 - s_3} \tag{2.21}$$

$$\nu = \frac{2e_2^p - e_1^p - e_3^p}{e_1^p - e_3^p}$$

In Equation (2.21), the stresses are the total principal stresses and the strains are the plastic portion of total principal strains defined as :

$$e^p = e^t - e^e \tag{2.22}$$

where e^t and e^e are the total and elastic principal strains respectively.

Lode showed that if a material is elastic-perfectly plastic, then the Prandtl-Reuss equations imply that the two parameters will be identical, i.e., $\mu = \nu$. The Lode parameters are a convenient way to test whether a given material follows the Pandtl-Reuss equations. The Lode parameters have been evaluated for a number of metals and metal alloys, including iron, copper, nickel, aluminum, and steel alloys [Morrison and Shepard (1950); Taylor and Quinney (1951)]. Typical experimental results are shown in Figure 2.2. As indicated, the correlation is usually not exact, and often a consistent deviation from predicted behavior can be identified. This deviation from theory is usually attributed to anisotropy of the test material and/or to experimental errors, although it is also likely that the material is not completely elastic-perfectly plastic. Despite these inconsistencies, the Prandtl-Reuss equations are considered to be one of the best theoretical approaches to modeling post-yield behavior currently available.

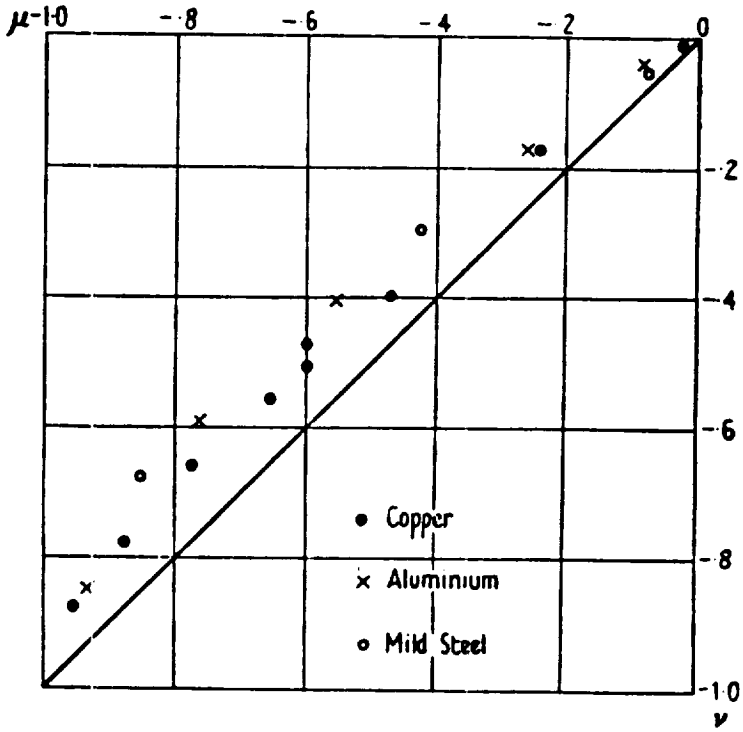

Figure 2.2: Lode Variables Measured by Taylor and Quinney for Copper, Aluminum, and Mild Steel Tubes Subjected to Combined Tension and Torsion (Taken from Hill [1950] pg 44).

Post-Yield Behavior of Anisotropic Materials

An anisotropic form of the power law was applied to polyethylene during the present study. The effective true stress and effective true strain for istropic materials have been defined in Equations (2.12) and (2.13). These definitions no longer apply for anisotropic materials. Hill [1950] modified these expressions for use with anisotropic materials. The effective true stress for an anisotropic material in terms of the true principal stresses is given by:

$$\bar{s} = \sqrt{\frac{3}{2}\frac{F(s_2-s_3)^2 + G(s_3-s_1)^2 + H(s_1-s_2)^2}{F + G + H}} \tag{2.23}$$

where:

$$H + G = \frac{1}{T_1^2} \qquad H + F = \frac{1}{T_2^2} \qquad G + F = \frac{1}{T_3^2}$$

and s_1, s_2, s_3 are the principal true stresses. Because the material is anisotropic, the normal stress coefficients F, G, and H are functions of the tensile yield strengths in the 1, 2, and 3 directions, T_1, T_2, and T_3 respectively.

Similarly, the effective true plastic strain for an anisotropic material in terms of the true principal strains is given by:

$$\bar{e} = \sqrt{\frac{2}{3}}\,(F+G+H)^{\frac{1}{2}} \sqrt{F\left[\frac{Ge_2^p - He_3^p}{\beta}\right] + G\left[\frac{Fe_1^p - He_3^p}{\beta}\right] + H\left[\frac{Fe_1^p - Ge_2^p}{\beta}\right]} \tag{2.24}$$

where e_1^p, e_2^p, and e_3^p are the principal plastic normal strains and $\beta = (FG + GH + HF)$. . Note that if anisotropy is negligible then Equations (2.23) and (2.24) reduce to Equations (2.12) and (2.13), respectively.

For an anisotropic material, the power law formulation may be used by the substitutions of Equations (2.23) and (2.24) into Equation (2.14). That is, the flow law for an anisotropic material is given by

$$\bar{s} = \bar{s}_{yield} + M\bar{e}^n$$

where $\bar{s}$ is now given by the anisotropic form of the equivalent stress (i.e., is given by Eq. 2.23), and $\bar{e}$ is now given by the anisotropic form of the equivalent strain (i.e., is given by Eq. 2.24). Note that Eq (2.25) is identical to Eq (2.14); the variables have simply been redefined to account for anisotropic behavior. The anisotropic form of the power law expression was applied during the present study, as will be described in a following section.

CHAPTER 3 - EXPERIMENTAL PROCEDURES

In this study thin-walled tubes of high-density polyethylene were subjected to monotonically increasing axial loads and internal pressures. This biaxial loading produced both hoop and axial stresses within the walls of the specimen. Loading was increased proportionaly at user-specified rates, and the yield and post-yield response of the specimen was monitored throughout each test.

Due to symmetry the axial and hoop stresses were the principal stresses in all cases. The axial and hoop stresses induced during a given test therefore define a radial "load path" in principal stress space. The load paths used during the present study are summarized in Figure 3.1. A total of 57 seperate tests were planned, involving three repeated tests along each of 19 load paths. The load paths are oriented at five degree increments in the first quadrant of principal stress space.

The yield behavior of polyethylene is highly rate-dependent. As discussed in the preceding chapter, in most yield- and post-yield criterion it is assumed that inelastic behavior is governed by the octahedral shear stress. Therefore a constant octahedral shear stress rate was maintained during all tests in order to minimize rate effects between individual tests and load paths. Note that although the octahedral shear stress rate remained constant from test-to-test, the hydrostatic stress rate, axial loading rate, and internal pressure rate all varied considerably from one load path to the next.

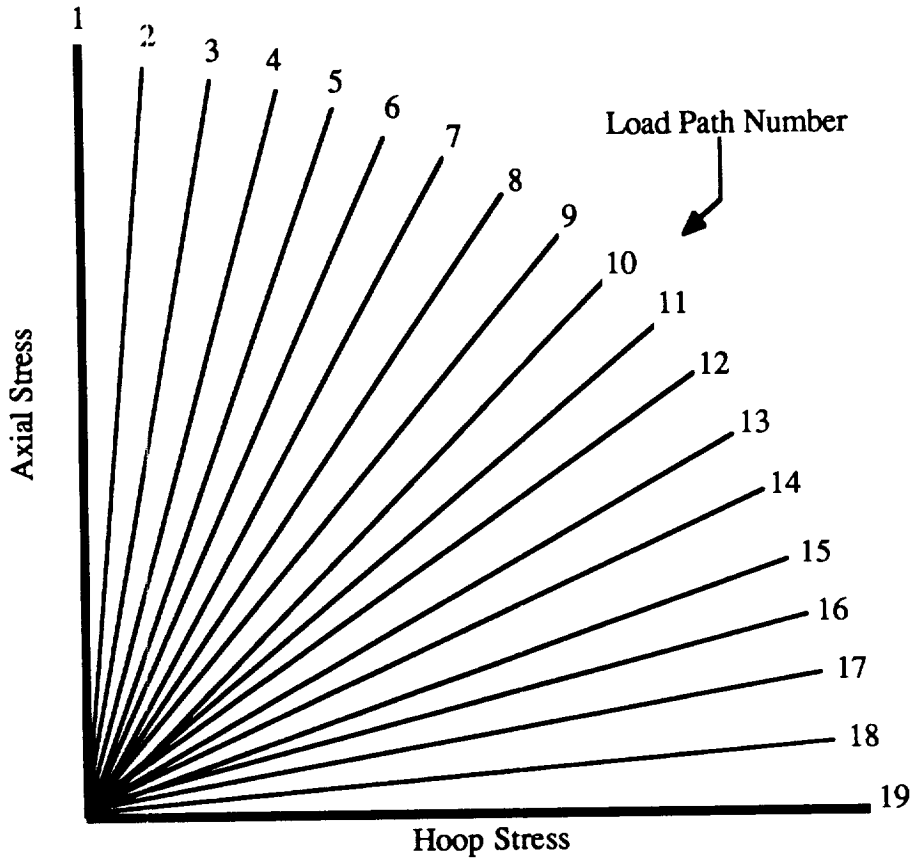

Figure 3.1 - Loading Paths in Principal Stress-Space

Derivation of Test Matrix

The axial load (L) was increased at a rate of k_1 and the internal pressure (P) was increased at a rate of k_2. Therefore at time t:

$$L = k_1 t \tag{3.1}$$

$$P = k_2 t \tag{3.2}$$

Under this loading condition, the stresses induced in the walls of the tube are:

$$\sigma_{AXIAL} = \sigma_1 = \frac{t}{2c}\left(\frac{k_1}{\pi r} + k_2 r\right) \tag{3.3}$$

$$\sigma_{HOOP} = \sigma_2 = \frac{k_2 r t}{c} \tag{3.4}$$

$$\sigma_{RADIAL} \cong -\frac{1}{2} k_2 t \cong 0 \tag{3.5}$$

with: r = average radius of tube

c = wall thickness

Note that the radial stress has been equated to zero. This is an appropriate assumption for thin-walled tubes, since the radial stress is typically an order of magnitude less than the hoop and axial stresses.

Normally, "σ_1" denotes the algebraically greatest principal stress, "σ_2" the intermediate principal stress, and "σ_3" the algebraically smallest principal stress. However, for purposes of consistent identification this convention was ignored in this study. Instead, "σ_1" was used to denote the axial stress, and "σ_2" was used to denote the hoop stress, even though along some load paths the hoop stress was in fact the algebraically greatest principal stress.

Substituting Eqs (3.3) and (3.4) into Eqs (2.1) and (2.2), the octahedral shear stress and hydrostatic stress at any time t are given by:

$$\tau_{oct} = \frac{t}{6c}\sqrt{\frac{2k_1^2}{\pi^2 r^2} + 6k_2^2 r^2} \tag{3.6}$$

$$\sigma_{hyd} = \frac{t}{2c}\left(\frac{k_1}{3\pi r} + k_2 r\right) \tag{3.7}$$

The slope M of any load path shown in Figure 3.1 can be expressed as:

$$M = \frac{\sigma_1}{\sigma_2} = \frac{1}{2\pi^2 r^2}\left(\frac{k_1}{k_2} + \pi r^2\right) \tag{3.8}$$

The combination of load rates k_1 and k_2 which produce a desired slope M are given by:

$$k_1 = k_2 \pi r^2 (2M-1) \tag{3.9}$$

Finally, given a desired octahedral shear stress rate, (τ_{oct}/t), and slope M, the required axial load rate and internal pressure rate are given by:

$$k_1 = \left(\frac{\tau_{oct}}{t}\right) 3\pi rc\,(2M-1)\sqrt{\frac{2}{3+(2M-1)^2}} \tag{3.10}$$

$$k_2 = \left(\frac{\tau_{oct}}{t}\right) \frac{3c}{r}\sqrt{\frac{2}{3+(2M-1)^2}} \tag{3.11}$$

An octahedral shear stress rate of 258 psi/min was selected for use since the axial loading rates and internal pressure rates for all loading paths falls within the range of the equipment available. A test matrix was defined in this fashion and is presented in Table 3.1. The numerical values given in Table 3.1 were obtained using Eqs (3.10) and (3.11), as well as the specimen dimensions presented in the following section.

Specimen Preparation

The material selected for testing was high-density polyethylene. Driscopipe 1000 (PE3408) SDR26 high-density polyethylene tubing was purchased in 20 foot lengths from a distributor in the Seattle area. Since the polyethylene tubes were produced by extrusion, significant residual stresses were present in the as-received tubes. Therefore, each specimen was subjected to a thermal annealing process prior to testing. To the authors' knowledge, there is no accepted procedure for annealing high-density polyethylene. An appropriate annealing cycle was determined by conducting several tests at different temperatures. Starting from an annealing temperature of 90°C, annealing temperatures were increased in 10°C increments from one test to the next until the melting temperature of roughly 130°C was reached. A Blue M forced air oven was used. The oven was preheated so as to achieve a constant annealing temperature with minimal thermal gradients throughout the oven chamber. The specimens were then placed in the oven and

Table 3.1: Axial and Internal Pressure Loading Rates Required to Perform Constant Octahedral Shear Stress Rate Tests

Load Path		Axial Load Rate	Int. Pressure Rate	τ_{oct}/t	σ_{hyd}/t
No	Slope (M)	(lb/min)	(psi/min)	(psi/min)	(psi/min)
1	∞	900	0	258	186
2	11.43	* 895	5	258	210
3	5.67	885	10	258	236
4	3.73	867	15	258	260
5	2.75	838	21	258	284
6	2.15	795	27	258	310
7	1.73	734	34	258	331
8	1.43	657	40	258	348
9	1.19	560	46	258	357
10	1.00	449	51	258	365
11	0.84	328	54	258	357
12	0.70	202	57	258	348
13	0.58	83	58.2	258	331
14	0.47	-31	58.4	258	310
15	0.36	-143	57.7	258	284
16	0.27	-230	56.5	258	260
17	0.18	-311	55	258	236
18	0.09	-384	53	258	210
19	0.00	-449	51	258	186

* Tests along Load Path 2 not completed.

annealed for one hour. The oven was then turned off and the specimens were slowly furnace cooled over approximately 10 hrs.

The effect of annealing temperatures was evaluated by means of a destructive sectioning technique. A 1 inch wide strip was removed along the length of a 12 inch tube to evaluate axial residual stresses . For the hoop direction, a 1-1/2 inch long "ring" specimens was cut from the tube, and a 1-1/2 wide section (corresponding to a 20° arc) was cut out of the circumference of this ring. After a period of 72 hours (to allow for any time-dependent response to develop) the strip and ring specimens were examined to determine whether any deformations had occurred.

It was found that large residual stresses existed in the tubes in the as-received condition. Compressive residual stresses existed in the hoop direction, while axial residual stresses were probably compressive at the outer diameter and tensile at the inner diameter. Figures 3.2 and 3.3 show the results of the various annealing temperatures on hoop and axial residual stresses. Note that at 130°C, the specimen had been extensively deformed by the annealing process, which indicated that the melting temperature had been reached. For the axial direction, the amount of deflection from the center of the strip was measured as shown in Figure 3.4. For the hoop direction, the angle of deflection from the center of the tube was measured as shown in Figure 3.5. Measured deformations were plotted functions of annealing temperature, and the results are summarized in Figure 3.6 and 3.7. The results show that deformation of the axial strip was minimized using an annealing temperature of approximately 115°C. However, higher annealing temperatures resulted in a algebraic sign change (i.e., a reversal in the curvature of the strip), indicating that axial residual stresses may still have existed in the tubes following an anneal at 115°C. Furthermore, the hoop deformations were not completely eliminated even at annealing temperatures approaching the melting temperature of polyethylene.

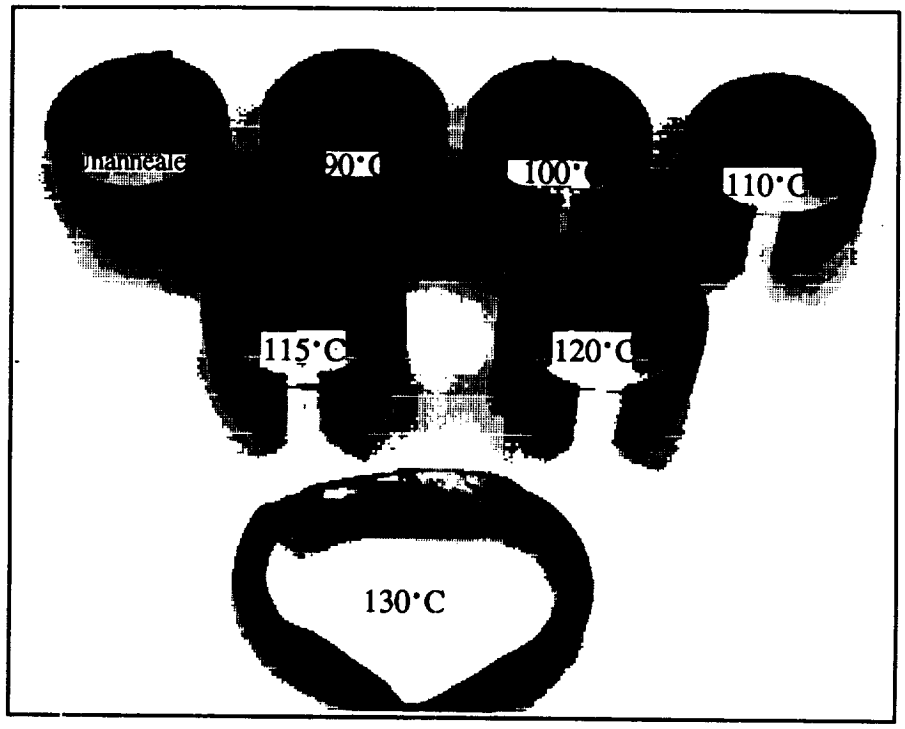

Figure 3.2 - Hoop Sections of Annealed Tubes at Various Temperatures

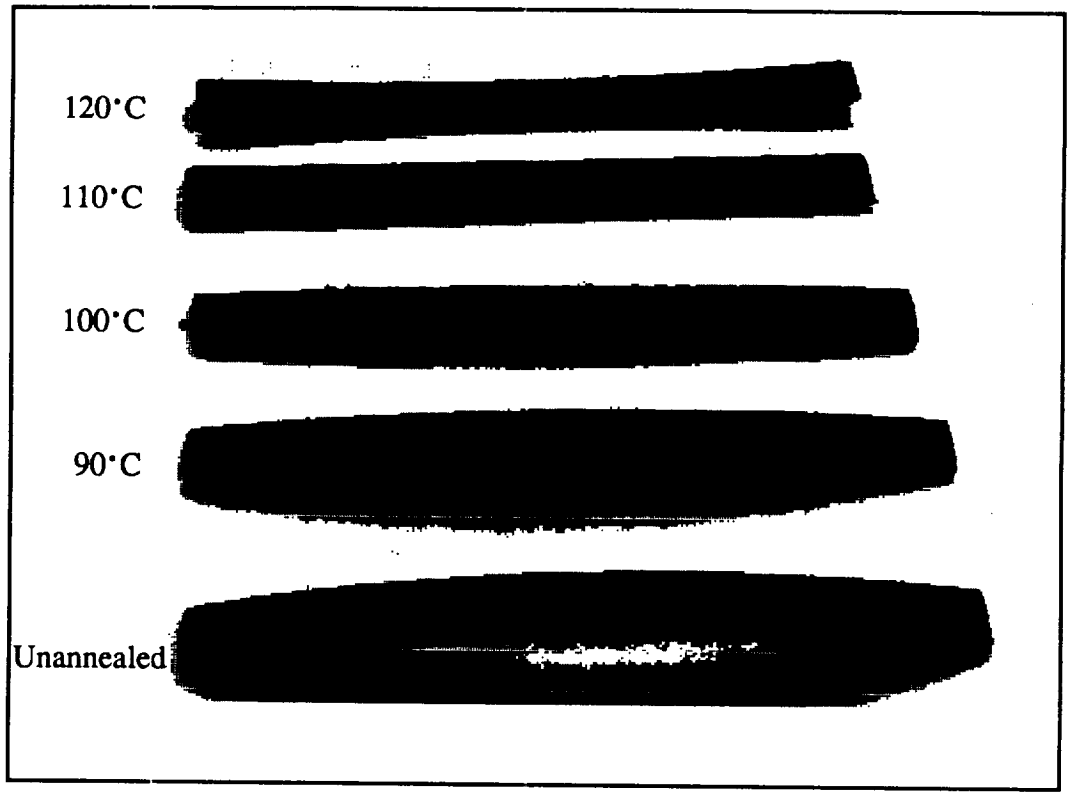

Figure 3.3 - Axial Sections of Annealed Tubes at Various Temperatures

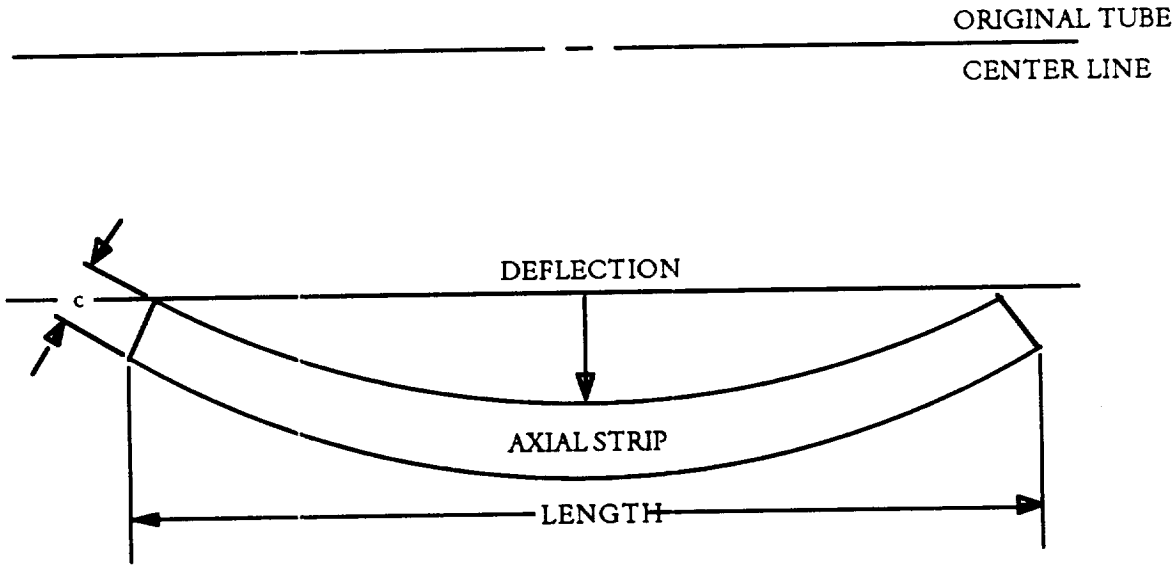

Figure 3.4: Measurement of deformations due to axial residual stresses. (Note: A deflection was defined as "positive" if the strip was concave with respect to the original centerline of this tube.)

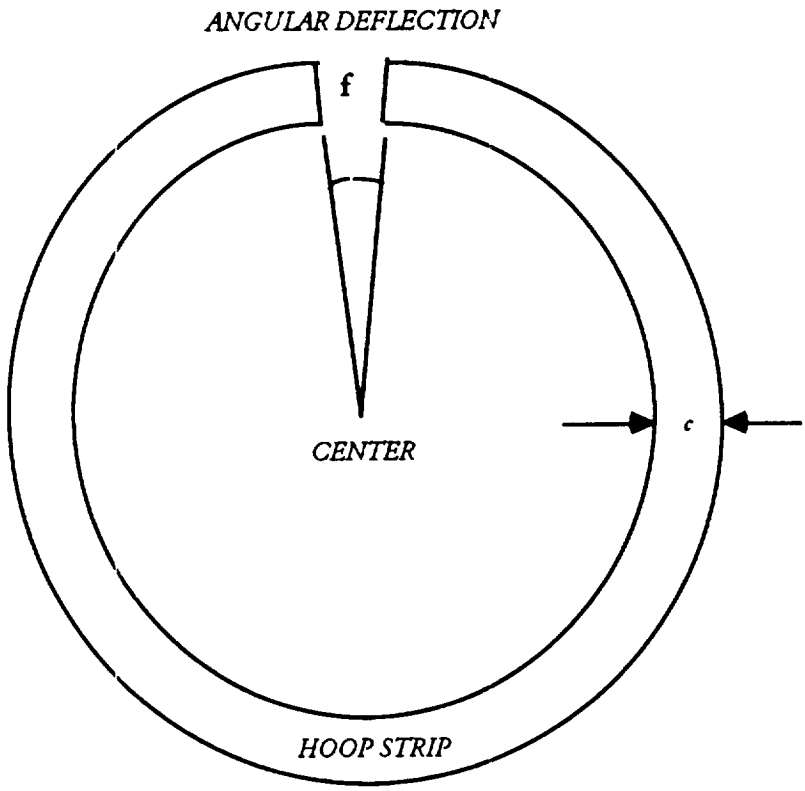

Figure 3.5: Measurement of deformations due to hoop residual stresses. (Note: Total angular deflection = 20° – 0.)

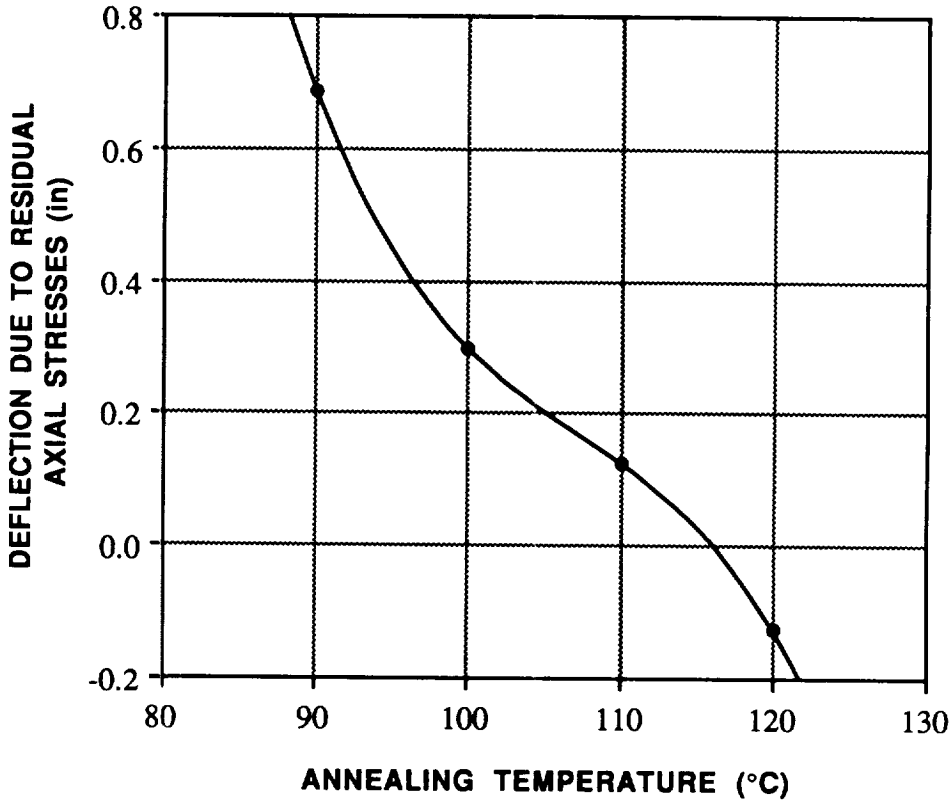

Figure 3.6: Transverse Deflections Due to Axial Residual Stresses as a Function of Annealing Temperature

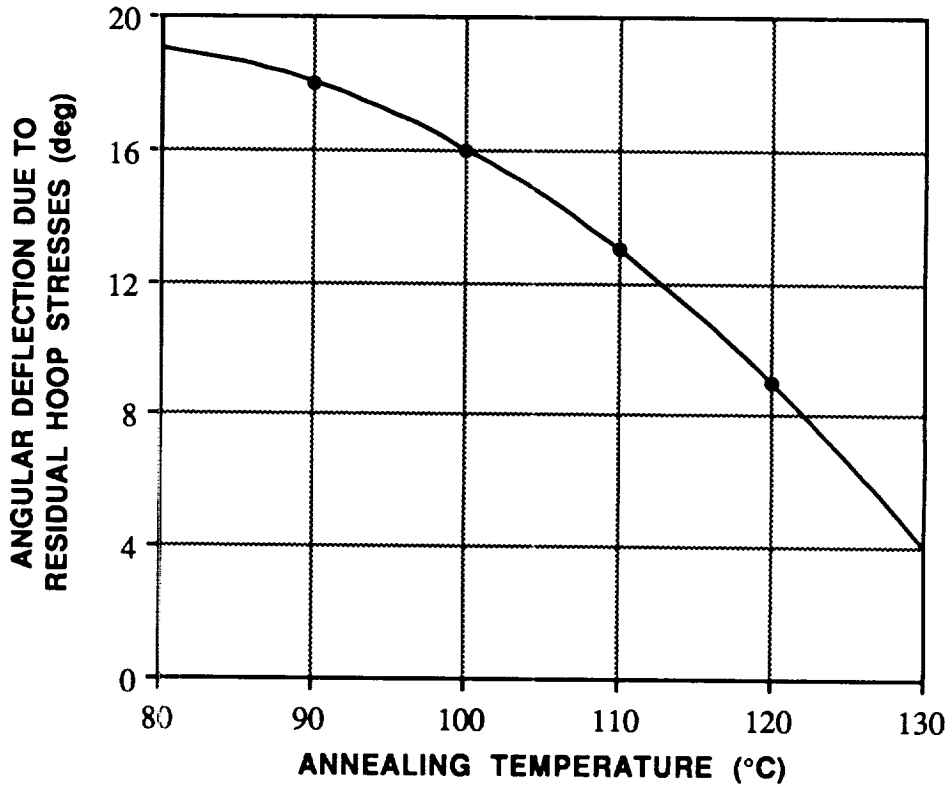

Figure 3.7: Angular Deflections Due to Residual Stress as a Function of Annealing Temperature

The annealing treatment finally selected for use consisted of a 2 hour anneal at 115°C followed by a 10 hr furnace cooling. It is believed that this annealing treatment minimized, but perhaps did not completely eliminate, residual stresses present in the as-received tubes.

Specimens were cut from "parent" tubes in 15-1/2 inch lengths and annealed. Specimen dimension measurements were taken on six different sections of the annealed tubes in order to determine average values. The average radius of the annealed tubes was 1.698", and the average wall thickness was 0.157".

Axial Load and Internal Pressure Control

Figure 3.8 shows the fixture used to apply axial loads and internal pressures to the tubular specimens. The specimens were mounted to two aluminum cylinders. The upper cylinder extended into the specimen in order to reduce the volume of air required to pressurize the specimen, which decreased the energy released in the event of catastrophic specimen failure. Two ports were machined in the lower cylinder. One was the supply port for the pressurized air from a bottled air cylinder and the other was the pressure transducer port for measuring internal pressures.

The tube specimens were seated on a shoulder machined in each aluminum cylinder. An O-ring was used to insure proper pressurization with no leakage. After seating the tube on the shoulder of each cylinder end, an aluminum clamp was attached at each end to firmly seal the tube and cylinder surfaces. The clamp also helped prevent slippage of the tubes during testing by pressing the specimen walls into the machined step of the cylinders, thus increasing the friction force between the mating surfaces of the tube and cylinder.

Axial loads were applied using an MTS electrohydraulic fatigue testing machine consisting of a Model 308.01 loading frame, a hydraulic cylinder and pump, a Model 442 control unit, a Model 410 digital function generator, and a Transducer Inc. Model WTC-FF42-CS-10K 10 kip load cell. A Tektronix Model 2213 60 MHz oscilliscope was used to monitor and verify the axial loading. Figure 3.9 illustrates the loading frame along with the load cell and specimen.

The MTS frame was used to apply a monotonically increasing axial load at a user-specified rate. The required axial loading rates have been previously listed in Table 3.1. The applied load rate was monitored throughout each test, and was maintained to within ±5% of the desired load rate in all cases.

A control system designed to produced a linearly increasing air pressure was developed during this study. The system is shown schematically in Figure 3.10, and a photograph of the assembled system is shown in Figure 11. The pressure regulation system involved two pressure regulators mounted in series. First, a Victor mode SR4G regulator was mounted directly on the stem of a compressed air bottle, and reduced the nominal air pressure from 3000 psi to 300 psi. This was referred to as the "knockdown" regulator. Air flow was then directed to a Watts R11-03D regulator. This second regulator was referred to as the "control" regulator. The control regulator outlet pressure can be adjusted from 0 to 250 psi. An angular rotation of the valve stem of the control regulator results in a pressure change at the outlet. The measured outlet pressure was found to be linearly proportional to the angular position of the valve stem. Thus, by rotating the valve stem at a constant angular rate the outlet pressure was increased at a constant linear rate.

The control regulator was coupled to a Slo-Syn M093-FD14 stepper motor. This motor was controlled by an Anaheim Automation BLB driver, which was in turn regulated by analog

voltage pulses from an A/D board mounted in a Macintosh II computer. A single pulse from the computer caused the stepper motor shaft to turn 1.8°. A pulse train of a given frequency would therefore cause the motor shaft to turn at a given angular frequency. Since the shaft was coupled to a linear pressure regulator, a given pressure rate was produced. The entire system was calibrated such that a specified pulse rate resulted in a known linear pressure rate. A computer program was written which allows the user to produce a pulse train of a desired frequency. Typical plots of pressure versus time recorded along load paths 5 and 10 are shown in Figure 3.12.

Data Acquistion

A total of five analog measurement devices were used during any test. Axial strains were measured using an MTS model number 632.25B-20 extensometer. Hoop strains were measured using two diametrically opposed Applied Test Systems (ATS) LVDT displacement transducers, with a range of 0.5 inch. Pressures applied to the specimen was measured using a Gulton GS616 pressure transducer. Finally, axial loads were measured using the load cell mounted to the MTS frame, as previously described. All five analog voltage signals were monitored using a National Instruments NB-MIO-16H A/D board mounted within a Macintosh II computer. The A/D board was controlled using "Labview", a National Instruments graphical programming language. The Labview package allowed scanning rates of up to 45000 samples per second and up to 8 double-ended input signals. One potential difficulty with the scanning process was that all 5 channels were not monitored at the same time but rather sequentially. A maximum time lag of 5 msec occurred between scanning each channel. Since the load and strain rates imposed during all tests were relatively low, the 5 msec lag between measurements was negligibly small, and all 5 measurements were treated as if obtained simultaneously.

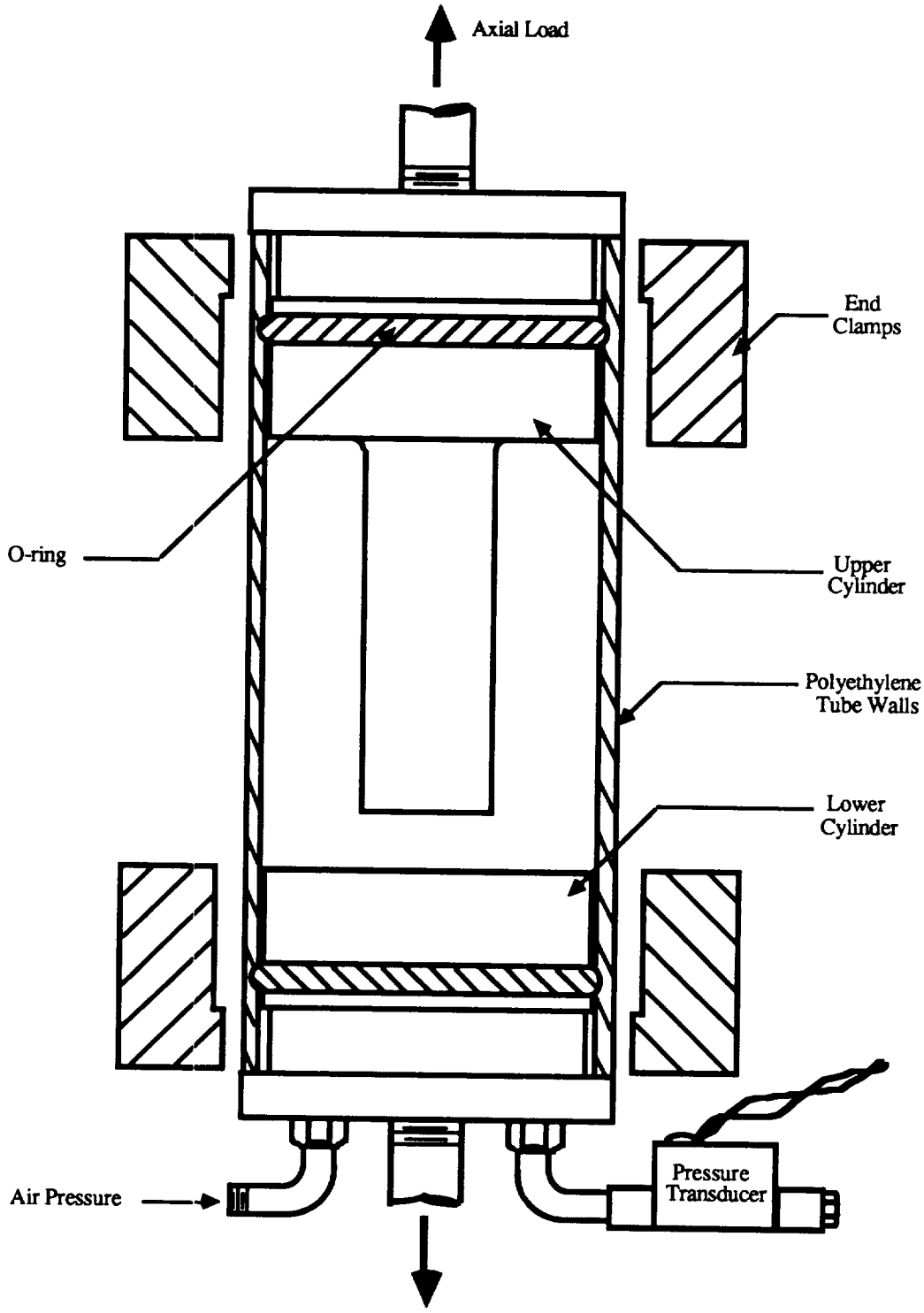

Figure 3.8 - Specimen Clamping Fixture

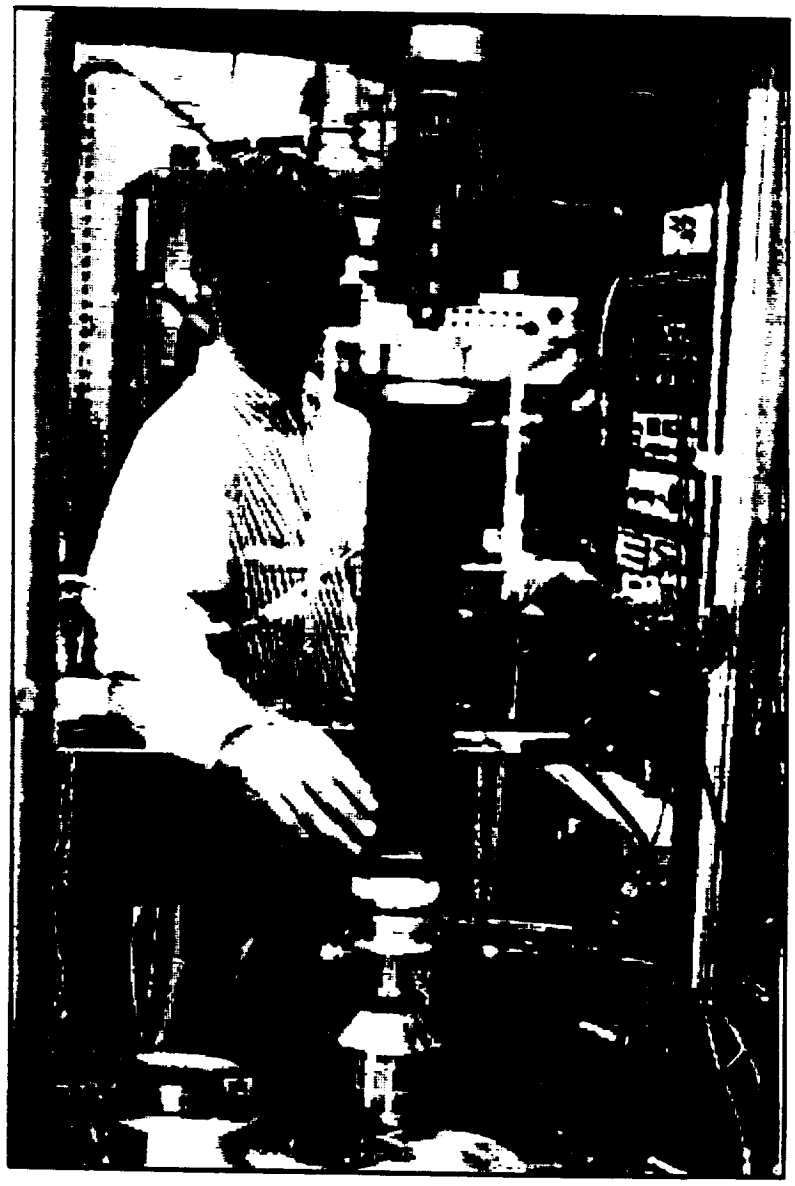

Figure 3.9 - Loading Frame along with Test Specimen.

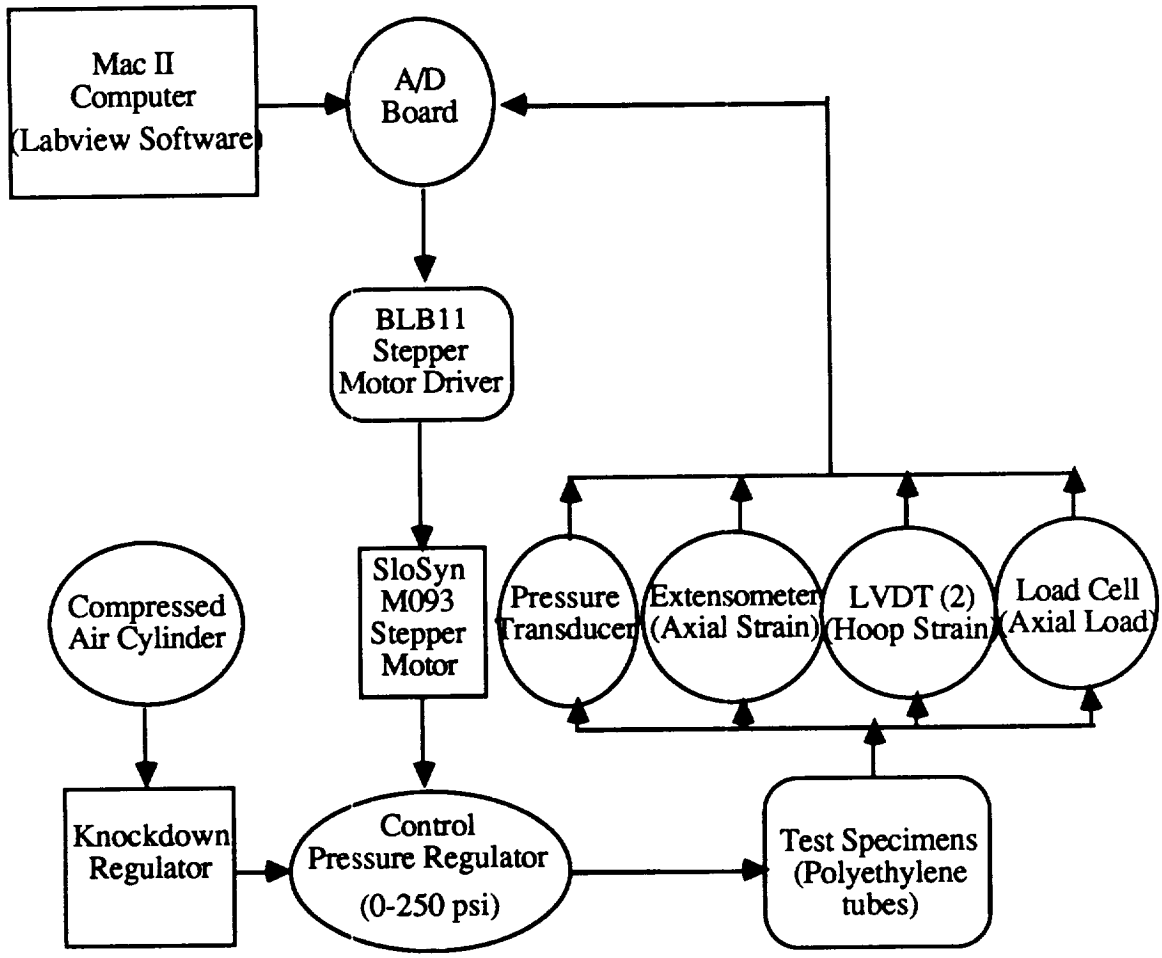

Figure 3.10 - Flow Chart of Pressure Regulation System

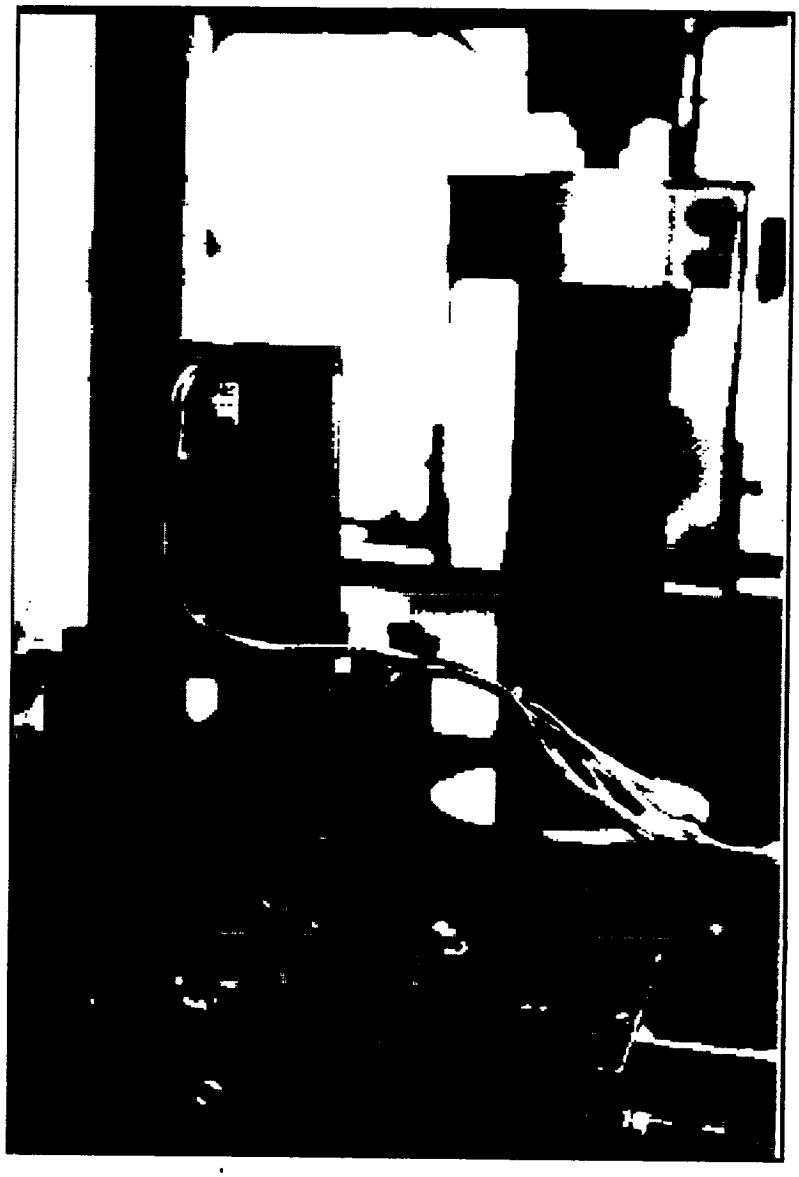

Figure 3.11 - Pressure Regulation System

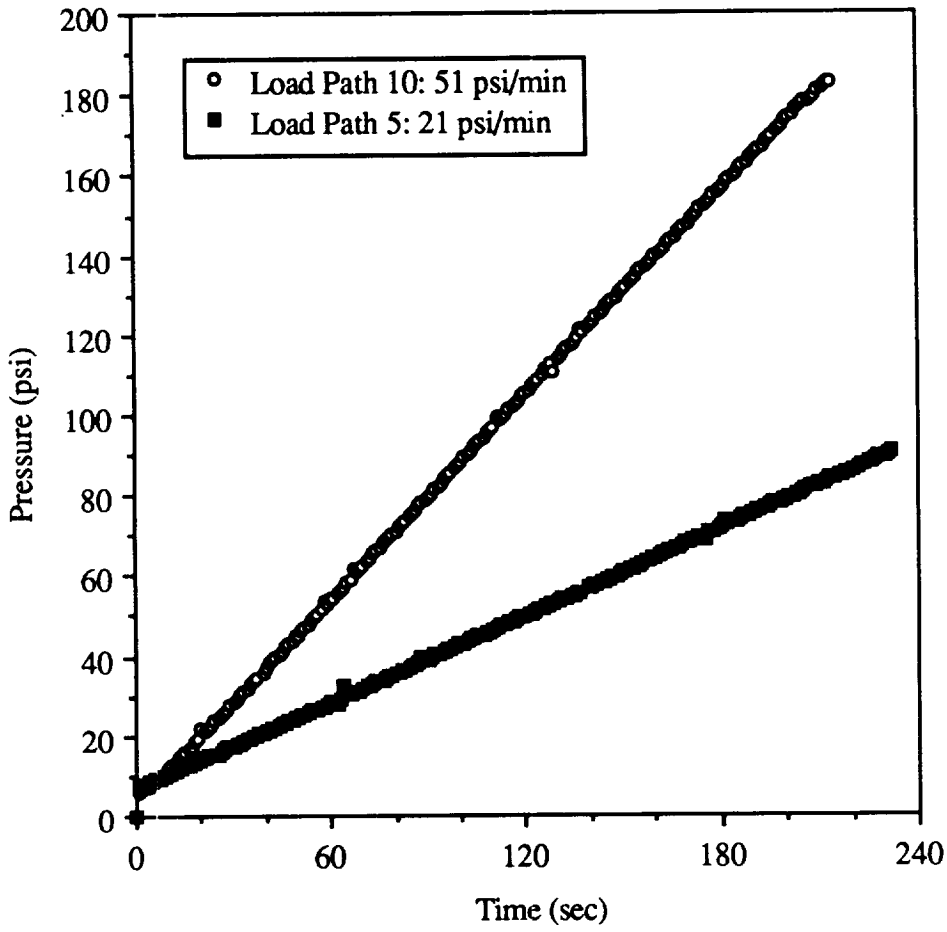

Figure 3.12 - Pressure versus Time for Load Paths 5 and 10

The scanning process created a binary data file. A computer program was then used to convert the binary data to numerical voltages. A second program converted the voltage readings to stress and strain values using calibration coefficients of the data measurement devices. Axial strain was calculated by: (1) converting the voltage reading at t = 0 sec to a corresponding gage length, (2) subtracting out the voltage reading at t = 0 sec from the entire set of voltage readings to determine the change in voltage, and (3) multiplying the voltage readings by the calibration coefficient 0.0992 inches/volt and dividing by the gage length for that test. Hoop strain was calculated by: (1) subtracting the voltage reading for t = 0 sec from all voltage readings for each LVDT, (2) multiplying the voltages for each LVDT by their corresponding calibration coefficient, 0.28457 inches/volt and 0.29379 inches/volt, to determine the displacement of each LVDT , (3) adding the displacement for LVDT 1 at time t to the displacement of LVDT 2 at time t to determine the total change in diameter of the tube at time t, and (4) dividing the change in diameter by the average hoop diameter of 3.396 inches. The pressure and axial load at any time t was calculated by multiplying the voltage reading from the pressure transducer and load cell at time t by their respective calibration coefficients, 59.386 psi/volt and 1000 lbs/volt. The hoop and axial stresses in the tube were calculated using thin-walled tube theory.

Summary of Test Procedure

Each specimen was mounted in the MTS frame, and a small offset preload (50 lbs) was applied to allow the grips to set. The axial load was then rezeroed. The desired axial load rate was entered into the MTS controller and all of the measurement devices and pressure hoses were attached.

Next, an offset pressure of approximately 7 psi was applied. The Labview program would then begin the pressure ramp and data acquisition and the MTS axial load ramp would be started manually. Although a small time offset existed between the start of the two ramps, the error induced was small. An X-Y chart recorder was used to obtain an axial load versus axial strain hardcopy plot, allowing for real-time monitoring of events. The test would end when the MTS bottomed out, when the maximum pressure of the system was reached, or when the specimen failed.

As mentioned, an offset pressure of approximately 7 psi existed in the specimen at the start of the test. This pressure induced small strains and stresses in both the hoop and axial directions. These strains were accounted for by plotting the hoop and axial strains versus the octahedral shear stress, as shown in Figure 3.13. The strain values went through zero since the instrumentation had been zeroed prior to the start of the test. The octahedral shear stress did not go through zero since there was initially pressure in the system inducing hoop and axial stresses. The two curves were linearly fit. An offset strain at time equal zero was then added to all strain values, shifting the entire curve so that it passed through the origin. Appendix A contains plots of the experimental hoop and axial stresses and strains obtained for each load path.

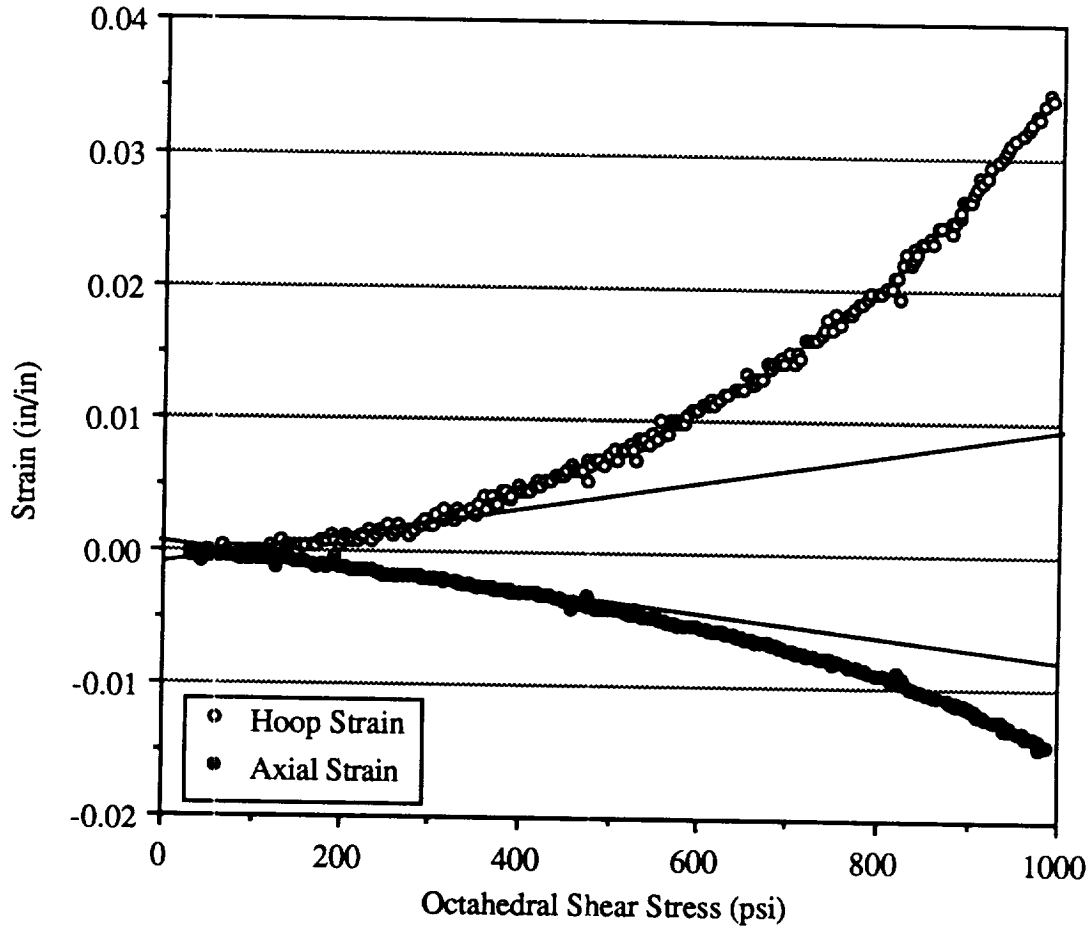

Hoop Strain Curve Fit: $y = -8.3268e^{-4} + 8.9596e^{-6}\,x$ $R^2 = 0.821$
Axial Strain Curve Fit: $y = 1.5582e^{-4} - 7.0471e^{-6}\,x$ $R^2 = 0.962$

Figure 3.13 - Axial and Hoop Strain versus Octahedral Shear Stress to Determine Offset Values of Strains due to Pressure Offset at time = 0 sec (Note: Data taken from Load Path 17, Test 57.)

CHAPTER 4 - DATA REDUCTION METHODS

Determination of Material Properties

Recall that load paths 1 and 19 (see Figure 3.1) define uniaxial stress tests, in which "pure" axial and hoop stress, respectively, were applied. Four repeated tests were completed for these two load paths. The stress and strain values recorded during these tests were used to determine Young's modulus E and Poisson ratio ν, in both the hoop and axial directions.

The experimentally determined material properties were:

E_1= 83,493 psi

E_2= 108,540 psi

ν_{12}= 0.39

ν_{21}= 0.52

As previously noted, the subscript "1" has been used to denote the axial direction, while the subscript "2" is used to denote the hoop direction. Previously reported values for E and ν range from 60,000 psi to 180,000 psi and 0.31 to 0.6, respectively [Manufacturing Chemists Association, 1957; Rodriguez, 1982; Ward, 1975]. Measurements obtained during this study therefore fall within the range of previously reported measurements.

The measured properties show that the annealed high-density polyethylene tubes were anisotropic. It can be shown that these properties should satisfy the following inverse relationship [Jones, 1975]:

$$\frac{\nu_{12}}{E_1} = \frac{\nu_{21}}{E_2} \tag{4.1}$$

Using the values of E_1, E_2, and ν_{12} listed above, the expected values of ν_{21} is 0.51. This compares very well with the experimental value of 0.52. For consistency, the value of ν_{21} in subsequent calculations was forced to fit the inverse relationship, i.e., ν_{21} was equated to 0.51.

Recall that the tubular specimens were produced by an extrusion process which resulted in significant residual stresses in the as-received tubes. It is likely that the extrusion process also caused the pronounced anisotropy in mechanical properties. The specimens were all subjected to a thermal annealing treatment prior to testing, so as to relieve the residual stresses. It had been hoped that the annealing process would also reduce or eliminate any anisotropic material behavior. This result was not achieved. The annealing process minimized residual stresses, but had little impact upon the anisotropy of the material.

Prediction of Yielding - Isotropic Model

Although the test material was clearly anisotropic, it was first modeled as an isotropic material. This approach may be of practical interest, since it avoids the additional mathematical complexities associated with anisotropic constituitive models. Average values were assigned to E and ν, 96000 psi and 0.46 respectively, and were assumed constant throughout the material.

Yield was based upon a 0.3% strain offset on the octahedral shear stress- octahedral shear strain curve. Octahedral shear stress and strain were used rather than individual axial and hoop stress and strain components in order to determine one value for the yield point and to bypass the

need to average values found on the individual stress-strain curves. This approach is in contrast to the method used by previous researchers [Raghava et al, 1973; Ely, 1968] wherein yield is defined based on axial stress and hoop stress versus effective strain curves. This latter approach results in two measurements of yield strength, which are subsequently averaged. A 0.3% offset was used because it was the most common offset in previous yield studies on polymers [Raghava and Caddell, 1974; Raghava et al, 1973].

The octahedral shear stress was calculated using Equation 2.2, repeated here for convenience:

$$\tau_{oct} = \frac{1}{3}\sqrt{(\sigma_1-\sigma_2)^2 + (\sigma_2-\sigma_3)^2 + (\sigma_3-\sigma_1)^2} \tag{4.2}$$

Octahedral shear strain is a similar function of the three principal strains:

$$\gamma_{oct} = \frac{2}{3}\sqrt{(\varepsilon_1-\varepsilon_2)^2 + (\varepsilon_2-\varepsilon_3)^2 + (\varepsilon_3-\varepsilon_1)^2} \tag{4.3}$$

Since no measurement of ε_3 was made during testing, it was necessary to determine ε_3 as a function of ε_1 and ε_2. Assuming that a plane stress state existed in the thin-walled tube, ε_3 is related to the two measured strains in the following manner:

$$\varepsilon_3 = \frac{-\nu}{1-\nu}[\varepsilon_1+\varepsilon_2] \tag{4.4}$$

Octahedral shear strain can now be written:

$$\gamma_{oct} = \frac{2}{3}\sqrt{(2+\frac{2\nu}{(1-\nu)^2})(\varepsilon_1^2+\varepsilon_2^2) + 2\varepsilon_1\varepsilon_2 \frac{-\nu^2+4\nu-1}{(1-\nu)^2}} \tag{4.5}$$

It can be shown [Semeliss, 1990] that the slope of the octahedral shear stress vs octahedral shear strain curve, assuming isotropic material behavior, is given by:

$$\frac{d\tau}{d\gamma} = \frac{E}{2(\nu+1)} = G \tag{4.6}$$

That is, the slope of the curve is independent of load rates and is simply equal to the shear modulus G. This simple relationship does not hold for anisotropic material behavior, as will be shown in a following section.

The procedure used to identify the yield point was as follows. Three repeated tests were conducted along each load path. All measurements for a given load path were combined into a single data set, and a fifth-order polynomial was fit to the data. The yield point was then identified by calculating the point of intersection between a 0.3% strain offset with a slope equal to G and the fifth-order polynomial. A typical result is shown in Figure 4.1. This numerical approach eliminated any need for estimating the intersection visually, and defined the yield point conveniently and consistently from one load path to the next. Since the axial stress to hoop stress ratio was constant for each test, the axial and hoop stresses which correspond to the yield point could be calculated based upon the octahedral shear stress at yield. Appendix B contains plots of octahedral shear stress versus octahedral shear strain for all load paths.

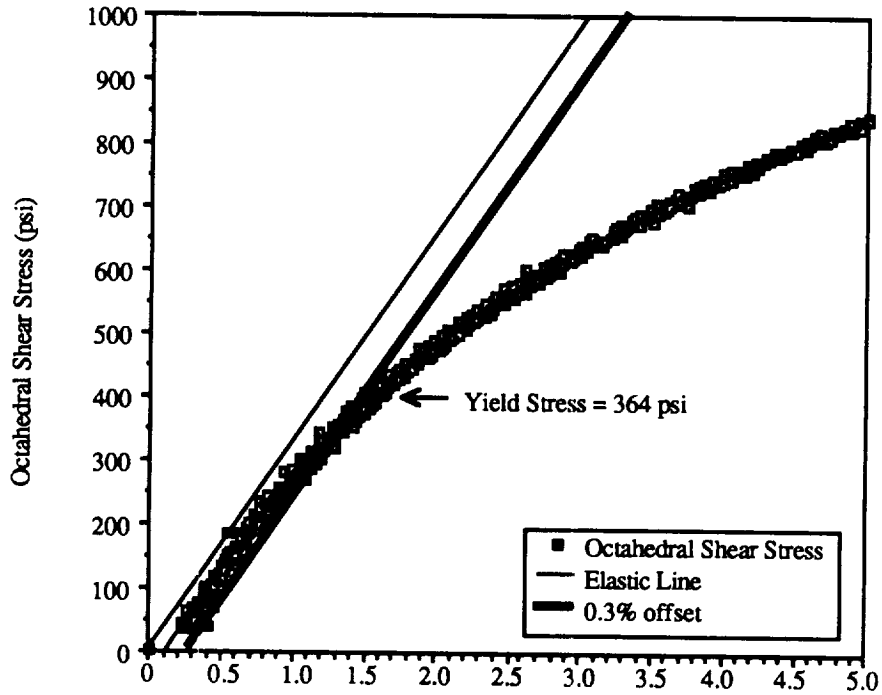

y = - 48.315 + 3.866(e+4x - 8.0732e+5x^2 + 1.1227e+7x^3 - 7.8266e+7x^4 + 1.8156e+8x^5 R^2 = 0.999

Figure 4.1 - Octahedral Shear Stress versus Octahedral Shear Strain for Load Path 3 with Isotropic Assumption: Axial Load Rate = 885 lb/min, Pressure Rate = 10 psi/min, Octahedral Shear Stress Rate = 258 psi/min, and Hydrostatic Stress Rate = 236 psi/min.

Prediction of Yielding - Transversely Isotropic Model

Hooke's law for an orthotropic (or transversely isotropic) material subjected to a plane stress state and referenced to the "principal" material coordinate system can be written [Jones, 1975]:

$$\begin{bmatrix} \varepsilon_1 \\ \varepsilon_2 \\ \gamma_{12} \end{bmatrix} = \begin{bmatrix} S_{11} & S_{12} & 0 \\ S_{12} & S_{22} & 0 \\ 0 & 0 & S_{66} \end{bmatrix} \begin{bmatrix} \sigma_1 \\ \sigma_2 \\ \tau_{12} \end{bmatrix} \tag{4.7}$$

$$\varepsilon_3 = S_{13}\sigma_1 + S_{23}\sigma_2 \tag{4.8}$$

where:

$$S_{11} = \frac{1}{E_1} \quad S_{12} = S_{21} = -\frac{\nu_{12}}{E_1} \quad S_{13} = S_{31} = -\frac{\nu_{13}}{E_1}$$

$$S_{22} = \frac{1}{E_2} \quad S_{23} = S_{32} = -\frac{\nu_{23}}{E_2}$$

It was assumed that the material was transversely isotropic, and hence $\nu_{13} = \nu_{23}$, $E_2 = E_3$, and $S_{13} = S_{12}$. Finally, ν_{23} was equated to the value of the average Poisson ratio in the axial and hoop direction, i.e., $\nu_{23} = 0.46$.

The radial strain was calculated assuming plane stress conditions:

$$\varepsilon_3 = \frac{-E_1\nu_{12}\,(1+\nu_{23})\,\varepsilon_1 - (E_2\nu_{12}^2 + E_1\nu_{23})\,\varepsilon_2}{E_1 - E_2\nu_{12}^2} \tag{4.9}$$

Octahedral shear strain for the transversely isotropic model can now be calculated as:

$$\gamma_{oct} = \frac{2}{3(E_1 - E_2\nu_{12}^2)} \sqrt{A\varepsilon_1^2 + B\varepsilon_1\varepsilon_2 + C\varepsilon_2^2} \tag{4.10}$$

where:

$$A = 2E_1^2 (\nu_{12}^2\nu_{23}^2 + 2\nu_{12}^2\nu_{23} + \nu_{12}^2 + \nu_{12}\nu_{23} + \nu_{12} + 1) - 2E_1E_2 (\nu_{12}^3\nu_{23} + \nu_{12}^3 + 2\nu_{12}^2) + 2E_2^2\nu_{12}^4$$

$$B = 2E_1^2 (2\nu_{12}\nu_{23}^2 + 3\nu_{12}\nu_{23} + \nu_{12} + \nu_{23} - 1) + 2E_1E_2 (\nu_{12}^3\nu_{23} + \nu_{12}^3 - \nu_{12}^2\nu_{23} + 3\nu_{12}^2) - 4E_2^2\nu_{12}^4$$

$$C = 2E_1^2 (\nu_{23}^2 + \nu_{23} + 1) + 2E_1E_2 (\nu_{12}^2\nu_{23} - \nu_{12}^2) + 2E_2^2\nu_{12}^4$$

Note that retention of the anisotropic material properties has a dramatic effect on the calculated value of octahedral shear strain. This fundamental difference between isotropic and anisotropic models will result in a difference in the measured yield point, as will be pointed out below.

It can be shown [Semeliss, 1990] that the predicted slope of the octahedral shear stress versus octahederal shear strain curve along each load path is given by:

$$\frac{d\tau}{d\gamma} = \frac{\frac{E_1E_2}{2\sqrt{2}} \sqrt{\frac{k_1^2}{2\pi^2r^2} + \frac{3r^2k_2^2}{2}}}{\sqrt{Dk_1^2 + Fk_1k_2 + Gk_2^2}} \tag{4.11}$$

where:

$$D = \frac{E_2^2 (\nu_{12} + 1)^2}{4r^2\pi^2}$$

$$F = \frac{1}{2\pi} [E_2^2 (-\nu_{12}^2 + 1) + E_1E_2 (-\nu_{12} + \nu_{12}\nu_{23} + \nu_{23} - 1)]$$

$$G = \frac{r^2}{4} [E_2^2 (\nu_{12}^2 - 2\nu_{12} + 1) + 2E_1E_2 (\nu_{12} - \nu_{12}\nu_{23} + \nu_{23} - 1) + 4E_1^2 (\nu_{23}^2 + \nu_{23} + 1)]$$

Unlike the isotropic case (i.e., Eq 4.6), the slope of the stress-strain curve for a transversely isotropic material is a function of load rates and therefore of load path.

The yield point was determined for the transversely isotropic model using the same procedure as described for the isotropic model. However, the slope is now a function of load path, and the octahedral shear strain values differ. Appendix B contains plots of octahedral shear stress versus octahedral shear strain for all load paths.

Prediction of Post-Yield Behavior

Power Law Models

Isotropic Form: The power law expression was given by Equation (2.11), repeated here for convenience:

$$\bar{s} = \bar{s}_{yield} + M\bar{e}^n \qquad (4.12)$$

where:

$$\bar{s} = \frac{1}{\sqrt{2}} [(s_1-s_2)^2 + (s_2-s_3)^2 + (s_3-s_1)^2]^{\frac{1}{2}} \tag{4.13}$$

$$\bar{e} = \frac{\sqrt{2}}{3} [(e_1-e_2)^2 + (e_2-e_3)^2 + (e_3-e_1)^2]^{\frac{1}{2}} \tag{4.14}$$

are the effective true stress and effective true strain defined as a function of the principal stresses and strains respectively. Assuming plane stress, then $s_3 \approx 0$, and Equation (4.13) can be simplified:

$$\bar{s} = [s_1^2 + s_2^2 + s_1 s_2]^{\frac{1}{2}} \tag{4.15}$$

Also by assuming the constancy of volume, Equation (4.14) can be rewritten as:

$$\bar{e} = [\frac{4}{3} (e_1^2 + e_2^2 + e_1 e_2)]^{\frac{1}{2}} \tag{4.16}$$

The true strains used in Equation (4.16) are the plastic portion of the total true strain defined earlier and repeated here:

$$e^p = e^t - e^e \tag{4.17}$$

where e^t and e^e are the total and elastic true strain components respectively. The total true strain e^t are the experimentally recorded values and the elastic true strains e^e are defined using the biaxial

form of Hooke's law. The principal stress and strain components in Equations (4.15) and (4.16) correspond to the axial and hoop directions, due to loading and specimen geometry symmetry.

Taking the logarithms of both sides of Equation (4.12) gives:

$$\log(\bar{s}\text{-}\bar{s}_{yield}) = n \log\bar{e} + \log M \tag{4.18}$$

which is in the form of a linear equation:

$$y = mx + b \tag{4.19}$$

where $y = \log \bar{s}\text{-}\bar{s}_{yield}$, $x = \log\bar{e}$ and $b = \log M$. Thus, a log-log plot of $\bar{s}\text{-}\bar{s}_{yield}$ versus $\bar{e}$ can be used to determine the constants M and n, where M is the y-intercept and n is the slope of Equation (4.19).

A polynomial curve-fit was used to achieve a smooth curve after shifting the individual tests to the isotropic yield points. A "new" data set consisting of axial stress strain and hoop stress strain values was generated using the polynomial curve-fitting equation. The effective true stresses and effective plastic strains were then calculated using Equations (4.15) and (4.16). A log-log plot of $\bar{s}\text{-}\bar{s}_{yield}$ versus $\bar{e}$ was performed and a linear curve-fit was used to achieve the best correlation coefficient. This linear curve-fitting equation provided easy calculation of the constants M and n, the strength coefficient and strain hardening exponent, respectively.

Anisotropic Form: For the anisotropic case, the power law relation is defined in the same way as the isotropic case given by Equation (4.12). On the other hand, the effective true stress and

effective true strain for an anisotropic material under complex loading condtions are very different from the isotropic case (compare Equations 2.12 and 2.13 with Equations 2.23 and 2.24). However, if it is assumed that only a biaxial stress state exists and the material is transversely isotropic, then Equations (2.23) and (2.24) can be simplified as:

$$\bar{s} = \sqrt{\frac{3}{2}\frac{Fs_2^2 + Gs_1^2 + H(s_1-s_2)^2}{F+G+H}} \tag{4.20}$$

$$\bar{e} = \frac{\sqrt{\frac{2}{3}(F+G+H)[F\{Ge_2+H(e_1+e_2)\}^2 - G\{Fe_1+H(e_1+e_2)\}^2 + H\{Fe_1-Ge_2\}^2]}}{FG + GH + HF} \tag{4.21}$$

where:

$$H + G = \frac{1}{T_{axial}^2}$$

$$H + F = \frac{1}{T_{hoop}^2}$$

$$H = G$$

The coefficients, F, G, and H, are now functions of the tensile yield strengths in the axial and hoop directions.

Using Equations (4.12), (4.20) and (4.21), the constants M and n can again be found using a linear curve-fit of a $\log \bar{s}\text{-}\bar{s}_{yield}$ versus $\log \bar{e}$ curve.

Prandtl-Reuss Model

The Prandtl-Reuss equation for an isotropic material was given in Equation (2.20), repeated here for convenience:

$$de_i^t = \frac{3}{2}\frac{s'_i\, d\bar{s}}{\bar{s}H} - \frac{ds'_i}{2G} + \frac{(1-2\nu)}{E} ds_{hyd} \tag{4.22}$$

where $\bar{s}$ is the isotropic form of the effective true stress defined by Equation (4.15). Equation (4.22) gives the incremental change in total true strain associated with an incremental increase in stress. Note that by definition the plastic true strains equal zero at the yield point. Therefore the total true strain induced by a given stress state beyond the yield point equals the sum of the elastic response (including any strain offset associated with the definition of yielding) plus the sum of incremental increases in strain calculated using Equation (4.22). The given stress state is represented by the effective true stress $\bar{s}$, the deviatoric stress , and the hydrostatic true stress s_{hyd}.

In order to apply the Prandtl-Reuss equation in practice, one must determine the material constants E and ν, as well as the plasticity modulus H. In the present case E and ν were assigned average values of 96000 psi and 0.46. The plasticity modulus H was determined using data collected along the two uniaxial stress load paths, specifically load path 1 (pure axial stress) and load path 19 (pure hoop stress). Four repeated tests were performed along both of these load paths. The resulting eight data files were combined into a single data set and a plot of effective plastic true strain versus effective true stress was generated, as shown in Figure 4.2. The data was

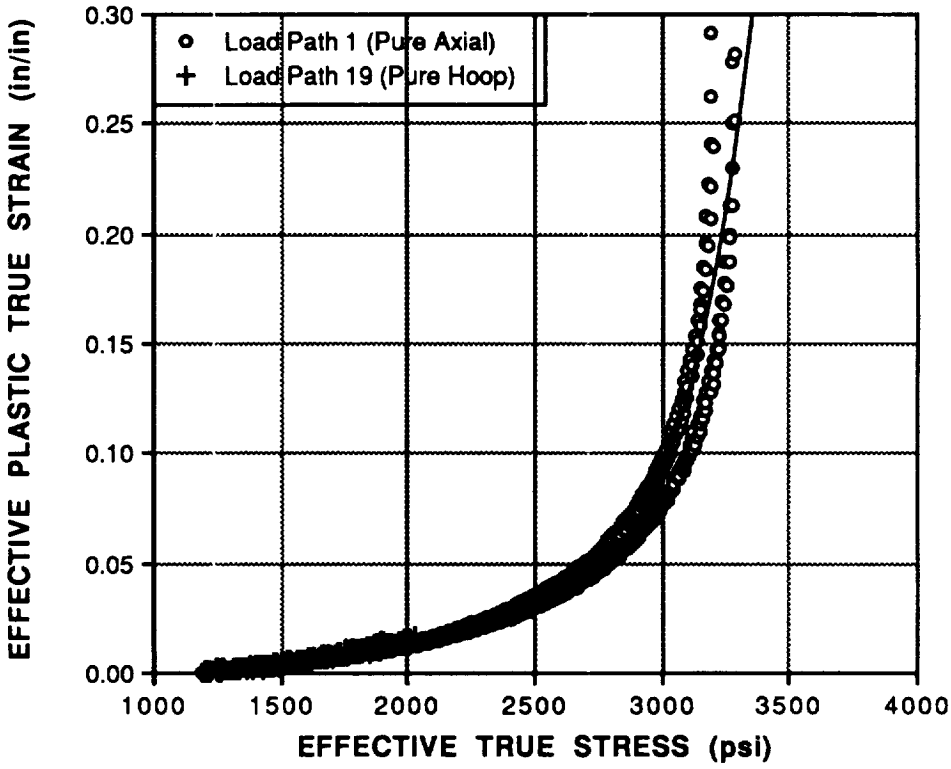

Figure 4.2: Plot of Effective Plastic True Strain versus Effective True Stress, Used to Determine the Plasticity Modulus H.

then curve-fit using a fifth-order polynomial such that the derivative of this equation represents the inverse of the plasticity modulus H:

$$\frac{1}{H} = \frac{d\bar{e}^p}{d\bar{s}} \tag{4.23}$$

As mentioned above and described in a preceding section, yielding was defined in terms of a 3% offset in octahedral shear strain, and the axial and hoop strain components associated with this strain offset were added to the calculated elastic strains.

Lode Parameters: The Lode parameters, μ and ν, provide a simple check to determine if the Prandtl-Reuss equations are valid for a given material. If the equations hold, then μ and ν are equal, as previously shown in Figure 2.2. For plane stress conditions the Lode parameters reduce to:

$$\mu = \frac{2s_2 - s_1}{s_1}$$

$$\nu = \frac{3e_2^p}{2e_1^p + e_3^p}$$

where in the present case the principal stresses and strains correspond to the axial and hoop directions. The stresses in Equation (4.26) are the total stresses, while the plastic strains were derived also from experimental values using Equation (4.17). The parameters μ and ν were calculated for the the entire post-yield history, and then an average value was determined for each particular load path.

CHAPTER 5 - RESULTS AND DISCUSSION

YIELD PREDICTIONS

Isotropic Models: The two isotropic yield criterion considered in this study were the Von Mises yield criterion and the Pressure-modified Von Mises yield criterion. Experimentally determined yield points are listed in Table 5.1, and are compared with predictions in Figure 5.1 Note that the shape and size of the theoretical Pressure-modified Von Mises locus is a function of the compressive to tensile yield strength ratio (see Eq 2.4). Since the compressive yield strength of polyethylene was not measured during this study, it was neccessary to use literature reference values for the compressive to tensile yield strength ratio (C/T) for high-density polyethylene. Two values have been reported in the literature for (C/T): 1.3 [Raghava and Caddell, 1973] and 1.08 [Raghava et al, 1973; Caddell et al, 1974]. Thus, the compressive yield strength is typically higher than the tensile yield strength.

The comparison presented in Figure 5.1 shows that the experimental measurements were not well predicted by either of the two isotropic yield criterion considered. The theoretical loci were symmetric with respect to the 45° line, while the experimental yield locus was skewed. This discrepancy is of course due to material anisotropy. As previously stated, the isotropic analysis was conducted because isotropic models avoid the additional mathematical complexities associated with anisotropic constituitive models, and hence are easier to apply in practice. The results represented by Figure 5.1 show that very significant errors are introduced by the assumption of isotropy.

Table 5.1 - Experimental Yield Stresses for the Isotropic and Transversely Isotropic Models

	Isotropic Model		Transversely Isotropic Model	
Load Path	Axial Stress (psi)	Hoop Stress (psi)	Axial Stress (psi)	Hoop Stress (psi)
1	931	0	1143	0
3	835	147	1127	199
4	748	200	1074	288
5	871	317	1205	438
6	906	421	1238	576
7	981	567	1295	749
8	1043	729	1325	926
9	1099	923	1288	1082
10	1283	1283	1262	1262
11	1209	1439	1243	1480
12	1024	1463	984	1406
13	928	1600	846	1459
14	735	1564	664	1413
15	644	1789	586	1627
16	424	1572	375	1390
17	323	1794	281	1560
18	116	1293	110	1220
19	0	1438	0	1279

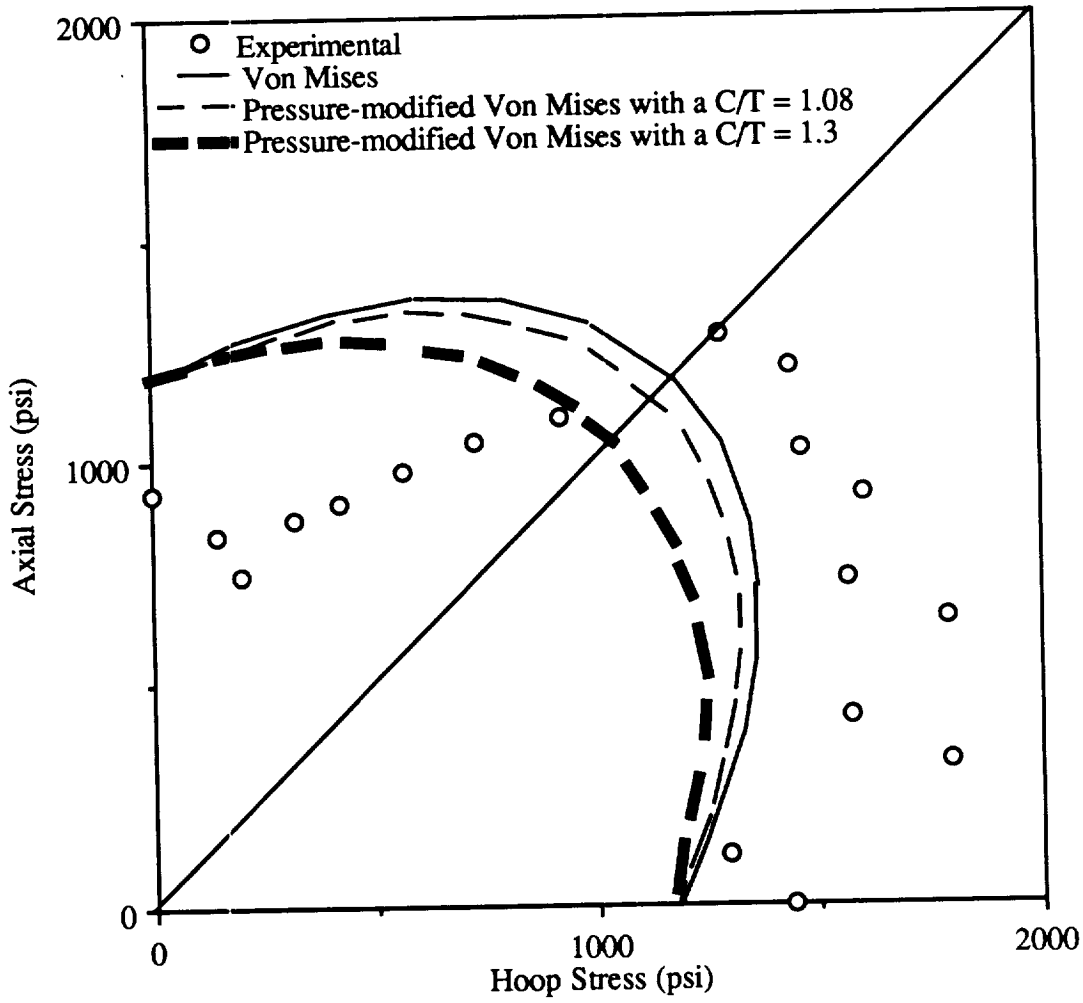

Figure 5.1 - Comparison of Experimental Measurements and Theoretical Yield Loci for the Isotropic Models

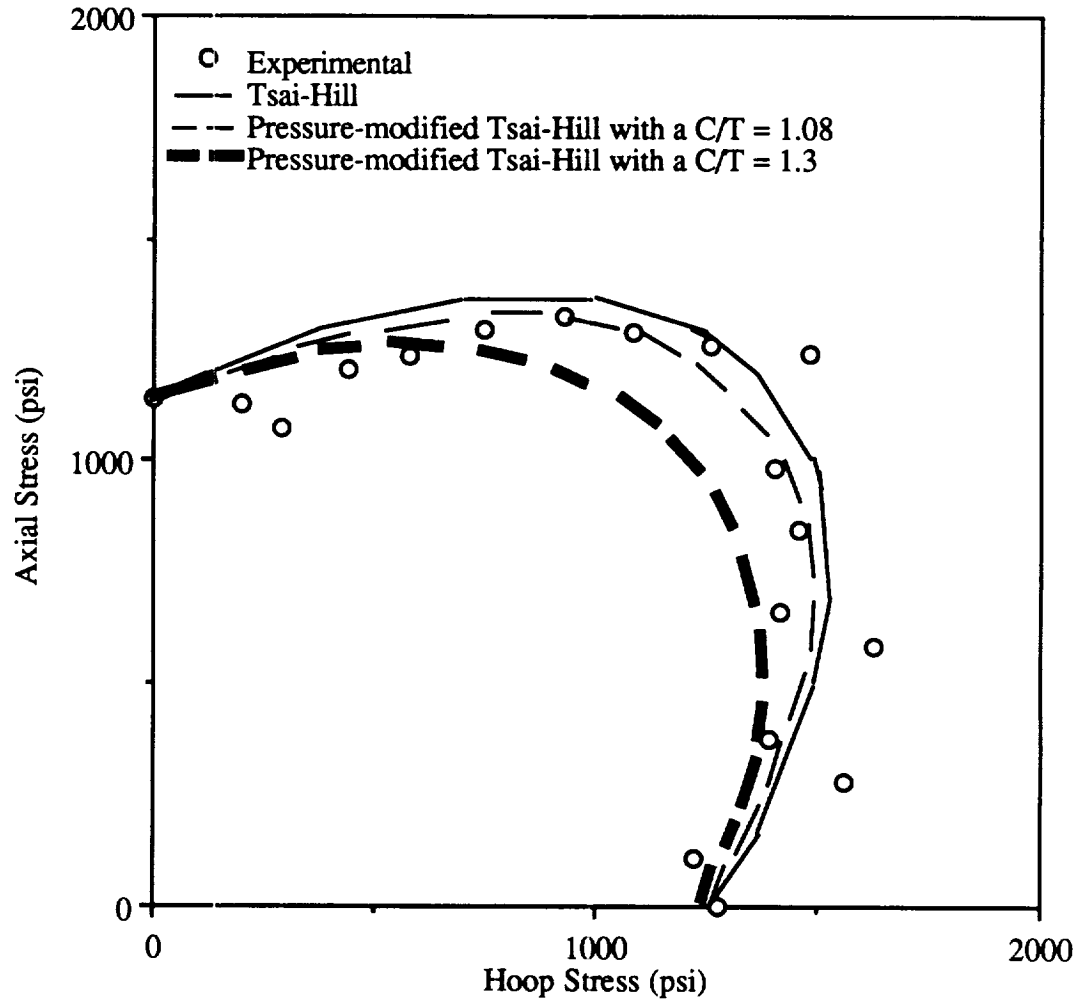

Figure 5.2 - Comparison of Experimental Measurements and Theoretical Yield Loci for the Transversely Isotropic Model

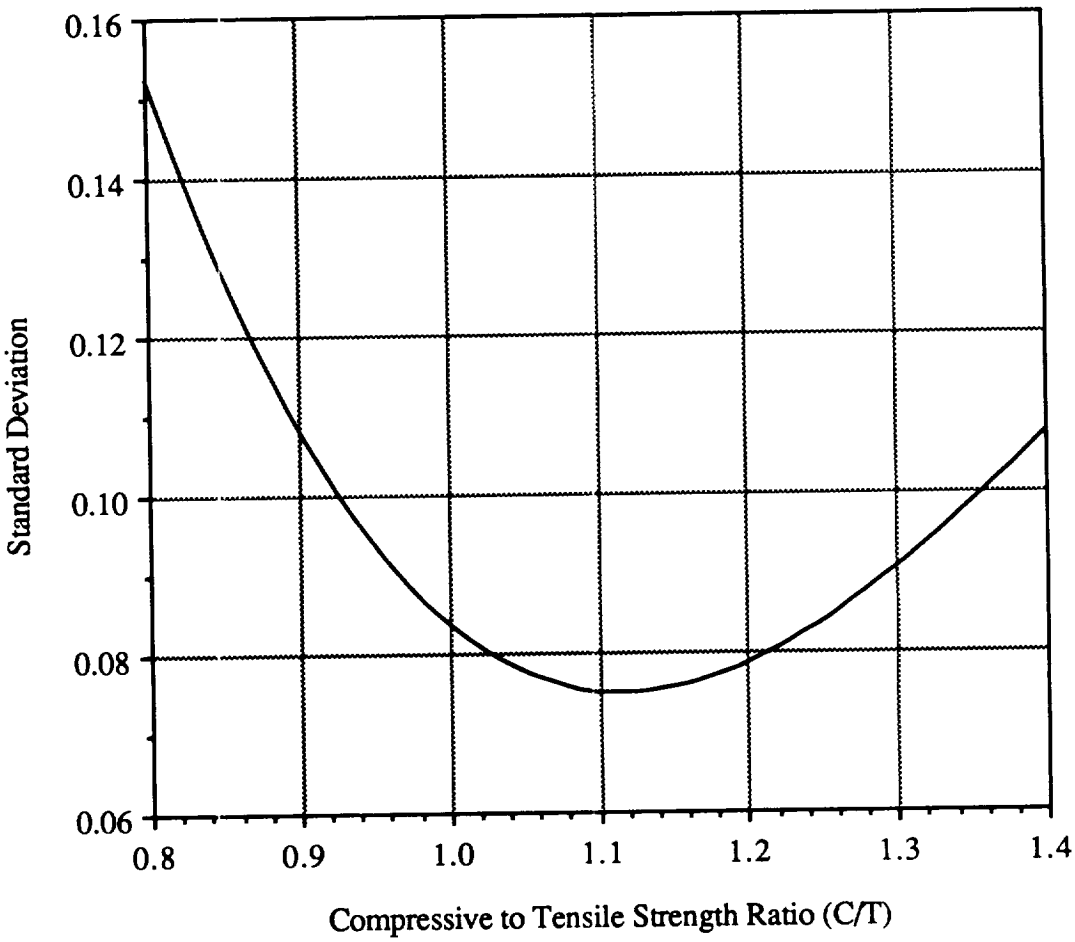

Figure 5.3 - Standard Deviation of Pressure-modified Tsai-Hill Yield Locus from Experimental Yield Locus as a Function of Compressive to Tensile Yield Strength Ratio (C/T)

It was concluded on the basis of these results that the yield behavior of high-density polyethylene cannot be adequately modeled using isotropic yield criterion. Further, this conclusion is likely to be true for the general class of semi-crystalline thermoplastic polymers.

Anisotropic Models: The two anisotropic yield criterion considered in this study were the Tsai-Hill criterion and the Pressure-modified Tsai-Hill criterion. Experimentally measured yield points based on the transversely isotropic model are listed in Table 5.1. A comparison of the experimental yield locus and the predicted loci of the two anisotropic models is shown in Figure 5.2. Once again, the compressive to tensile yield strength ratio was needed to define the theoretical Pressure-modified Tsai-Hill yield locus (see Eq 2.6). In this case both hoop and axial strength ratios are required. The same values for the strength ratios mentioned above were used (i.e., C/T = 1.3, 1.08), and the ratios were assumed to be the same for both hoop and axial directions.

Comparing Figs 5.1 and 5.2, it is immediately obvious that the anisotropic models predict the experimental behavior much better than the isotropic models. However, by inspection alone it is difficult to determine whether the Pressure-modified Tsai-Hill yield criterion or the Tsai-Hill yield criterion best fit the experimental results. A calculation based on the standard deviation between measurement and prediction was conducted to determine which criterion correlated best with experimental results. The procedure is fully described in Appendix C. Briefly, the standard deviation was based on the difference between the radial distance to an experimentally measured yield point and the radial distance to the corresponding point on the theoretical yield locus defined by the Pressure-modified Tsai-Hill criterion and some given C/T ratio. In essense, the procedure determined the particular C/T ratio which resulted in the best fit between measured and predicted yield response.

The standard deviation as a function of the C/T ratio is shown in Figure 5.3. The results indicate a minimum standard deviation when the strength ratio was 1.11. As discussed above, C/T ratios for high density polyethylene equal to 1.08 and 1.3 have been reported. Hence, the C/T ratio deduced from the data collected during this study is in close agreement with previously reported values.

To summarize, the yield response of annealed high-density polyethylene is best predicted using the Pressure-modified Tsai-Hill criterion, with a C/T ratio of 1.11. This criterion adequately models both the anisotropic nature of polyethylene, and also accounts for the effects of hydrostatic stress on yielding.

POST-YIELD PREDICTIONS

Power Law Model

Isotropic Form: Plots of log $\bar{s}$-$\bar{s}_{yield}$ versus log $\bar{e}$ curves for load paths 1 and 19 of the isotropic case are shown in Figures 5.4 and 5.5 respectively. The straight line is the linear curve-fit of the experimental data points. The equation shown in the figures is the equation of the straight line and the corresponding correlation coefficent R^2. The correlation coefficient for all load paths achieved a value of 0.99 or better.

Figures 5.6 and 5.7 show the experimentally obtained values of M and n for all load paths. As indicated, the values of M and n varied substantially with load path. These large variations imply that the plastic flow of polyethylene cannot be adequately modeled using the isotropic power law, since M and n must be independent of load path. The values of the strength coefficient M

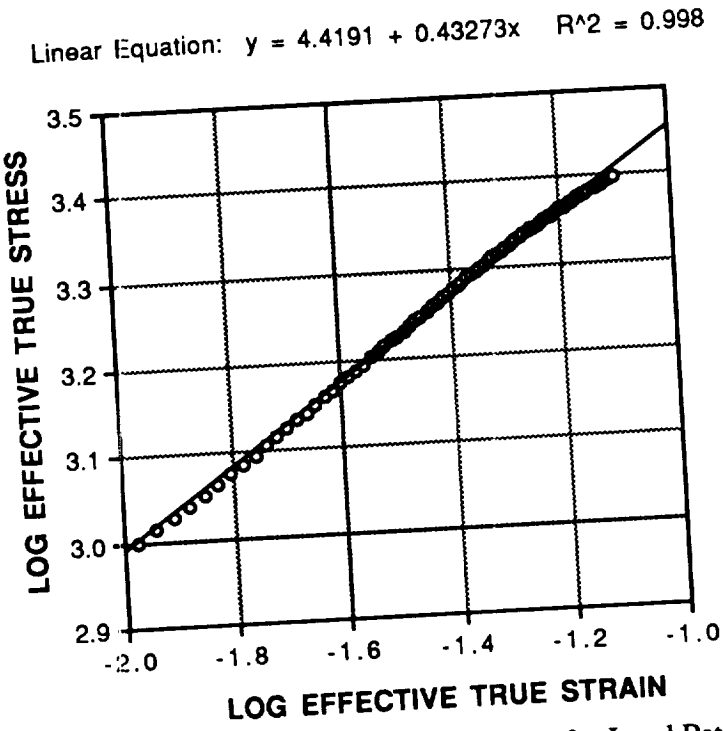

Figure 5.4: Log $\bar{s}$-$\bar{s}$yield versus Log $\bar{e}$ Curve for Load Path 1

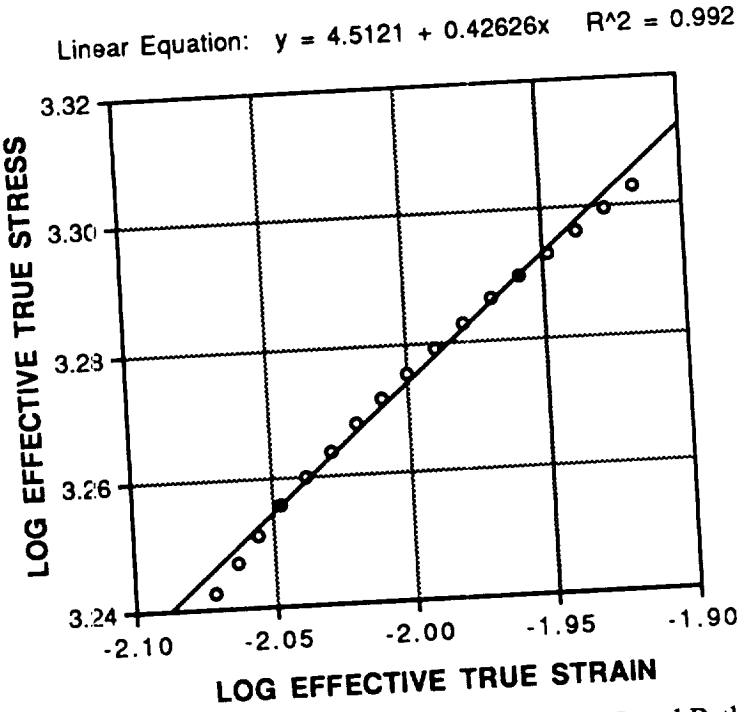

Figure 5.5: Log $\bar{s}$-$\bar{s}$yield versus Log $\bar{e}$ Curve for Load Path 19

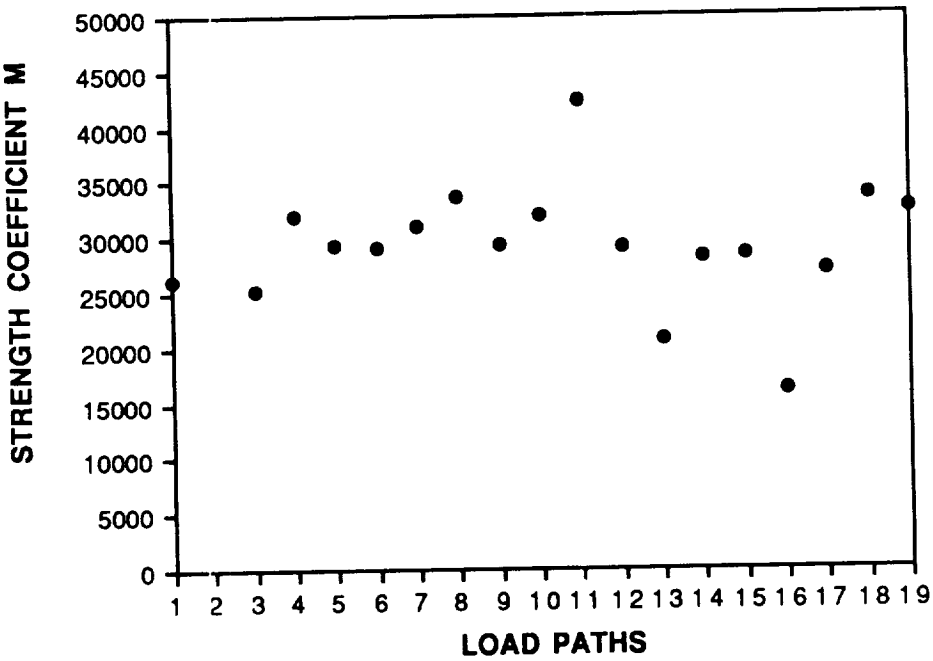

Figure 5.6: Strength Coefficient M versus Load Path for Isotropic Power Law Model

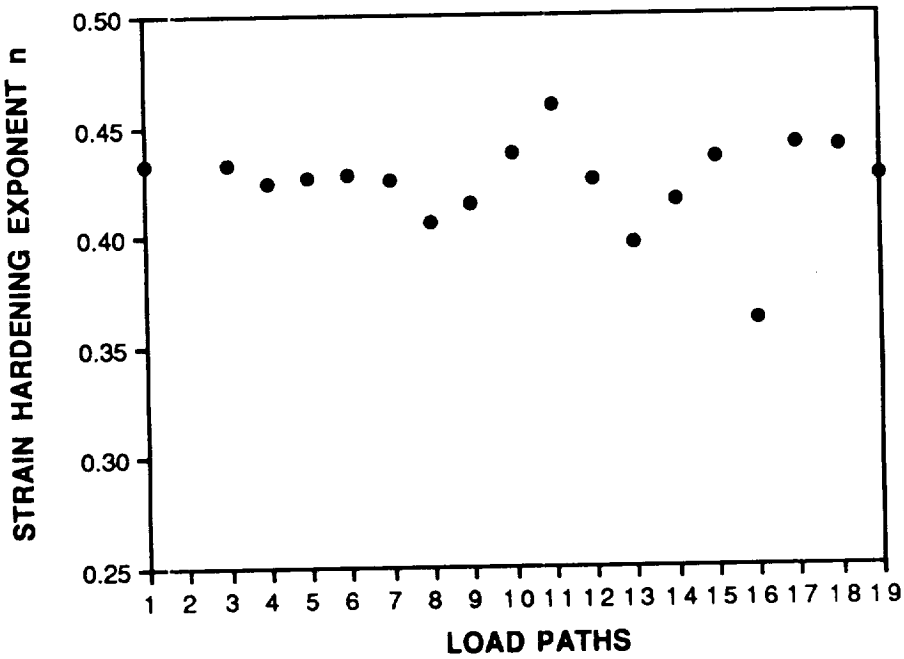

Figure 5.7: Strain Hardening Exponent n versus Load Path for Isotropic Power Law Model

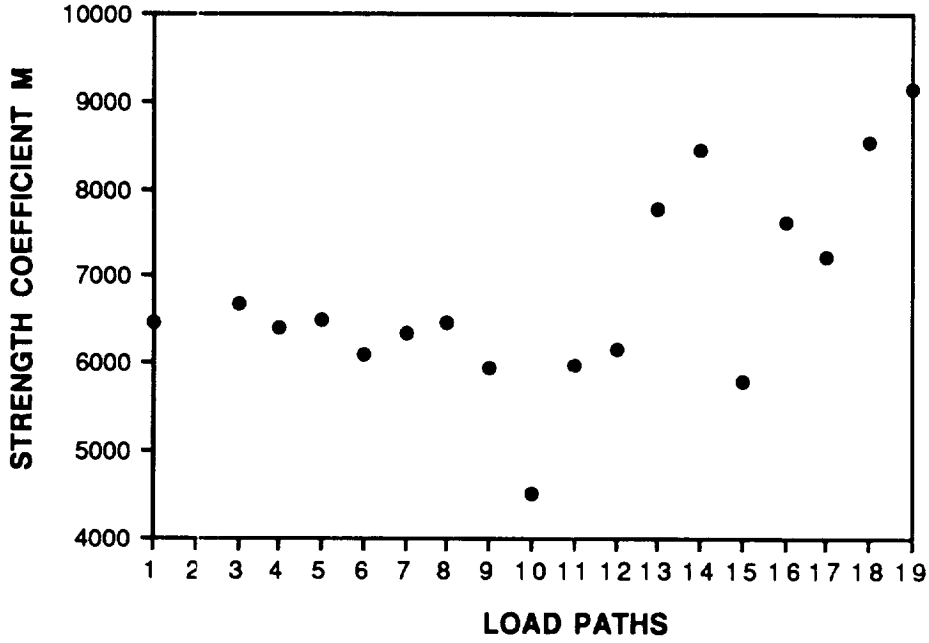

Figure 5.8: Strength Coefficient M versus Load Path for Anisotropic Power Law Model

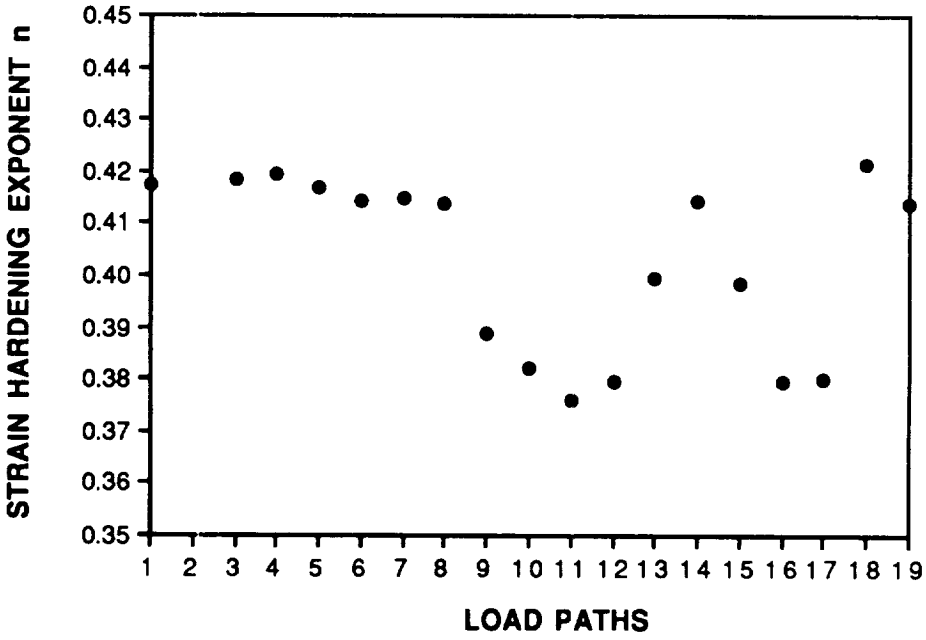

Figure 5.9: Strain Hardening Exponent n versus Load Path for Anisotropic Power Law Model

range from about 15,000 psi to over 40,000 psi , while the values of the strain hardening exponent n range from about 0.36 to about 0.46.

Since both M and n varied substantially with load path, the isotropic form of the power law was not further pursued during the study.

Anisotropic Form: A plot of the experimentally determined values of M and n versus load path for the anisotropic power law are shown in Figures 5.8 and 5.9 respectively. Once again, M and n do not have the same values for all load paths, although the deviations in M and n are less than in the corresponding isotropic analysis. Values range from M = 4500 psi to 9000 psi, and n = 0.38 to 0.42. Although the anisotropic power law showed improvement over the isotropic version, the agreement between load paths was still considered poor. In particular, the deviation in M was considered excessive. As discussed in Chapter 2, the power law is essentially an empirical relationship, and even for initially isotropic materials deviation from the power law are common. The lack of agreement in the present study is therefore not suprising.

Since both M and n varied substantially with load path, the anisotropic form of the power law was not further pursued during the study.

Prandtl-Reuss Model

Calculation of the Lode Parameters: An evaluation of whether the Prandtl-Reuss relations are appropriate for use with polyethylene was first performed by calculating the Lode parameters for each load path. As discussed in Chapter 4, a material is suited for use with the Prandtl-Reuss equations if the Lode parameters are equal. The Lode parameters calculated during this study are

shown in Figure 5.10. Although the parameters were not absolutely identical, the deviations are similar in magnitude to those reported by other researchers for other materials (see, for example, Figure 2.2). Hence, the Lode parameters indicate that the Prandtl-Reuss relations will predict the post-yield response to within engineering accuracy, which in essence implies that high-density polyethylene can be modeled approximately as an elastic-perfectly plastic material.

Prandtl-Reuss Predictions: Figures 5.11- 5.28 show a comparison between experimental and predicted axial strain and hoop strain for each load path, based upon the Prandtl-Reuss equations. The reader should note several details during interpetation of these plots. First, the stress and strains plotted in these figures are true stress/strains, as compared to engineering stress/strains. Second, only the post-yield response is plotted. As previously discussed, all curves (both measured and predicted) begin at the axial or hoop strain level associated with the yield point for the given load path. These strain levels were calculated as the sum of the elastic strain at yield (calculated using the average measured values of E and ν), and a strain value corresponding to the 0.3% offset in octahedral shear strain. Third, strains are plotted against both axial and hoop stress in these figures, to emphasize that the measured and predicted response is for a particular biaxial loading condition. Fourth, the maximum plastic strain which could be induced was not constant for all load paths. Recall that axial loads were applied using an MTS fatigue frame capable of applying loads as high as 20,000 lbs. In contrast, internal pressures were applied using a bottled air and regulator system, and the maximum pressure which could be applied was roughly 250 psi. Hence, the maximum plastic strain which could be induced for a given load path was a function of whether the axial load or internal pressure was the dominant loading mechanism. In order to make a consistent comparison, the strain range for Figs 5.11 through 5.18 (i.e., for load paths 1 through 9) is 0 to 0.20 in/in, whereas the strain range for Figs 5.19 through 5.28 (load paths 10 through 19) is 0 to 0.10 in/in. Fifth, in each plot the predicted response is

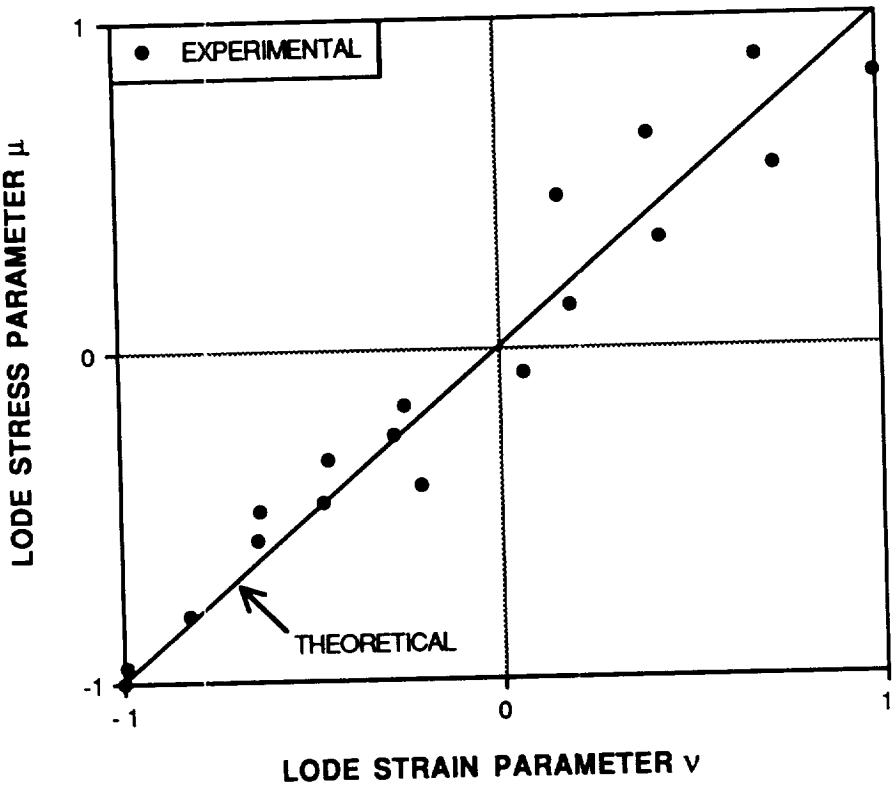

Figure 5.10: Comparison of Lode Variables Calculated Using Experimental Data with Theoretical Result

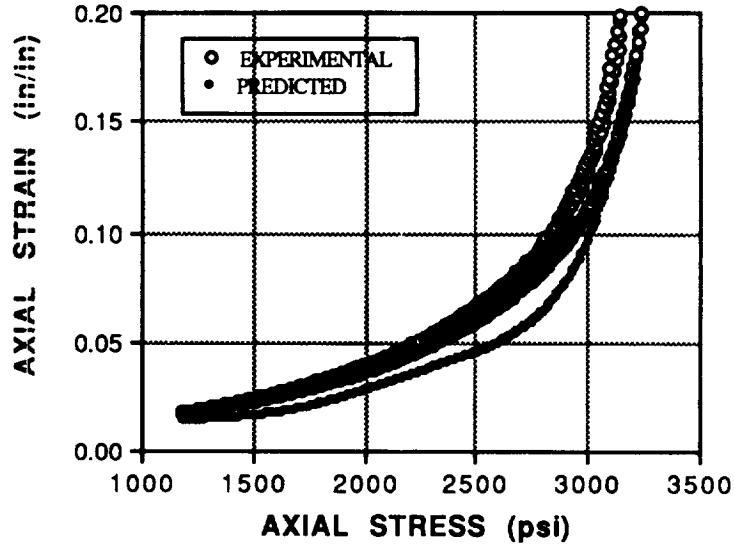

(a) Axial Strains (Tensile)

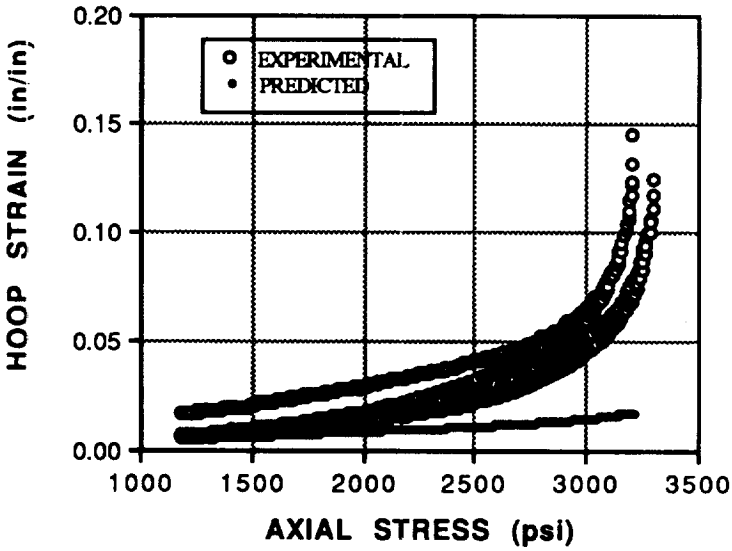

(b) Hoop Strains (Compressive)

Figure 5.11: Measured vs Predicted Plastic Strains for Load Path 1

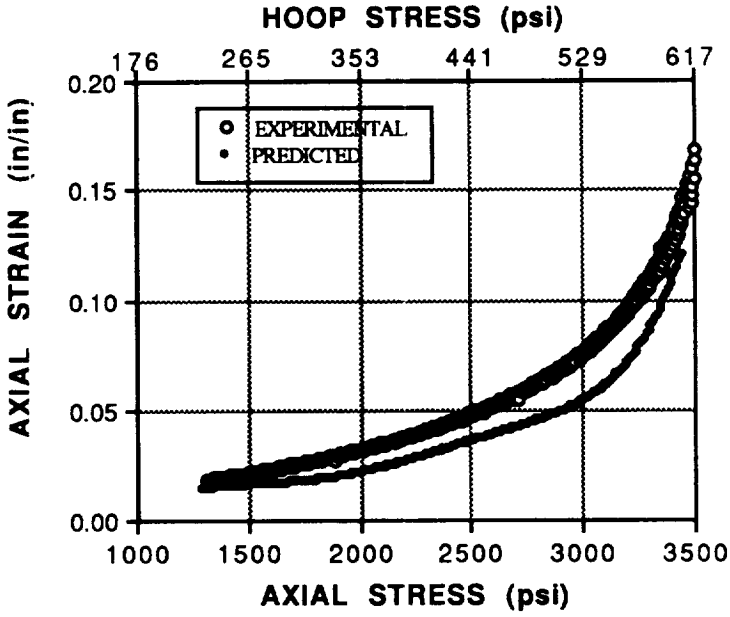

(a) Axial Strains (Tensile)

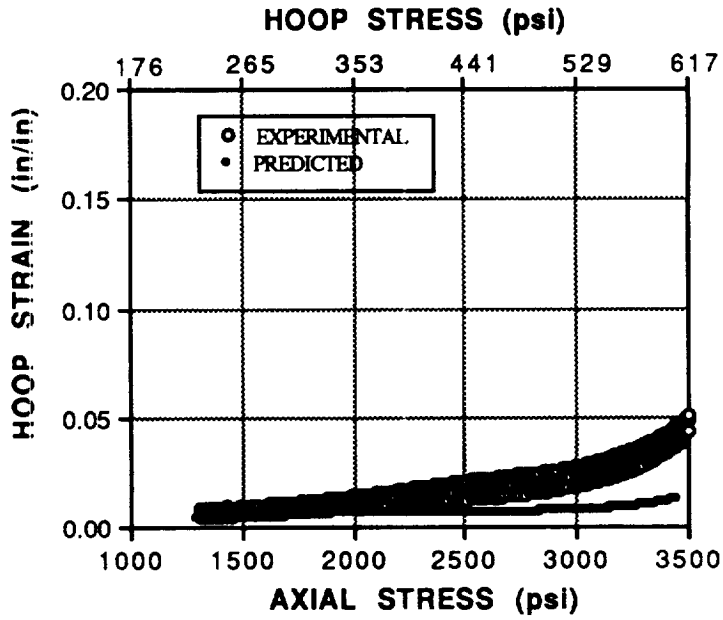

(b) Hoop Strains (Compressive)

Figure 5.12: Measured vs Predicted Plastic Strains for Load Path 3

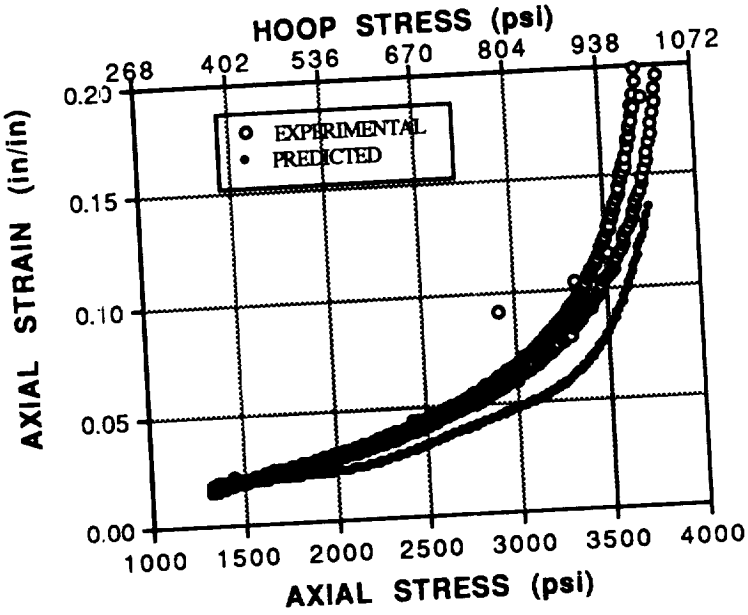

(a) Axial Strains (Tensile)

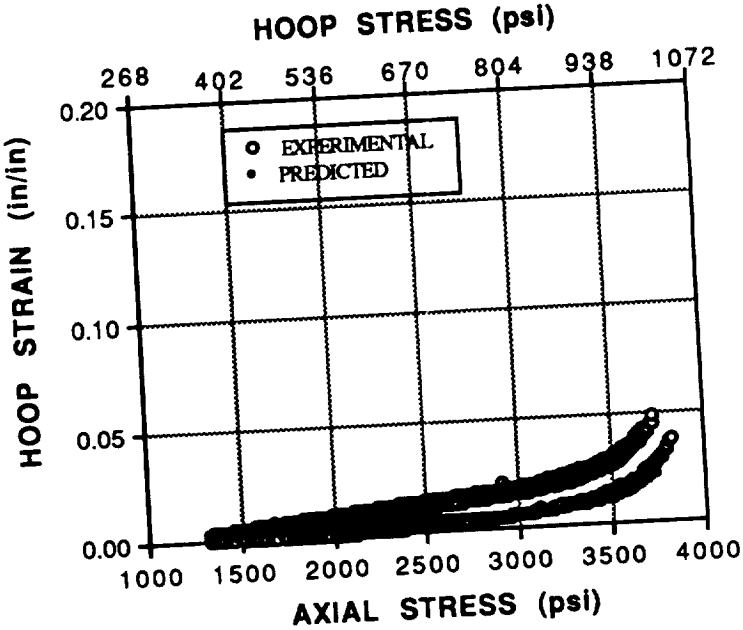

(b) Hoop Strains (Compressive)

Figure 5.13: Measured vs Predicted Plastic Strains for Load Path 4

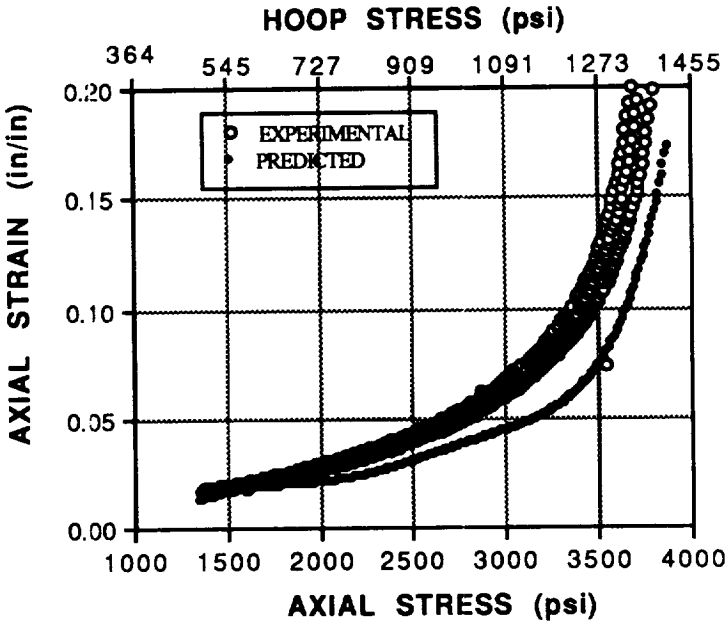

(a) Axial Strains (Tensile)

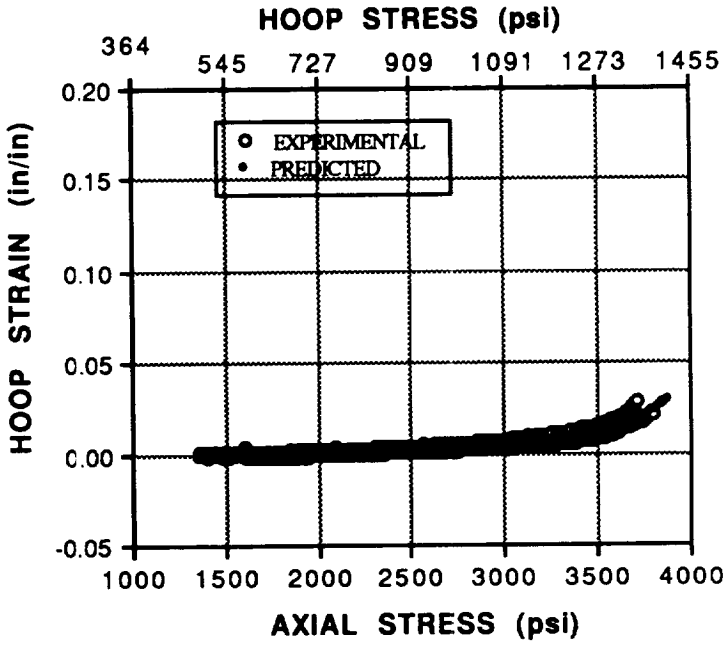

(b) Hoop Strains (Compressive)

Figure 5.14: Measured vs Predicted Plastic Strains for Load Path 5

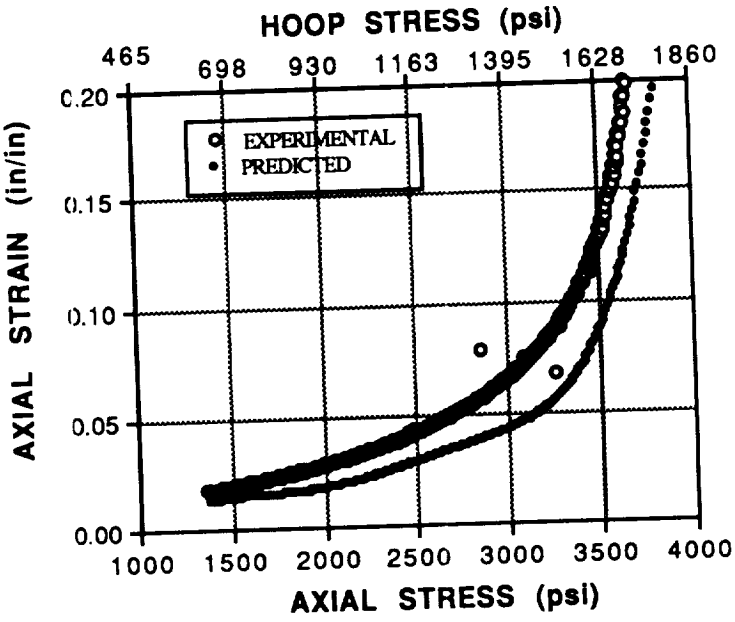

(a) Axial Strains (Tensile)

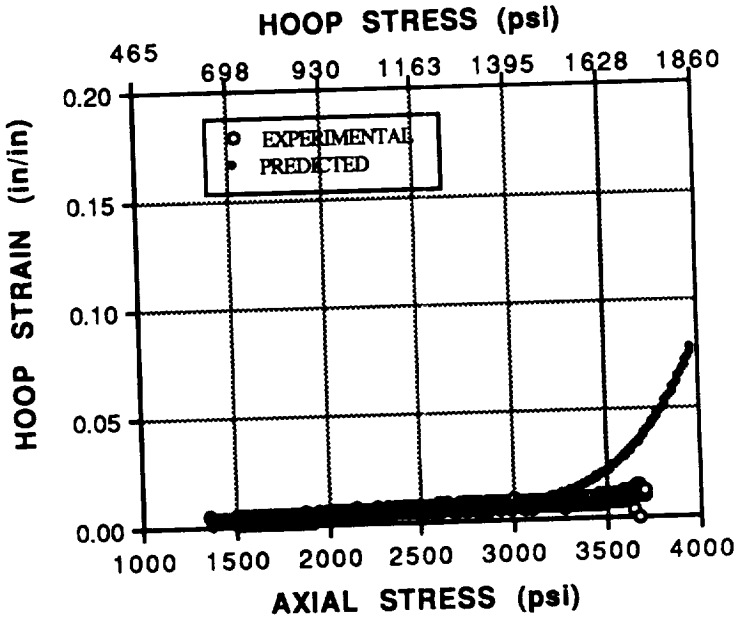

(b) Hoop Strains (Compressive)

Figure 5.15: Measured vs Predicted Plastic Strains for Load Path 6

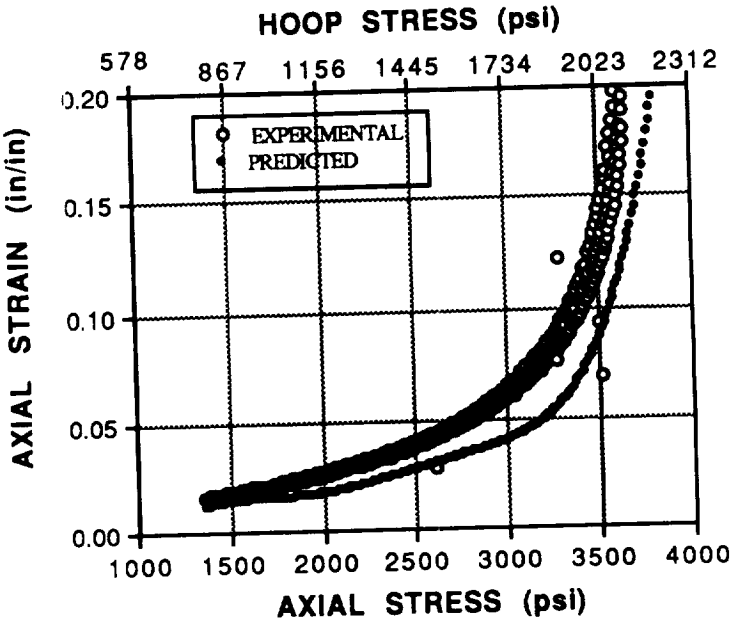

(a) Axial Strains (Tensile)

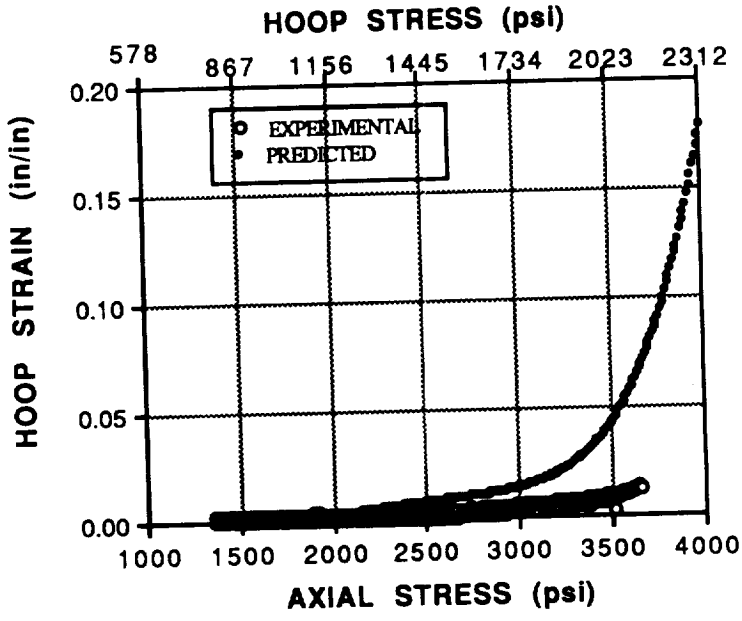

(b) Hoop Strains (Tensile)

Figure 5.16: Measured vs Predicted Plastic Strains for Load Path 7

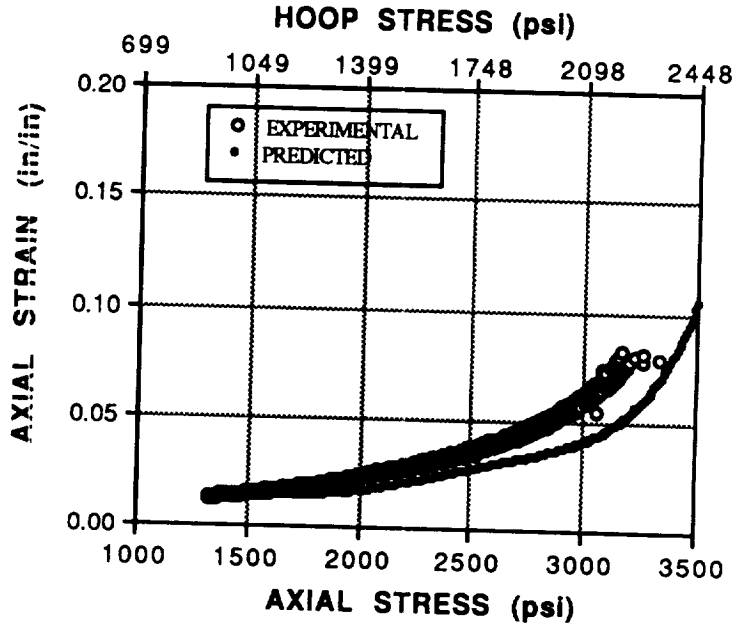

(a) Axial Strains (Tensile)

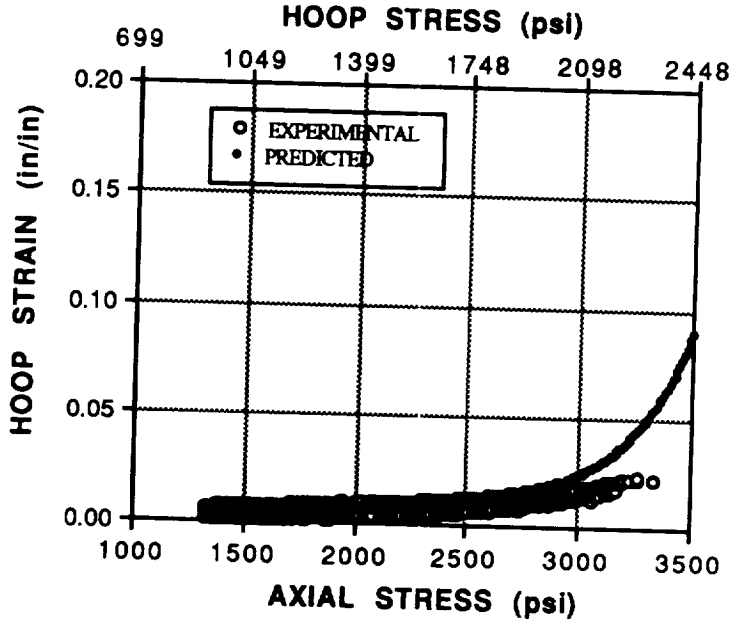

(b) Hoop Strains (Tensile)

Figure 5.17: Measured vs Predicted Plastic Strains for Load Path 8

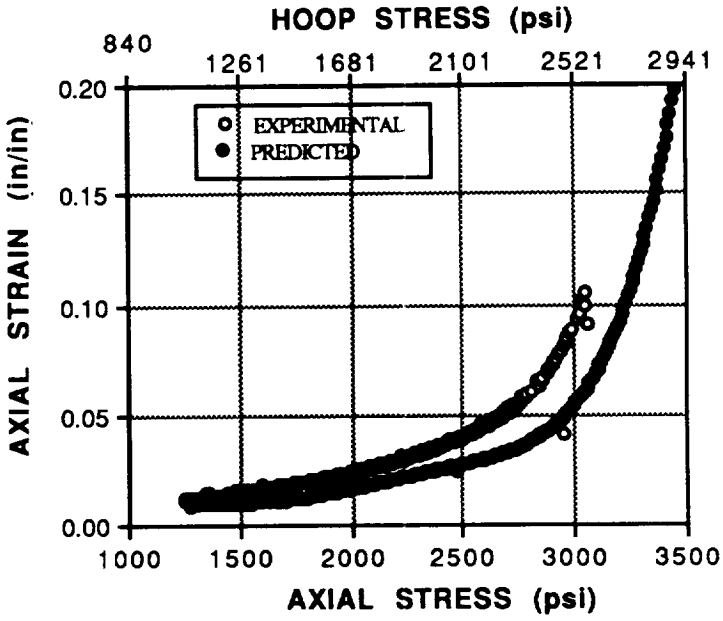

(a) Axial Strains (Tensile)

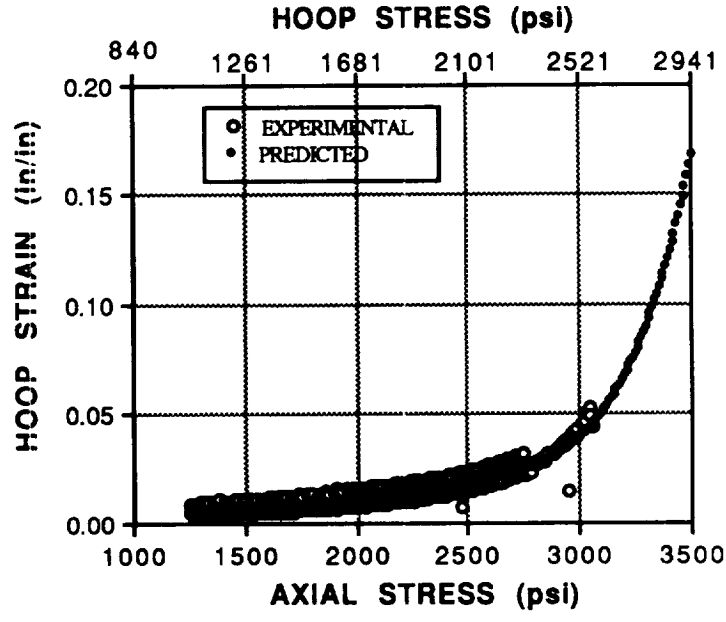

(b) Hoop Strains (Tensile)

Figure 5.18: Measured vs Predicted Plastic Strains for Load Path 9

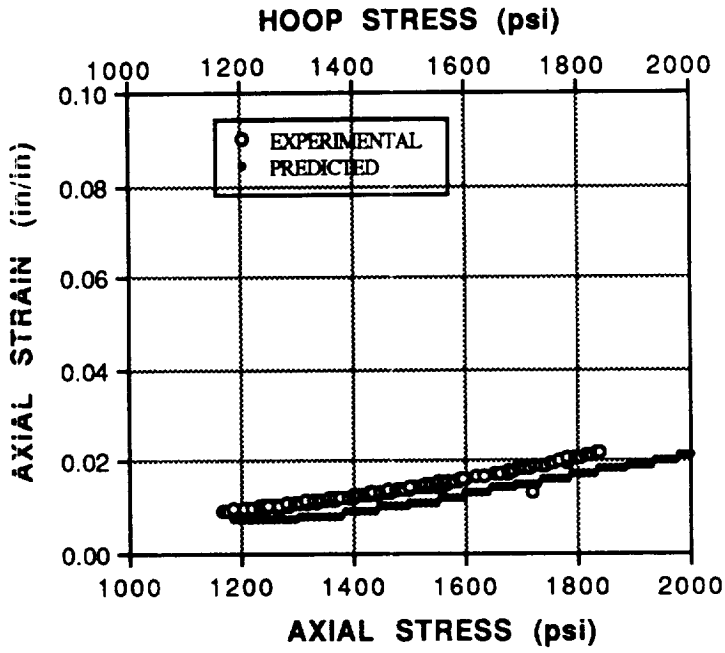

(a) Axial Strains (Tensile)

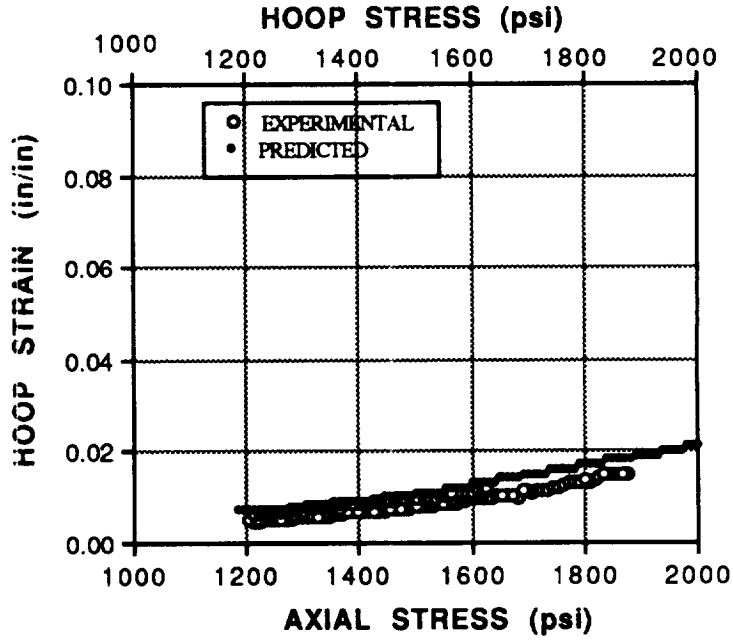

(b) Hoop Strains (Tensile)

Figure 5.19: Measured vs Predicted Plastic Strains for Load Path 10

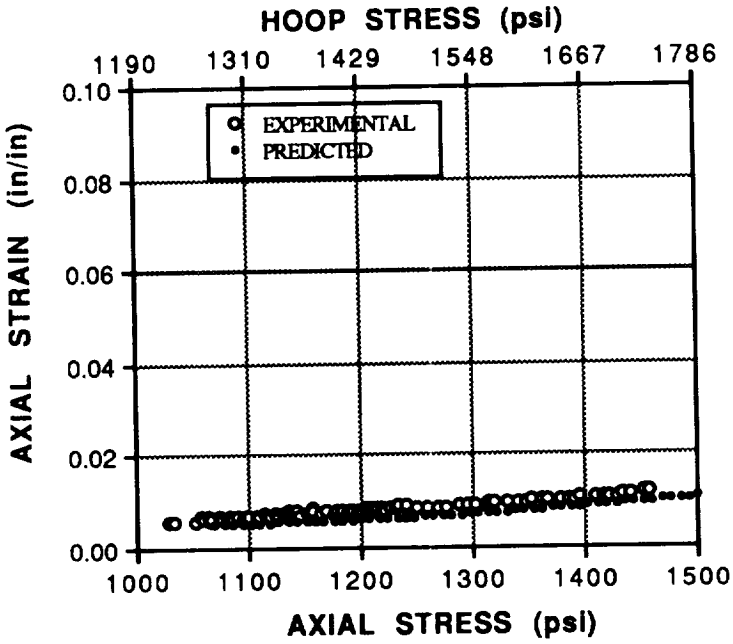

(a) Axial Strains (Tensile)

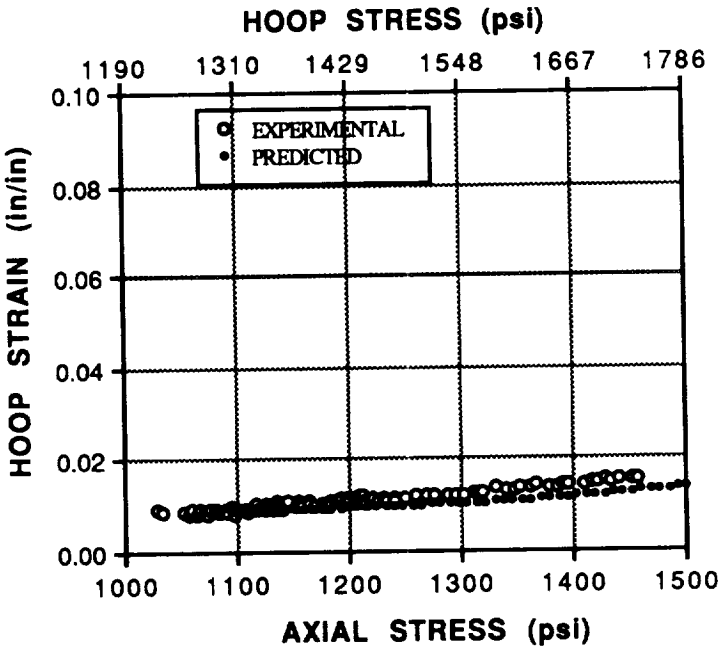

(b) Hoop Strains (Tensile)

Figure 5.20: Measured vs Predicted Plastic Strains for Load Path 11

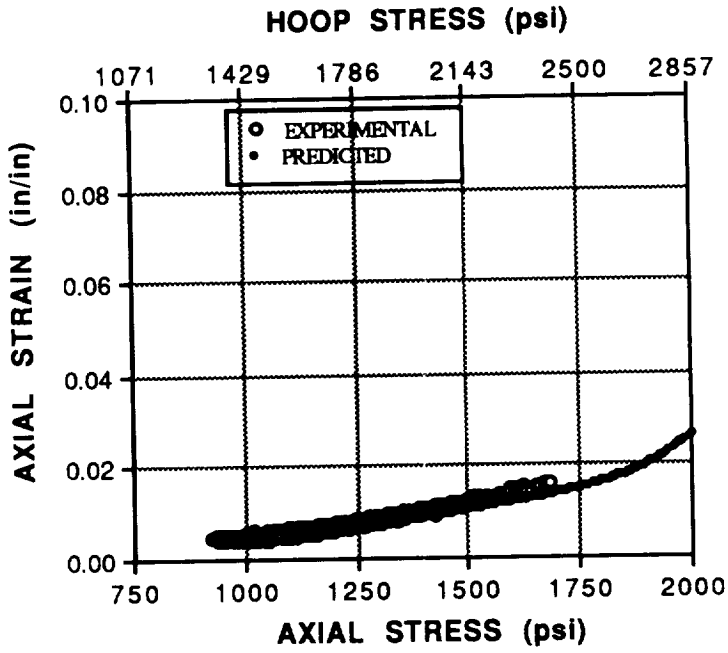

(a) Axial Strains (Tensile)

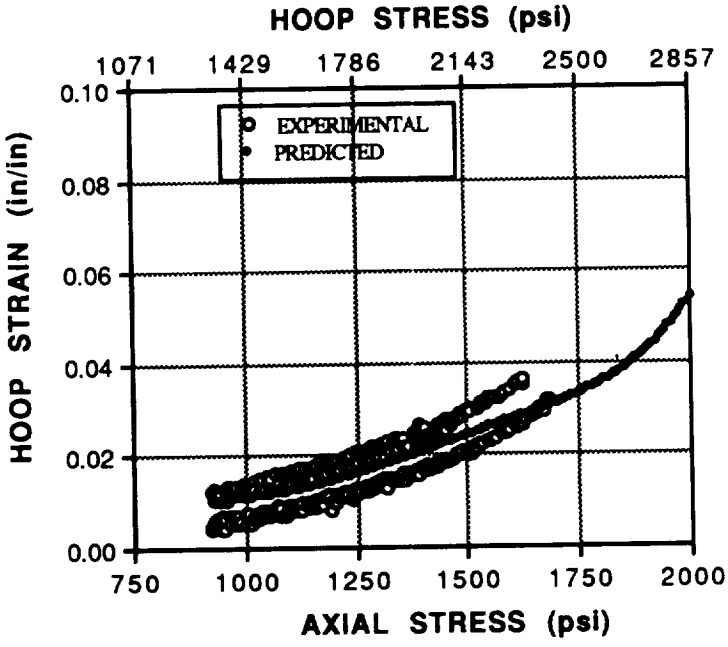

(b) Hoop Strains (Tensile)

Figure 5.21: Measured vs Predicted Plastic Strains for Load Path 12

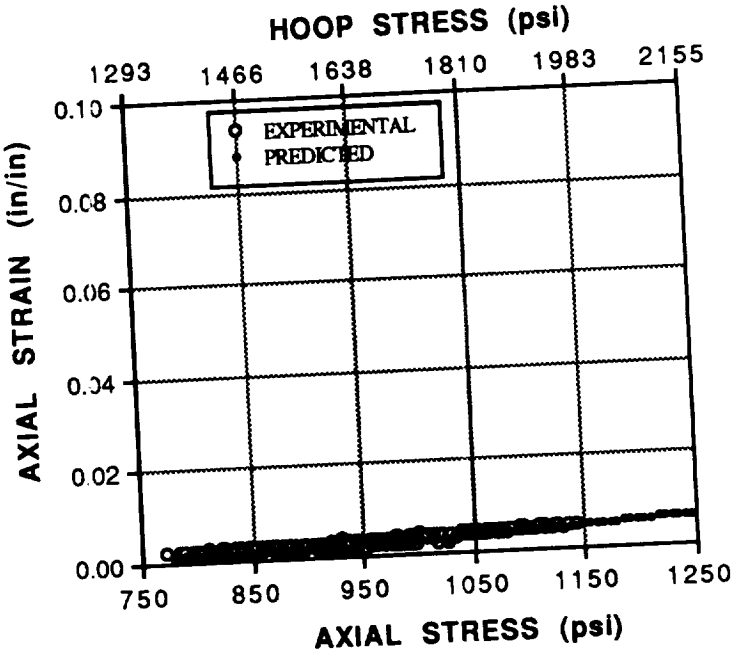

(a) Axial Strains (Tensile)

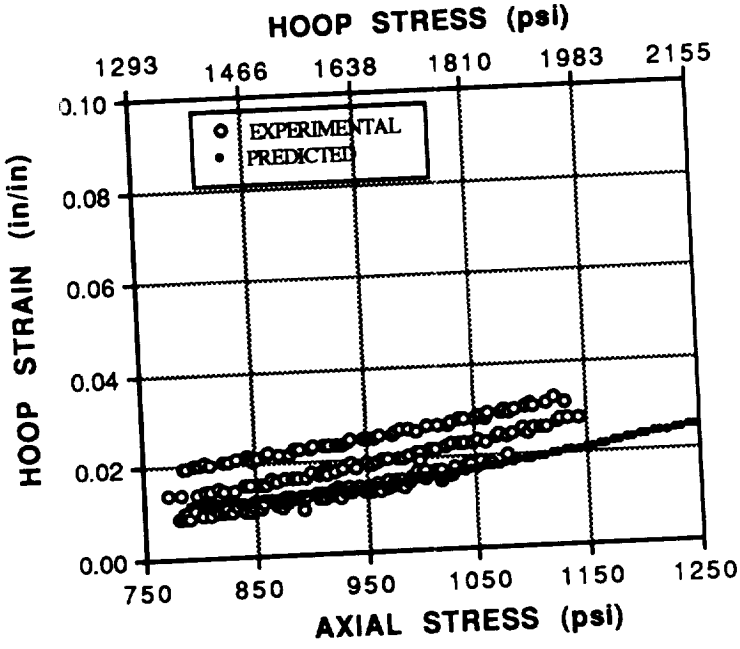

(b) Hoop Strains (Tensile)

Figure 5.22: Measured vs Predicted Plastic Strains for Load Path 13

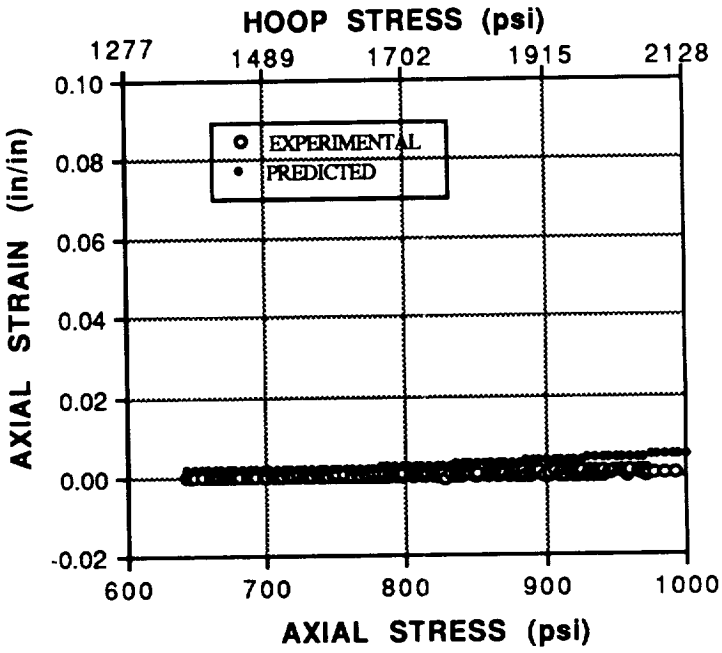

(a) Axial Strains (Tensile)

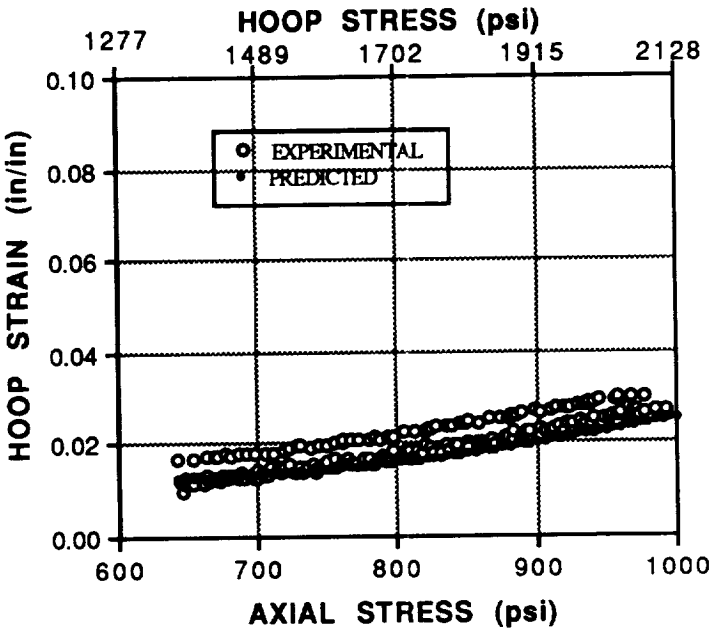

(b) Hoop Strains (Tensile)

Figure 5.23: Measured vs Predicted Plastic Strains for Load Path 14

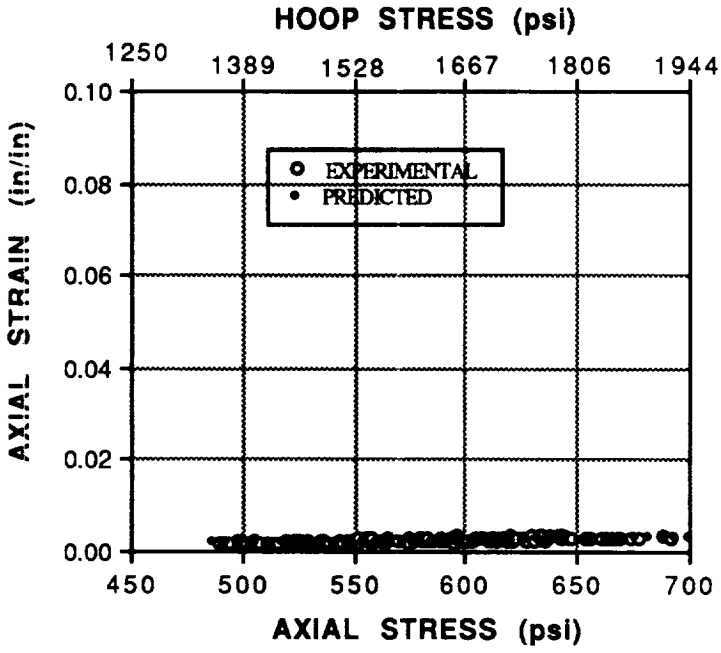

(a) Axial Strains (Compressive)

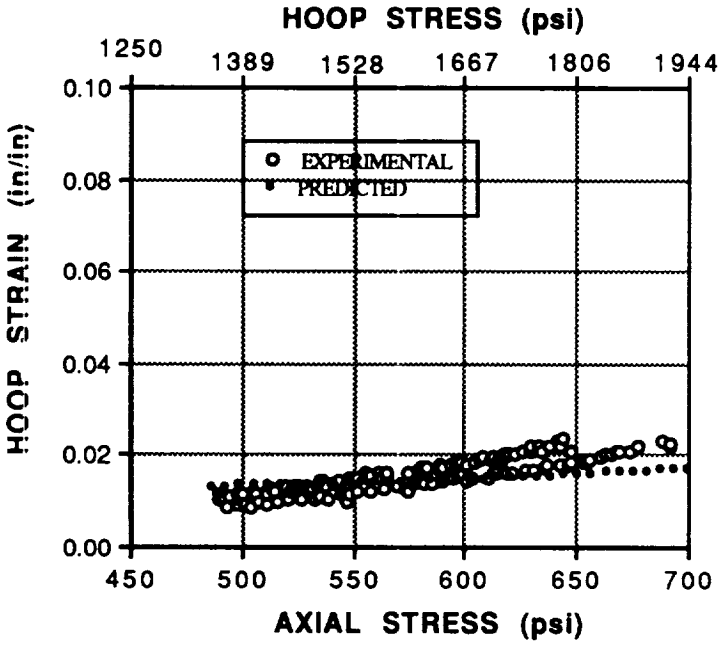

(b) Hoop Strains (Tensile)

Figure 5.24: Measured vs. Predicted Plastic Strains for Load Path 15

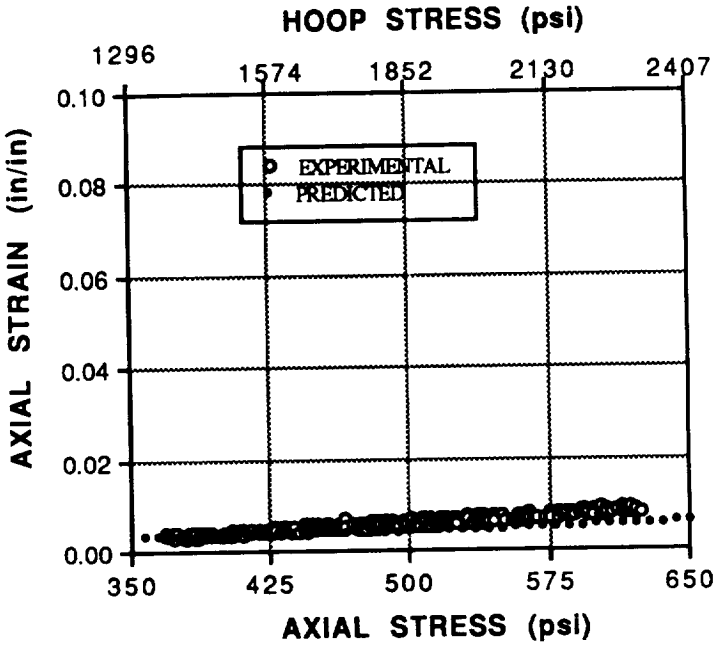

(a) Axial Strains (Compressive)

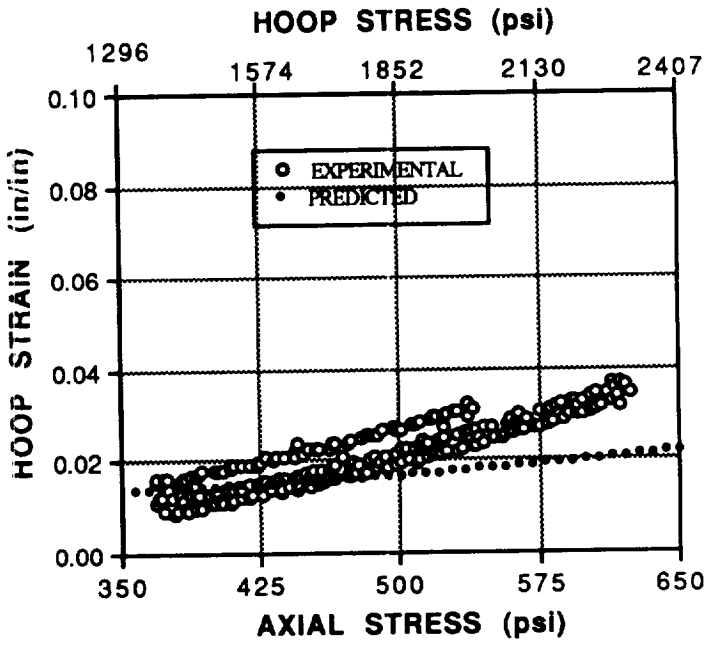

(b) Hoop Strains (Tensile)

Figure 5.25: Measured vs Predicted Plastic Strains for Load Path 16

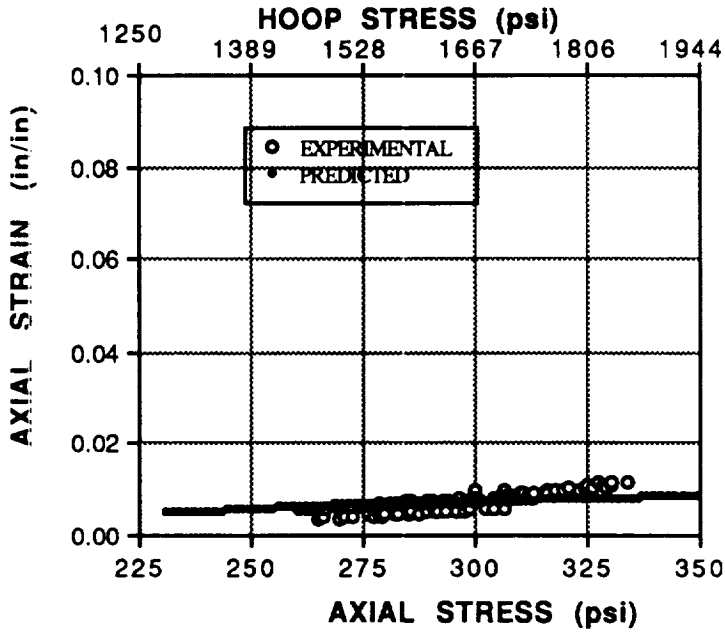

(a) Axial Strains (Compressive)

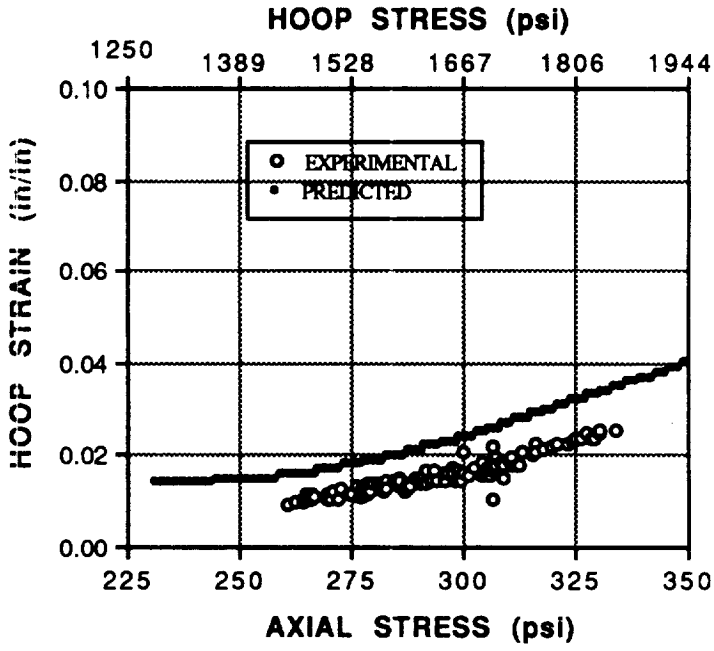

(b) Hoop Strains (Tensile)

Figure 5.26: Measured vs Predicted Plastic Strains for Load Path 17

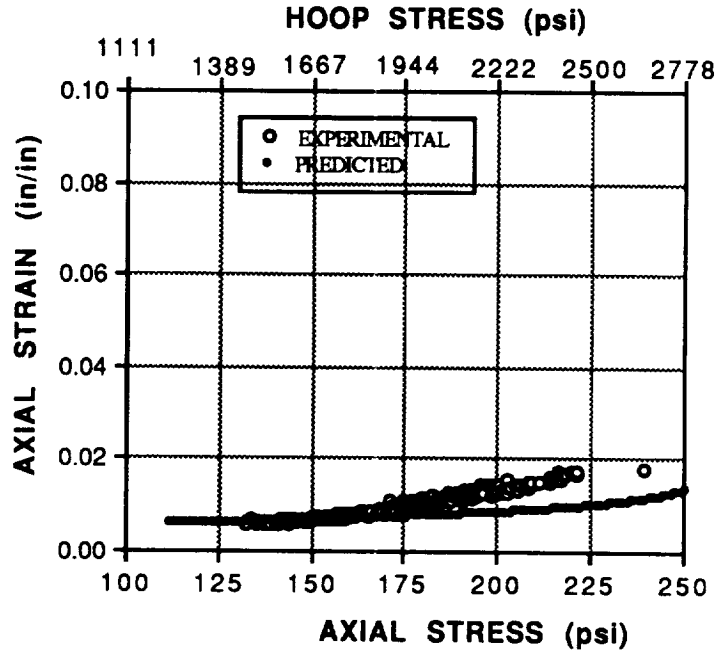

(a) Axial Strains (Compressive)

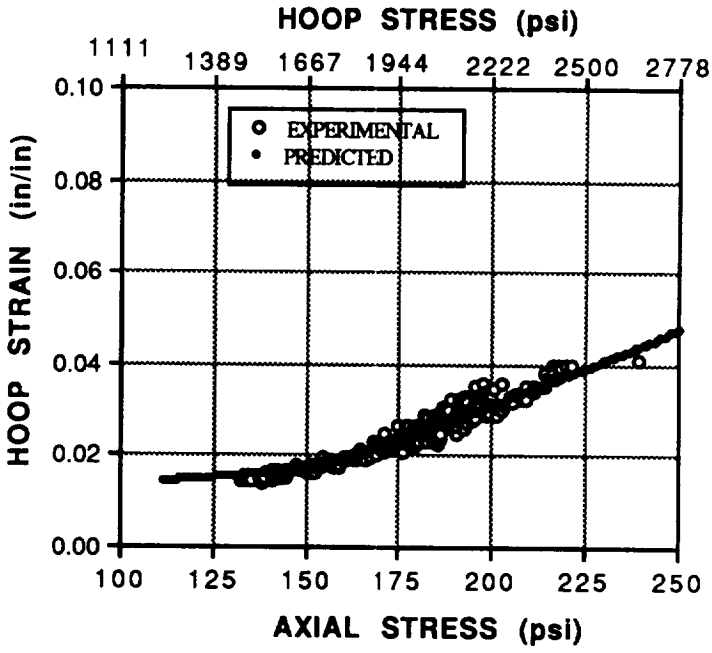

(b) Hoop Strains (Tensile)

Figure 5.27: Measured vs Predicted Plastic Strains for Load Path 18

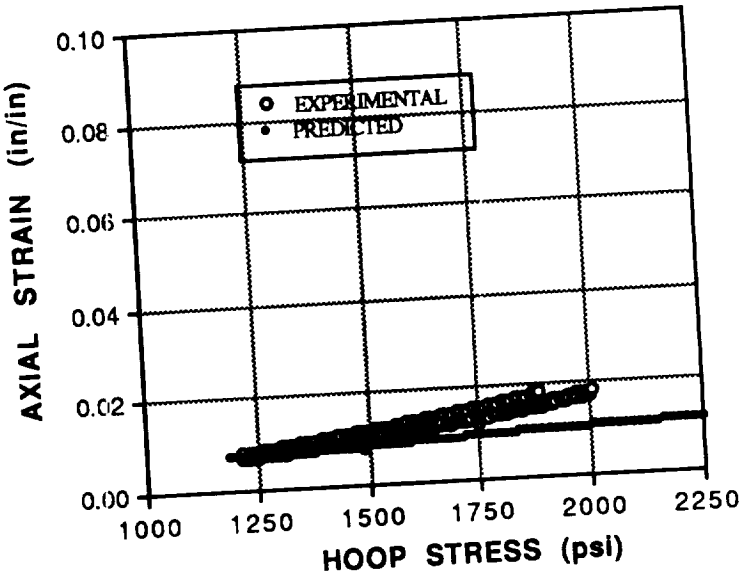

(a) Axial Strains (Compressive)

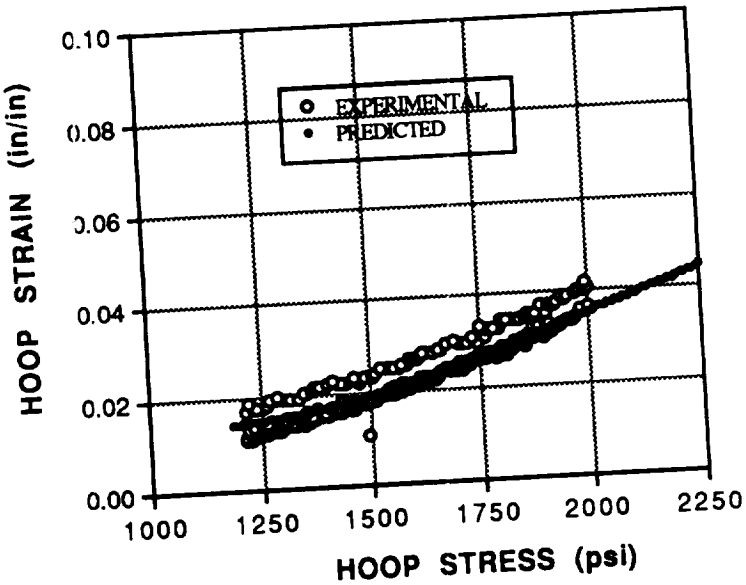

(b) Hoop Strains (Tensile)

Figure 5.28: Measured vs Predicted Plastic Strains for Load Path 19

compared with results measured during three repeated tests (exceptions are Figs 5.11 and 5.28, which show results for four repeated tests along load paths 1 and 19, respectively). Finally, note that all strains are plotted as positive values. The actual algebraic sign in each case is noted in the figure caption.

The comparison between measurement and prediction is considered suprisingly good, since these predictions are based on the Prandtl-Reuss equations, which are strictly valid only for initially isotropic materials. Nevertheless, in most cases the predicted response falls within the data scatter. The greatest errors are the hoop strain predictions for the first few load paths (i.e., part b in Figure 5.11 through 5.15, corresponding to load paths 1 - 6). In these cases the predicted hoop strains at high stress levels fall below the measured hoop strains. It is believed that these discrepancies are due to necking of the specimen. That is, for near-uniaxial loadings and at high stresses the specimen began to neck, resulting in an unstable increase in the measured hoop strain. The Prandtl-Reuss equations do not account for the necking phenomena, and hence the predicted hoop strains are lower than measured in these cases.

Discussion of Pre- and Post-Yield Behavior

On the basis of the results discussed above, it has been concluded that the pre-yield behavior of high-density polyethylene in extruded tubular form is anisotropic (i.e., transversely isotropic), and yet the post-yield behavior is effectively isotropic. Two hypotheses which may explain this behavior have been considered. In the first hypothesis the polymer is visualized as consisting of stiff crystalline regions, completely surrounded by relatively flexible amorphous material. Upon the application of elastic stress levels, motions/distortions occur at the molecular level in both the amorphous and crystalline regions of the polymer. Since the crystalline regions were oriented

during the extrusion process, the initial elastic response is anisotropic. Now, as the load is increased and plastic stress levels are induced, the molecular motions in the crystalline regions reach a maximum. All additional strains are associated with molecular motions which occur within the amorphous regions alone. Hence, the post-yield behavior is isotropic. If this hypothesis is valid, then no increase in the degree of crystallinity would occur as a result of the strain levels imposed, although the crystalline regions may become reoriented. Orientation of the crystalline regions due to high levels of stress (or strain) certainly occurs for polyethylene; the initial orientation of the as-received tubular specimens was induced during the extrusion process, for example. However, the strains levels induced during this study (which in all cases were < 20%) are relatively modest compared to those encountered in the extrusion process (in which strains on the order of several hundred percent are typically imposed).

In the second hypothesis the elastic response is again due to molecular motions within amorphous and crystalline regions of the polymer, and hence the elastic response is anisotropic . However, as plastic stress levels are reached additional stress- (or strain-) induced crystallization of the polyethylene molecular structure occurs, such that initially amorphous regions become crystallized. In this second hypothesis the crystalline regions are oriented along the prevailing maximum stress or strain direction, and hence the post-yield response is identical for all load paths. If this second hypothesis is valid, then the degree of crystallinity would increase as a result of plastic deformation. Stress-induced crystallization of polyethylene is well documeted [Rodriguez, 1989, pg 299]. However, the stress- and strain-levels associated with these documented cases are far higher than those imposed in this study. Thus, it is unclear whether this mechanism can account for the isotropic post-yield behavior observed during the present study.

CHAPTER 6: SUMMARY AND CONCLUSIONS

This study was devoted to an experimental and analytical evaluation of the yield and post-yield behavior of high-density polyethylene, a semi-crystalline thermoplastic. Polyethylene was selected for study because it is very inexpensive and readily available in the form of thin-walled tubes. Thin-walled tubular specimens were subjected to axial loads and internal pressures, such that the specimens were subjected to a known biaxial loading. A constant octahederal shear stress rate was imposed during all tests. The measured yield and post-yield behavior was compared with predictions based on both isotropic and anisotropic models. Of particular interest was whether inelastic behavior was sensitive to the hydrostatic stress level.

The major achievements and conclusions reached during the study are itemized below.

(1) A suitable testing facility was designed, fabricated, assembled, and fully calibarated during the course of the study. One of the unique features of the testing apparatus is a pressure control system which allows the internal pressure to be increased at a user-defined rate, such that the octahedral shear stress induced in the tube wall is increased at a user-defined rate. A data aquisition system utilizing Labview software package and Macintosh II computer was developed and used to collect data automatically. The system is fully operational, and will be used during the coming year to study the mechanical behavior of other engineering thermoplastic polymers.

(2) An annealing process for use with extruded high-density polyethylene tubes was developed. Experimental measurements show that the annealing process reduces the residual stresses induced during the extrusion process to minimal levels. However, the annealed polyethylene specimens were found to exhibit a pronounced anisotropy. A 30% difference in

Young's modulus for the axial and hoop directions existed in the annealed specimens, for example. Thus, the annealing process removed residual stresses, but did not remove or minimize anisotropic material behavior. The anisotropic elastic behavior of high-density polyethylene is clearly due to the semi-crystalline nature of molecular structure of this polymer.

(3) An effort was made to determine whether relatively simple isotropic yield criterion could be used to predict yielding to within engineering accuracies. Predictions obtained using the Von Mises and Pressure-Modified Von Mises criteria were compared with the measured data. Neither of these models adequately predicted the experimental results. It is likely that this conclusion will hold for other semi-crystalline thermoplastics of current structural interest (e.g., polyetheretherketone or polyamide), which can also exhibit a pronounced anisotropy.

(4) The tubular specimens were subsequently treated as transversely isotropic materials, with the principal material coordinate system defined by the axial and hoop directions. Predictions obtained using two anisotropic yield criteria (the Tsai-Hill and Pressure-modified Tsai-Hill criteria) were then compared with the measured data. Yielding was best predicted by the Pressure-Modified Tsai-Hill criterion, which indicates that the yield behavior of high-density polyethylene is both anisotropic and sensitive to the hydrostatic stress state. It was deduced that the compressive-to-tensile yield strength ratio of high density polyethylene is 1.11, which compares very well with previously reported measurements.

(5) An attempt to model the post-yield behavior using the power law were made. Both an isotropic form as well as an anisotrpic form was used. Neither power law formulation adequately modeled the post-yield behavior; in both cases the strength coefficient M and the strain hardening exponent n varied substantially, depending on load path.

(6) The post-yield behavior was best predicted using the isotropic form of the Prandtl-Reuss equations. This was an unexpected and suprising result, since the initiation of yielding was sensitive to both the anisotropic nature of the polyethylene tubes and the hydrostatic stress level. Neither of these factors are included in the Prandtl-Reuss formulation. The post-yield behavior of polyethylene is essentially isotropic, even though the initial elastic response is anisotropic.

Two possible explanations of the isotropic post-yield response have been proposed. In the first hypothesis it is suggested that molecular motions associated with plastic strains occur primarily within the amorphous regions of the polymer, and hence the post-yield behavior is effectively isotropic. If this hypothesis is valid, then no increase in the degree of crystallinity would occur as a result of plastic deformation.

In the second hypothesis it is suggested that stress-induced crystallization of the amorphous regions of the molecular structure occurs, and further that during the loading process the crystalline regions become oriented in the prevailing direction of maximum stress or strain. Therefore the post-yield response would be identical for all load paths considered during this study. If this second hypothesis is valid, then the degree of crystallinity would increase as a result of plastic deformation. Monitoring the degree of crystallinity before and after testing, as well as the orientation of the crystalline regions, may provide a means of determining whether either of these hypotheses is valid.

LIST OF REFERENCES

Ainbinder, S.B., Laka, M.G., Maiors, I.Y., 1965, "Effect of Hydrostatic Pressure on Mechanical Properties of Polymers," *Polymer Mechanics*, Volume 1(1), pp. 50-67.

Bauwens, J.C., 1970, "Yield Condition and Propogation of Luders' Lines in Tension-Torsion," *Journal of Polymer Science*, Volume A2(8), pp. 893-901.

Betten, J., Frosch, H.G., and Borrmann, M., 1982, "Pressure-dependent Yield Behavior of Metals and Polymers, " *Materials Science and Engineering*, Volume 56, pp. 233-246.

Bowden, P.B., and Jukes, J.A., 1968, "The Plastic Yield Behavior of Polymethylmethacrylate," *Journal of Materials Science*, Volume 3, pp. 183-190.

Bowden, P.B., and Jukes, J.A., 1972, "The Plastic Flow of Isotropic Polymers," *Journal of Materials Science*, Volume 7, pp. 52-63.

Caddell, R.M., Raghava, R.S., and Atkins, A.G., 1973, "A Yield Criterion for Anisotropic and Pressure Dependent Solids such as Oriented Polymers," *Journal of Materials Science*, Volume 8, pp. 1641-1646.

Caddell, R.M., Raghava, R.S., and Atkins, A.G., 1974, "Pressure Dependent Yield Criteria for Polymers," *Materials Science and Engineering*, Volume 13, pp. 113-120.

Caddell, R.M., and Woodliff, A.R., 1977, "Macroscopic Yielding of Oriented Polymers," *Journal of Materials Science*, Volume 12, pp. 2028-2036.

Carapellucci, L.M., and Yee, A.F., 1986, "The Biaxial Deformation and Yield Behavior of Bisphenol-A Polycarbonate: Effect of Anisotropy," *Polymer Engineering and Science*, Volume 26(13), pp. 920-930.

Chakrabarty, J., 1987, Theory of Plasticity, McGraw-Hill Inc, p. 60.

Christiansen, A.W., Baer, E., and Radcliffe, S.V., 1971, "The Mechanical Behavior of Polymers under High Pressure," *Philosophical Magazine*, Volume 24, pp. 451-467.

Dieter, G.E., 1986, Mechanical Metallurgy, 3rd Ed, McGraw-Hill, pp 87-89.

Ely, R.E., 1967, "Biaxial Stress Testing of Acrylic Tube Specimens," *Polymer Engineering and Science*, Volume 7(1), pp. 40-44.

Ely, R.E., 1968, "Biaxial-stress Results for Nylon," *Experimental Mechanics*, Volume 8(6), pp. 267-271.

Freire, J.L.F., and Riley, W.F., 1980, "Yield Behavior of Photoplastic Materials," *Experimental Mechanics*, Volume 20, pp. 118-125.

Hill, R., 1950, The Mathematical Theory of Plasticity, Oxford University Press, p. 20.

Hundy, B.B., and Green, A.P., 1954, "A Determination of Plastic Stress-Strain Relations", *Journal on Mechanics & Physics of Solids*, p 16.

Jones, R.M., 1975, Mechanics of Composite Materials, McGraw-Hill Book Co., pp. 37-47.

Manufacturing Chemists Association, Inc, 1957, Technical Data on Plastics, Manufacturing Chemists Association Publ, p. 536.

Mears, D.R., Pae, K.D.,, and Sauer, J.A., 1969, "Effects of Hydrostatic Pressure on the Mechanical Behavior of Polyethylene and Polypropylene, " *Journal of Applied Physics*, Volume 40(11), pp. 4229-4237.

Morrison, J.L.M., and Shepard, 1950, "An Experimental Investigation of Plastic Stress-Strain Relations," *Proc. Instn. Mech. Engrs.*, p 163.

Nielsen, L.E., 1974, Mechanical Properties of Polymers and Composites-Volume 2, Marcel Dekker Inc, p. 265.

Pae, K.D., and Mears, D.R., 1968, "The Effects of High Pressure on Mechanical Behavior and Properties of Polytetrafluoroethylene, and Polyethylene," *Journal of Polymer Science*, Volume B6, pp. 269-273.

Pae, K.D., 1977, "The Macroscopic Yielding Behavior of Polymers in Multiaxial Stress Fields," *Journal of Materials Science*, Volume 12, pp. 1209-1214.

Raghava, R.S., and Caddell, R.M., 1973, "A Macroscopic Yield Criterion for Crystalline Polymers," *International Journal of Mechanical Sciences*, Volume 15, pp. 967-974.

Raghava, R.S., Caddell, R.M., and Yeh, G.S.Y., 1973, "The Macroscopic Yield Behavior of Polymers," *Journal of Materials Science*, Volume 8, pp. 225-232.

Raghava, R.S., and Caddell, R.M., 1974, "Yield Locus Studies of Oriented Polycarbonate: An Anisotropic and Pressure-dependent Solid," *International Journal of Mechanical Sciences*, Volume 16, pp 789-799.

Rider, J.G., and Hargreaves, E., 1969, "Yielding of Oriented Poly(vinylchloride)," *Journal of Polymer Science*, Volume A2(7), pp. 829-844.

Rodriguez, F., 1982, Principles of Polymer Systems, 3rd edition, Hemisphere Publishing Co.

Sardar, D., Radcliffe, S.V., Baer, E., 1968, "Effects of High Hydrostatic Pressure on the Mechanical Behavior of a Crystalline Polymer - Polyoxymethylene," *Polymer Engineering and Science*, Volume 8(4), pp. 290-301.

Semeliss, M.A., 1990, The Yield Behavior of High-Density Polyethylene, M.S. Thesis, Department of Mechanical Engineering, University of Washington.

Shinozaki, D., and Groves, G.W., 1973, "The Plastic Deformation of Oriented Polypropylene: Tensile and Compressive Yield Criteria," *Journal of Materials Science*, Volume 8, pp. 71-78.

Slater, R.A.C., 1977, Engineering Plasticity - Theory and Application to Metal Forming Processes, John Wiley & Sons, pp 90-117.

Sokolnikoff, I.S., and Sokolnikoff, E.S., 1941, Higher Mathematics for Engineers and Physicists, McGraw-Hill Book Co., p 136.

Spitzig, W.A., Sober, R.J., and Richmond, O., 1976, "The Effect of Hydrostatic Pressure on the Deformation Behavior of Maraging and HY-80 Steels and Its Implications for Plasticity Theory," *Metallurgical Transactions*, Volume 7A, pp. 1703-1710.

Spitzig, W.A., and Richmond, O., 1979, "Effect of Hydrostatic Pressure on the Deformation Behavior of Polyethylene and Polycarbonate in Tension and Compression," *Polymer Engineering and Science*, Volume 19(16), pp. 1129-1138.

Stassi-D'Alia, F, 1967, "Flow and Fracture of Materials according to a New Limiting Condition of Yielding," *Meccannica*, Volume 2(3), pp. 178-195.

Stassi-D'Alia, F, 1969, "Limiting Conditions of Yielding for Anisotropic Materials," *Meccannica*, Volume 4, pp. 349-364.

Taylor, G.I., and Quinney, H., "The Plastic Distortion of Metals, *Phil Trans Roy Society*, p 323.

Ward, I.M., 1975, Structures and Properties of Oriented Polymers, John Wiley & Sons, p. 298.

Whitfield, J.K., and Smith, C.W., 1972, "Characterization Studies of Potential Photoelastoplastic Material," *Experimental Mechanics*, Volume 12(2), pp. 67-74.

Williams, J.G., 1980, Stress Analysis of Polymers, 2nd Ed., John Wiley and Sons, p 77.

Wong, R., 1990, The Post-Yield Behavior of High-Density Polyethylene, M. S. Thesis, Department of Mechanical Engineering, University of Washington, Seattle.

APPENDIX A - EXPERIMENTAL STRESSES AND STRAINS

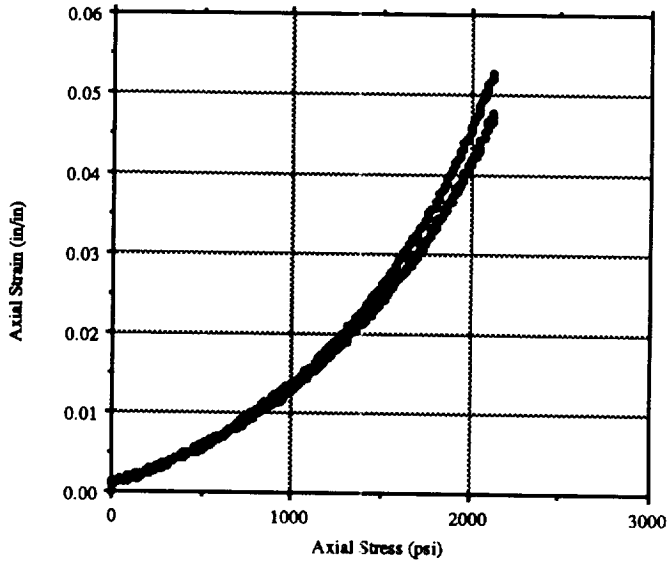

(a) Axial Strain versus Axial Stress (Hoop Stress = 0)

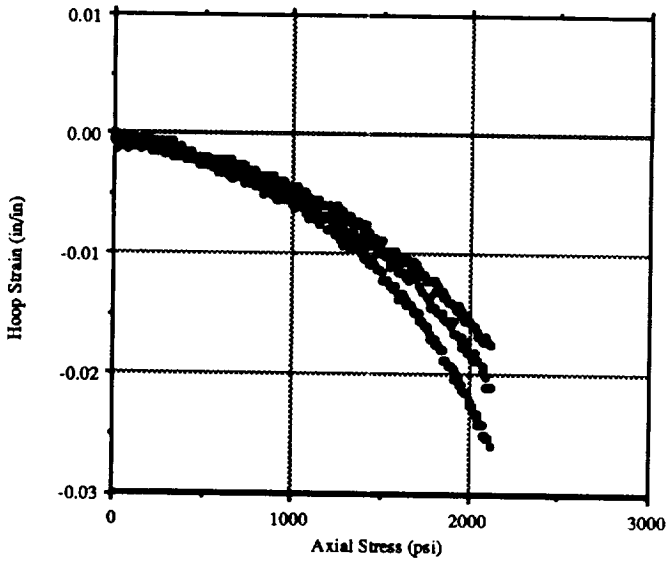

(b) Hoop Strain versus Axial Stress (Hoop Stress = 0)

Figure A.1 - Axial Strain and Hoop Strain versus Axial Stress or Hoop Stress for Load Path 1: Axial Load Rate = 900 lb/min, No Pressure, Octahedral Shear Stress Rate = 258 psi/min, and Hydrostatic Stress Rate = 186 psi/min.

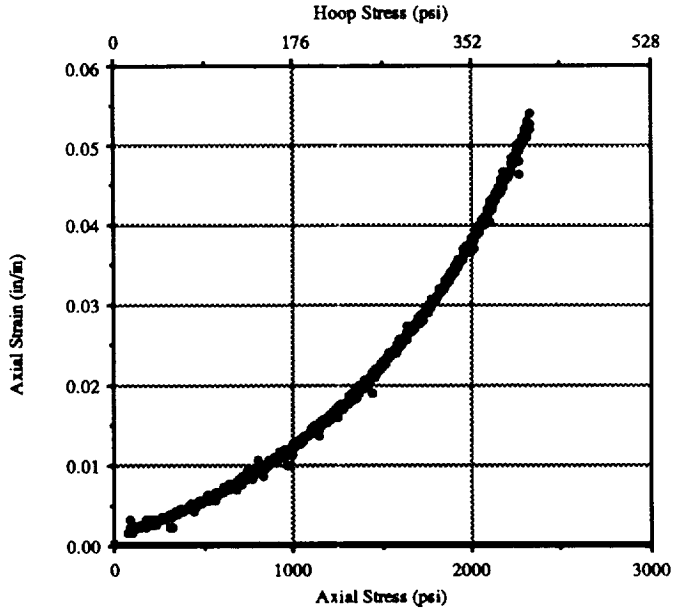

(a) Axial Strain versus Axial Stress or Hoop Stress

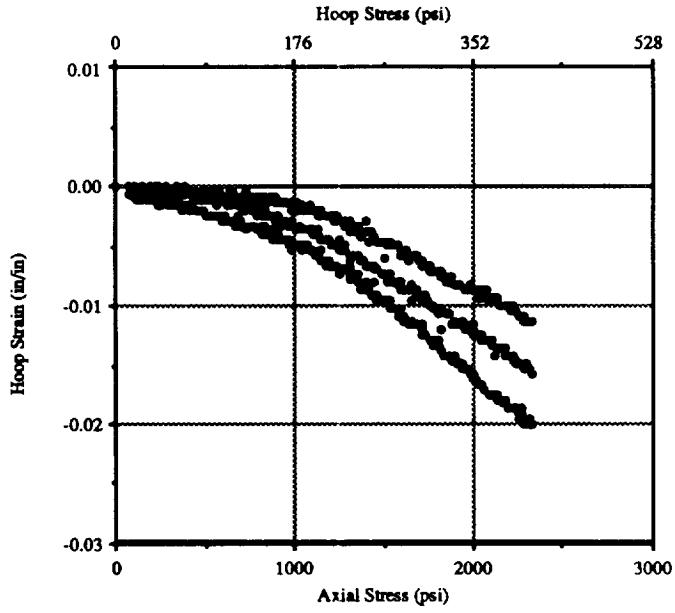

(b) Hoop Strain versus Axial Stress or Hoop Stress

Figure A.2 - Axial Strain and Hoop Strain versus Axial Stress or Hoop Stress for Load Path 3: Axial Load Rate = 885 lb/min, Pressure Rate = 10 psi/min, Octahedral Shear Stress Rate = 258 psi/min, and Hydrostatic Stress Rate = 236 psi/min.

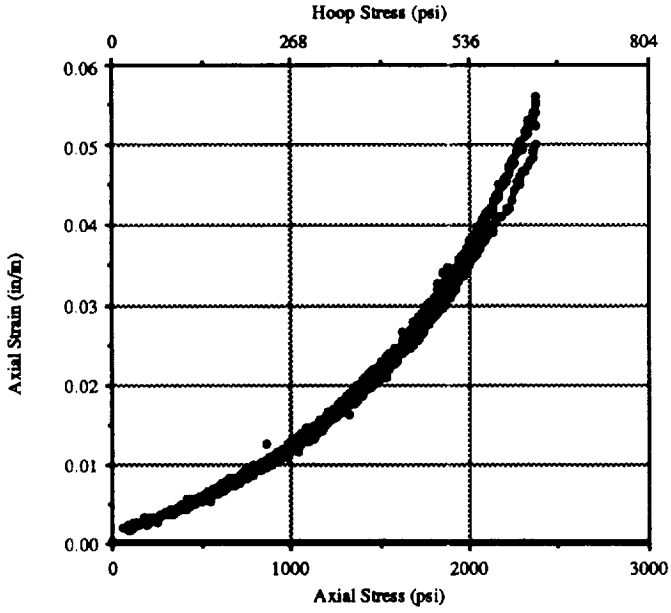

(a) Axial Strain versus Axial Stress or Hoop Stress

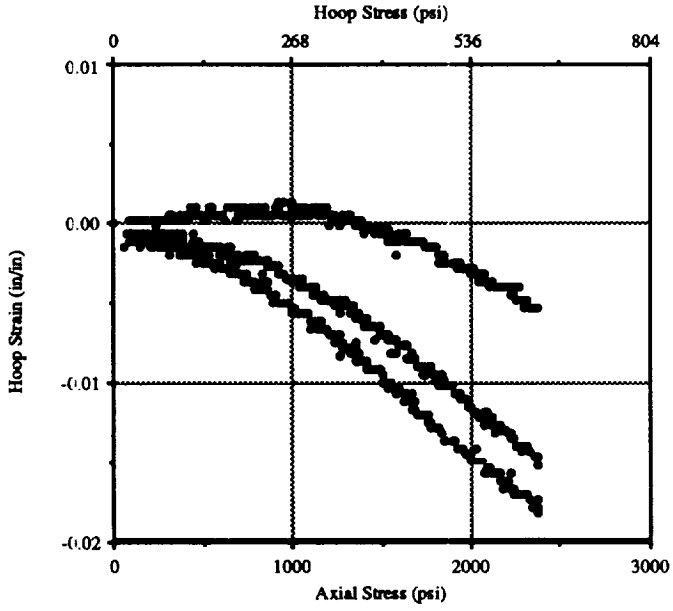

(b) Hoop Strain versus Axial Stress or Hoop Stress

Figure A.3 - Axial Strain and Hoop Strain versus Axial Stress or Hoop Stress for Load Path 4: Axial Load Rate = 867 lb/min, Pressure Rate = 15 psi/min, Octahedral Shear Stress Rate = 258 psi/min, and Hydrostatic Stress Rate = 260 psi/min.

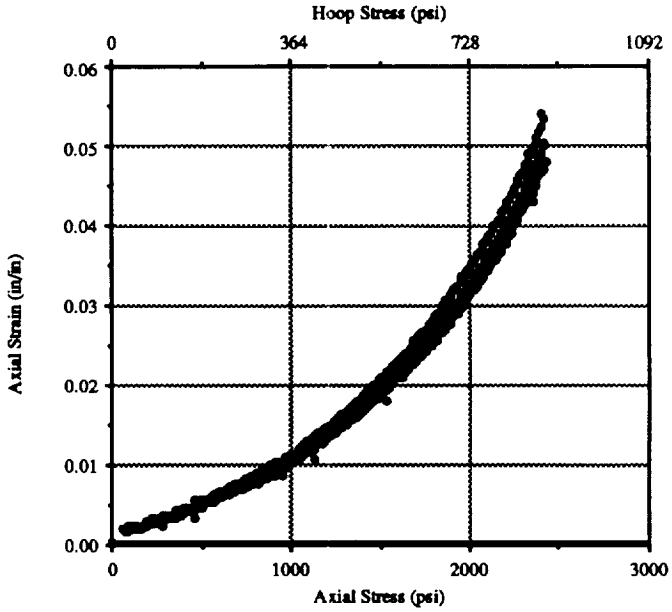

(a) Axial Strain versus Axial Stress or Hoop Stress

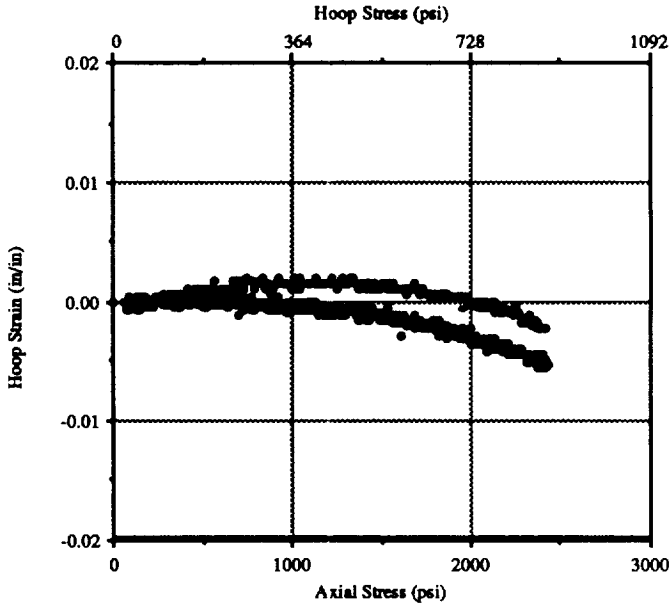

(b) Hoop Strain versus Axial Stress or Hoop Stress

Figure A.4 - Axial Strain and Hoop Strain versus Axial Stress or Hoop Stress for Load Path 5: Axial Load Rate = 838 lb/min, Pressure Rate = 21 psi/min, Octahedral Shear Stress Rate = 258 psi/min, and Hydrostatic Stress Rate = 284 psi/min.

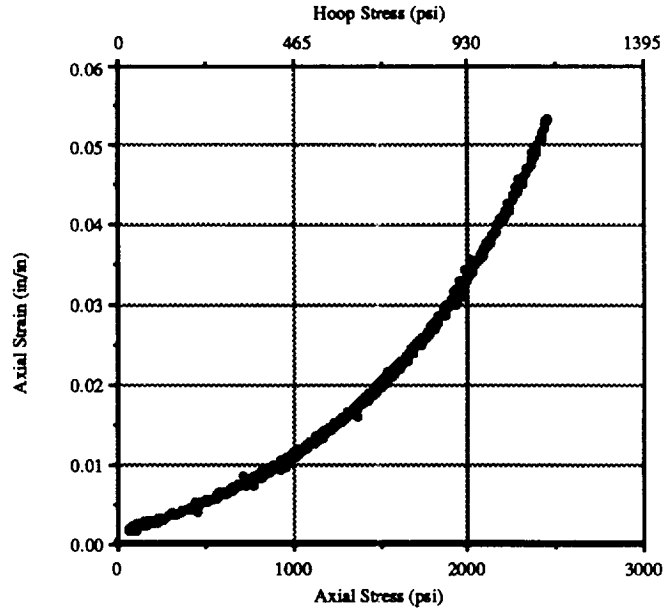

(a) Axial Strain versus Axial Stress or Hoop Stress

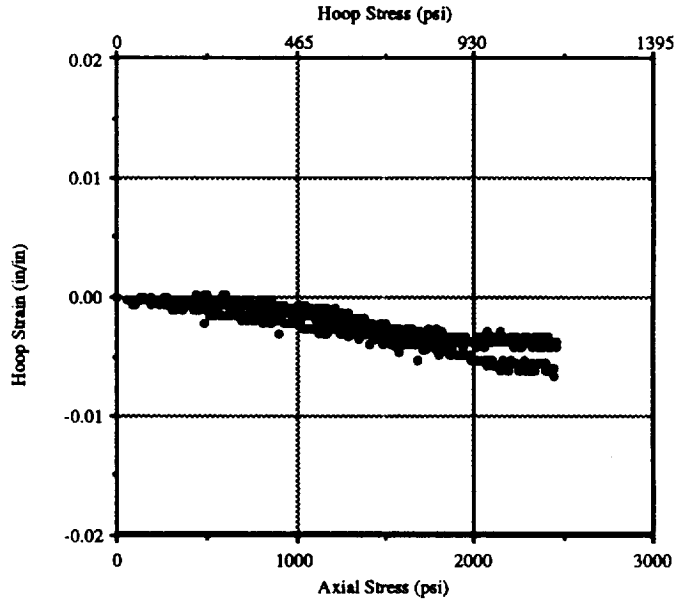

(b) Hoop Strain versus Axial Stress or Hoop Stress

Figure A.5 - Axial Strain and Hoop Strain versus Axial Stress or Hoop Stress for Load Path 6: Axial Load Rate = 795 lb/min, Pressure Rate = 27 psi/min, Octahedral Shear Stress Rate = 258 psi/min, and Hydrostatic Stress Rate = 310 psi/min.

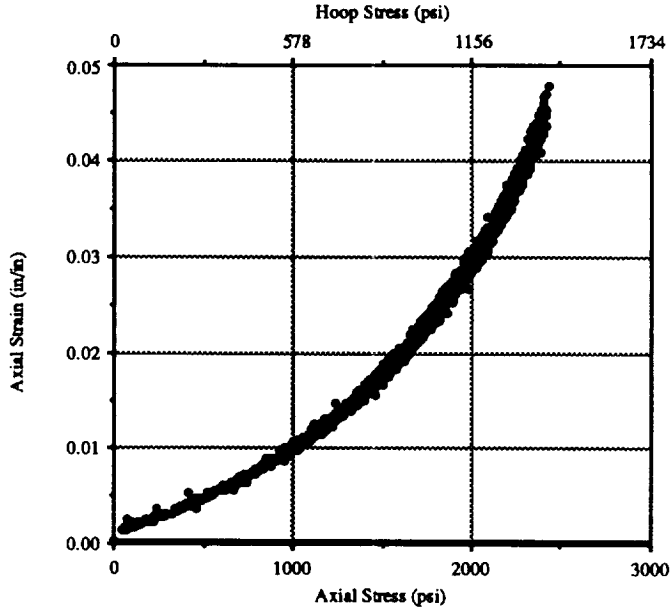

(a) Axial Strain versus Axial Stress or Hoop Stress

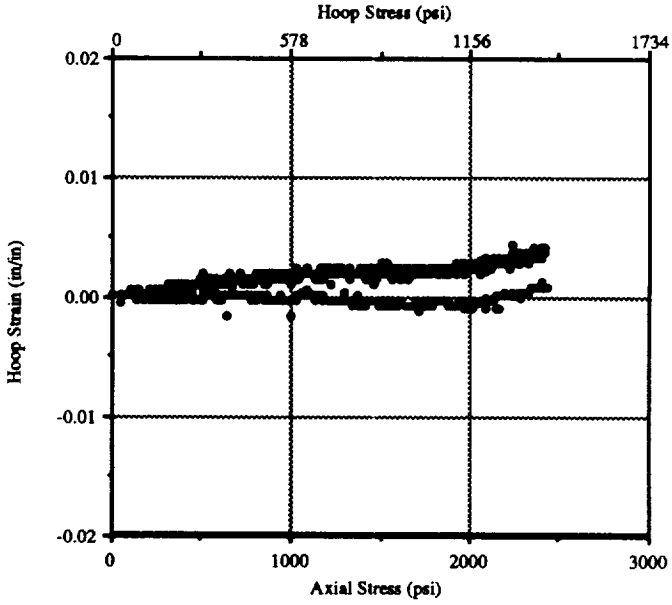

(b) Hoop Strain versus Axial Stress or Hoop Stress

Figure A.6 - Axial Strain and Hoop Strain versus Axial Stress or Hoop Stress for Load Path 7: Axial Load Rate = 734 lb/min, Pressure Rate = 34 psi/min, Octahedral Shear Stress Rate = 258 psi/min, and Hydrostatic Stress Rate = 331 psi/min.

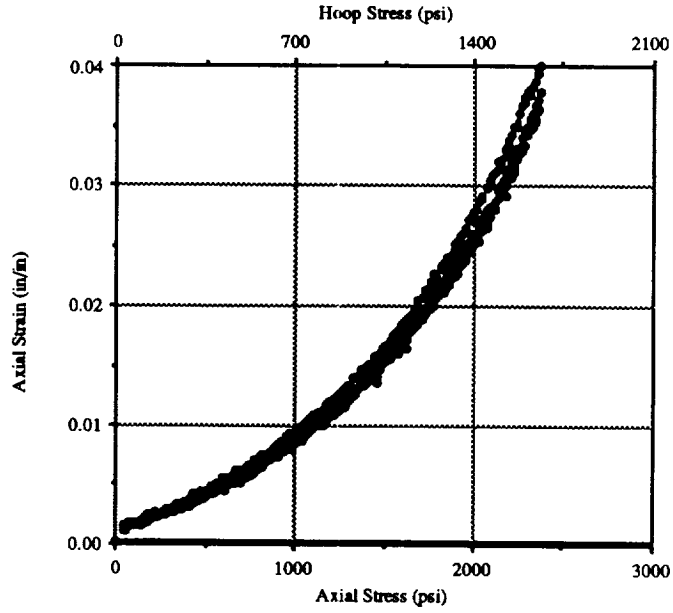

(a) Axial Strain versus Axial Stress or Hoop Stress

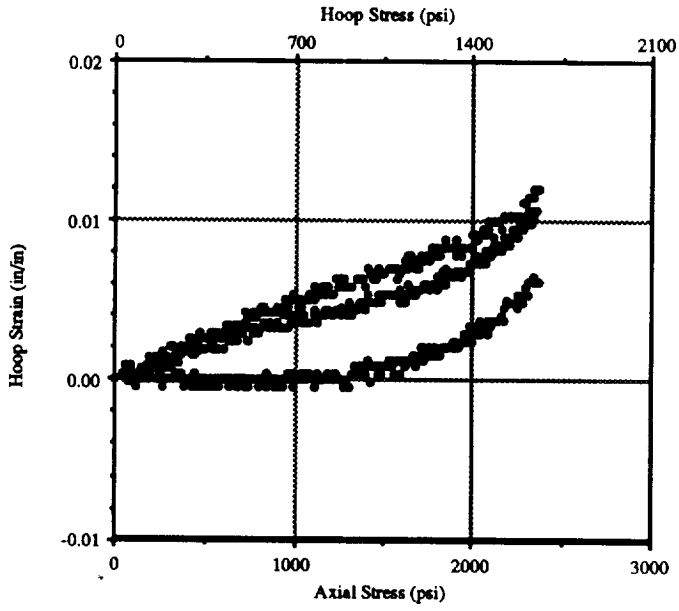

(b) Hoop Strain versus Axial Stress or Hoop Stress

Figure A.7 - Axial Strain and Hoop Strain versus Axial Stress or Hoop Stress for Load Path 8: Axial Load Rate = 657 lb/min, Pressure Rate = 40 psi/min, Octahedral Shear Stress Rate = 258 psi/min, and Hydrostatic Stress Rate = 348 psi/min.

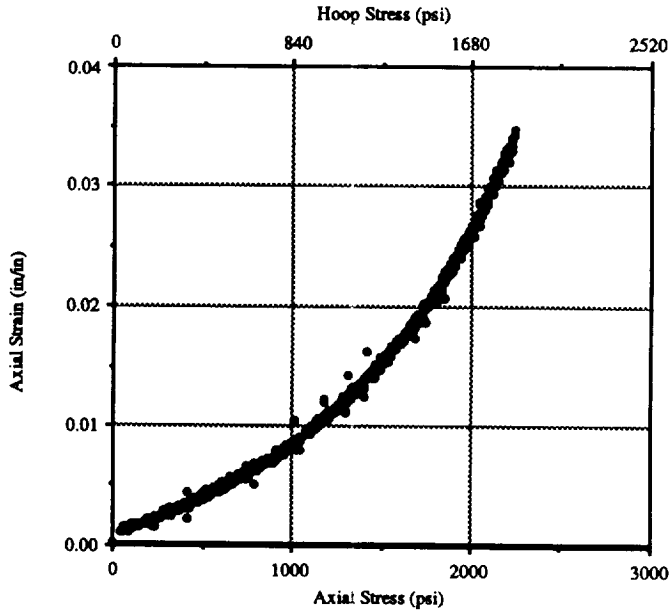

(a) Axial Strain versus Axial Stress or Hoop Stress

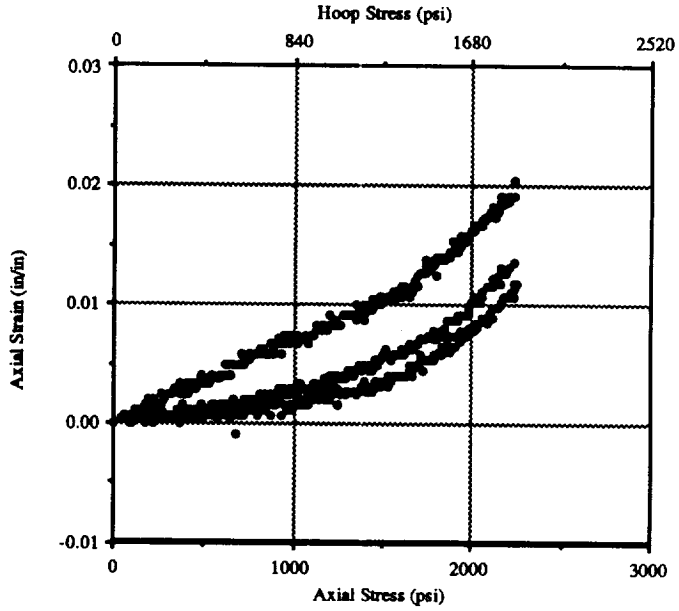

(b) Hoop Strain versus Axial Stress or Hoop Stress

Figure A.8 - Axial Strain and Hoop Strain versus Axial Stress or Hoop Stress for Load Path 9: Axial Load Rate = 560 lb/min, Pressure Rate = 46 psi/min, Octahedral Shear Stress Rate = 258 psi/min, and Hydrostatic Stress Rate = 357 psi/min.

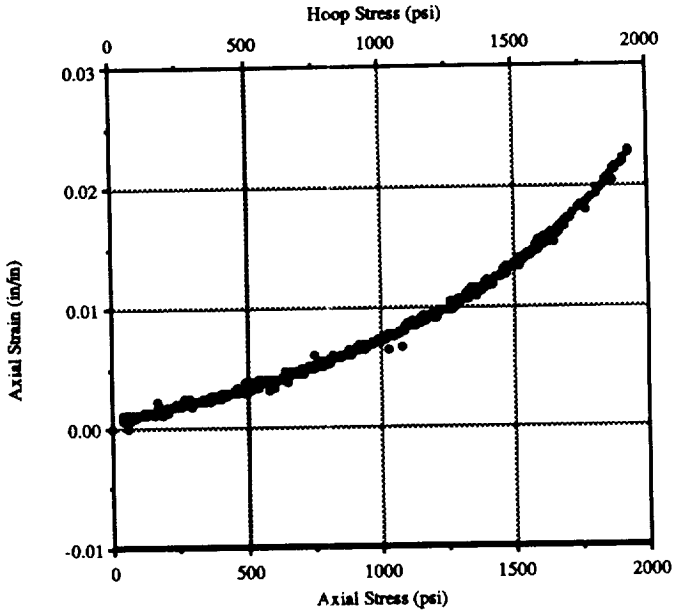

(a) Axial Strain versus Axial Stress or Hoop Stress

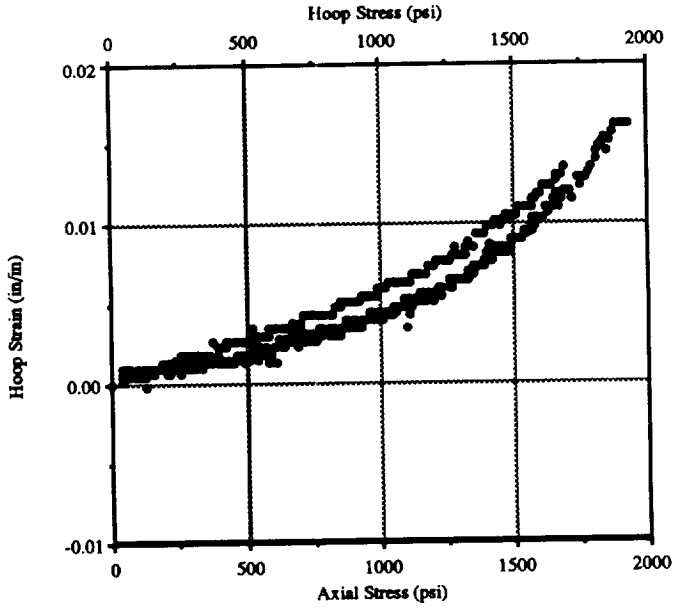

(b) Hoop Strain versus Axial Stress or Hoop Stress

Figure A.9 - Axial Strain and Hoop Strain versus Axial Stress or Hoop Stress for Load Path 10: Axial Load Rate = 449 lb/min, Pressure Rate = 51 psi/min, Octahedral Shear Stress Rate = 258 psi/min, and Hydrostatic Stress Rate = 365 psi/min.

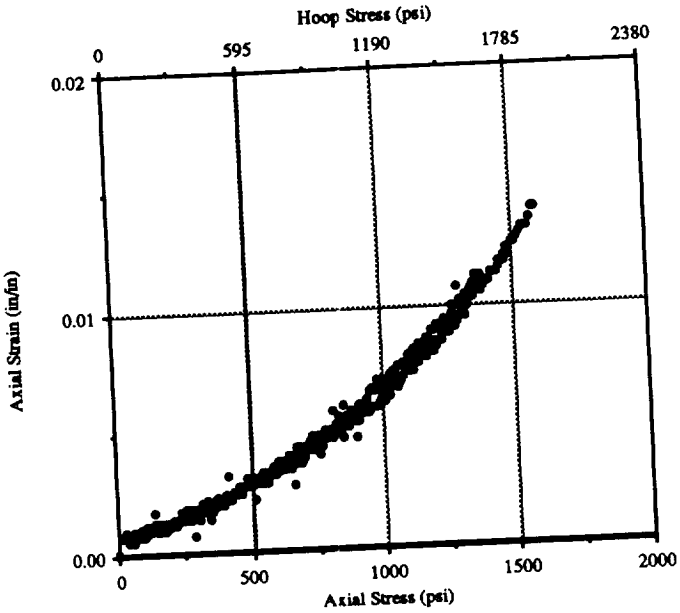

(a) Axial Strain versus Axial Stress or Hoop Stress

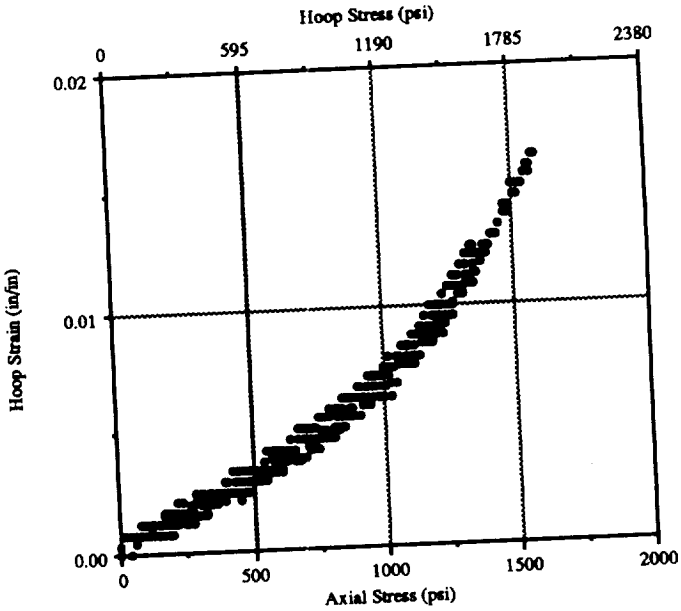

(b) Hoop Strain versus Axial Stress or Hoop Stress

Figure A.10 - Axial Strain and Hoop Strain versus Axial Stress or Hoop Stress for Load Path 11: Axial Load Rate = 328 lb/min, Pressure Rate = 54 psi/min, Octahedral Shear Stress Rate = 258 psi/min, and Hydrostatic Stress Rate = 357 psi/min.

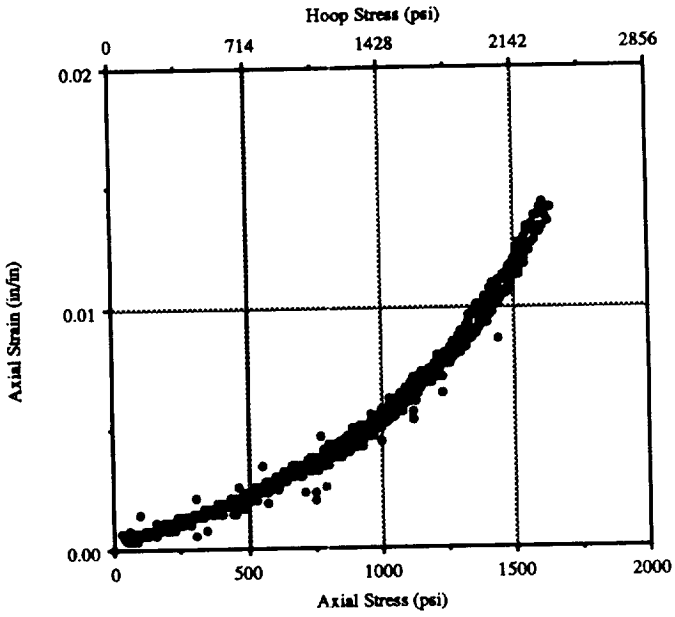

(a) Axial Strain versus Axial Stress or Hoop Stress

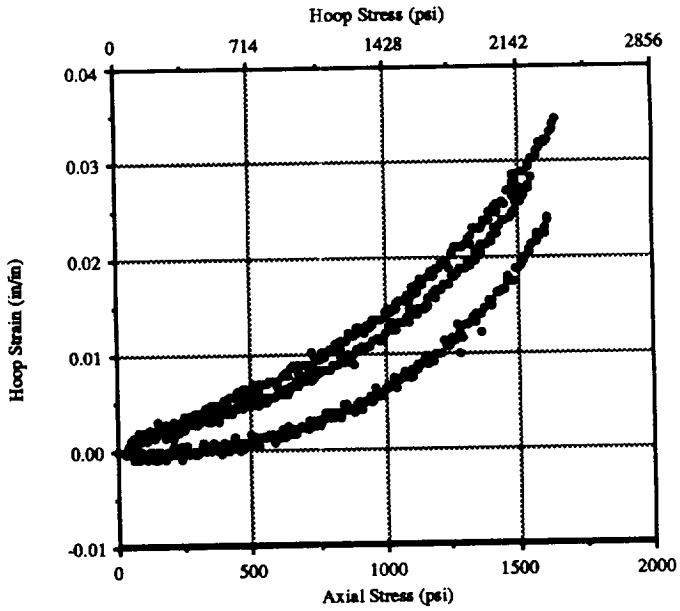

(b) Hoop Strain versus Axial Stress or Hoop Stress

Figure A.11 - Axial Strain and Hoop Strain versus Axial Stress or Hoop Stress for Load Path 12: Axial Load Rate = 202 lb/min, Pressure Rate = 57 psi/min, Octahedral Shear Stress Rate = 258 psi/min, and Hydrostatic Stress Rate = 348 psi/min.

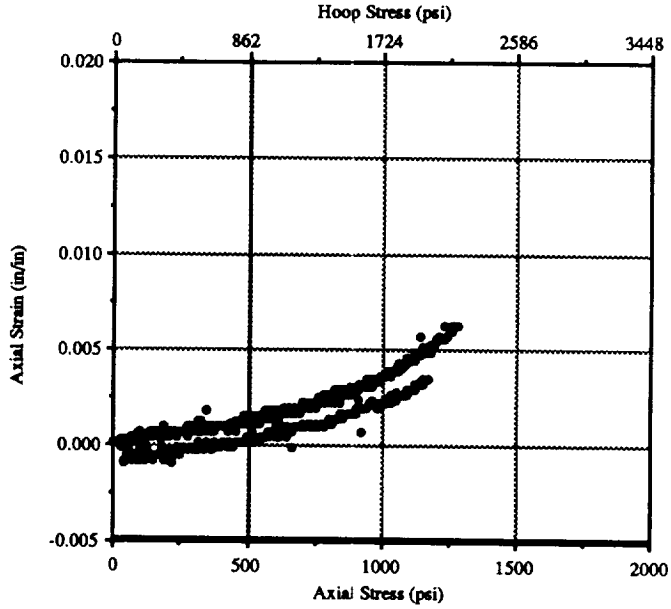

(a) Axial Strain versus Axial Stress or Hoop Stress

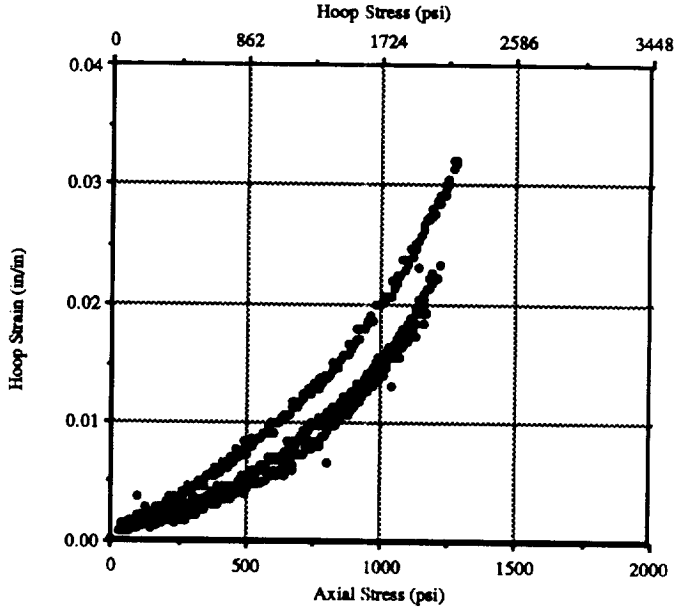

(b) Hoop Strain versus Axial Stress or Hoop Stress

Figure A.12 - Axial Strain and Hoop Strain versus Axial Stress or Hoop Stress for Load Path 13: Axial Load Rate = 83 lb/min, Pressure Rate = 58.2 psi/min, Octahedral Shear Stress Rate = 258 psi/min, and Hydrostatic Stress Rate = 331 psi/min.

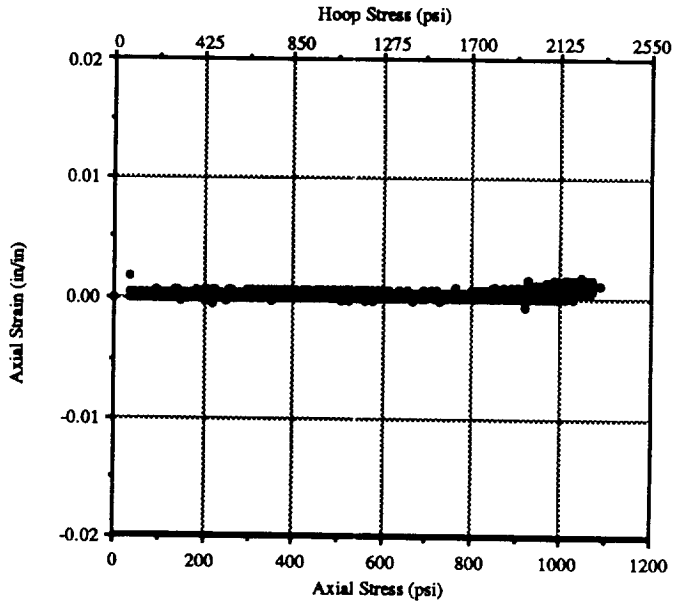

(a) Axial Strain versus Axial Stress or Hoop Stress

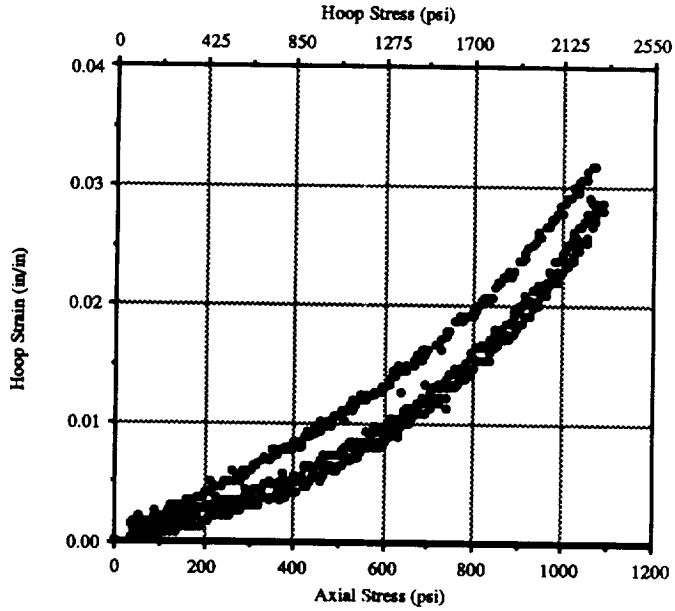

(b) Hoop Strain versus Axial Stress or Hoop Stress

Figure A.13 - Axial Strain and Hoop Strain versus Axial Stress or Hoop Stress for Load Path 14: Axial Load Rate = -31 lb/min, Pressure Rate = 58.4 psi/min, Octahedral Shear Stress Rate = 258 psi/min, and Hydrostatic Stress Rate = 310 psi/min.

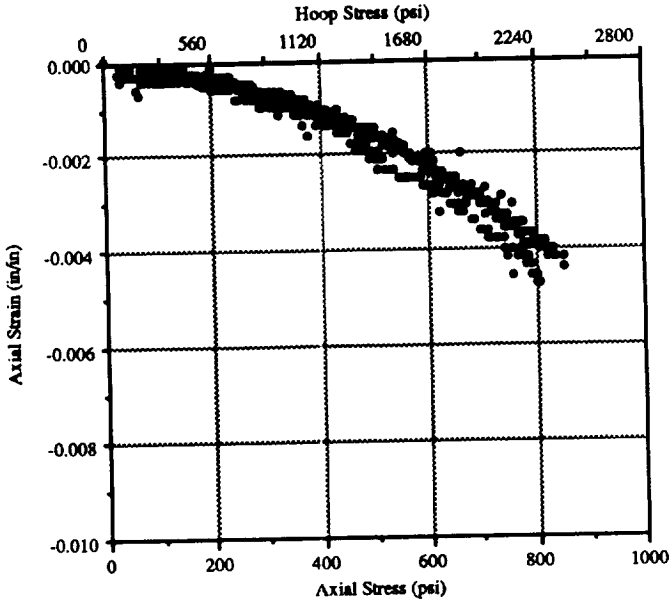

(a) Axial Strain versus Axial Stress or Hoop Stress

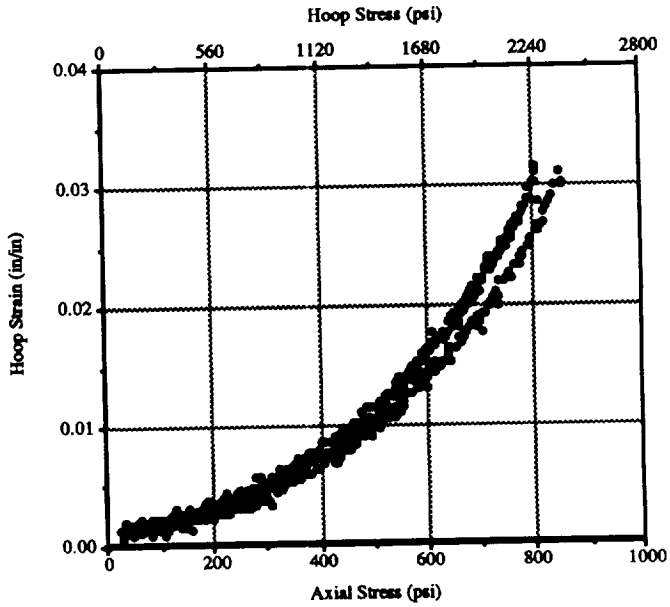

(b) Hoop Strain versus Axial Stress or Hoop Stress

Figure A.14 - Axial Strain and Hoop Strain versus Axial Stress or Hoop Stress for Load Path 15: Axial Load Rate = -143 lb/min, Pressure Rate = 57.7 psi/min, Octahedral Shear Stress Rate = 258 psi/min, and Hydrostatic Stress Rate = 284 psi/min.

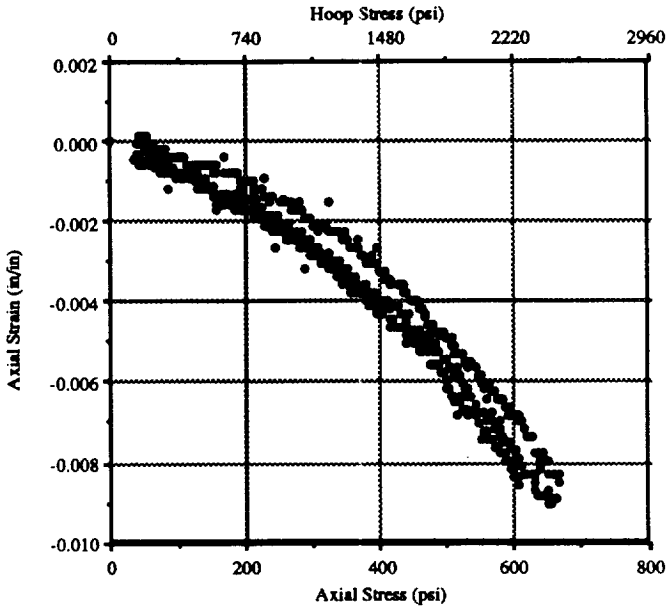

(a) Axial Strain versus Axial Stress or Hoop Stress

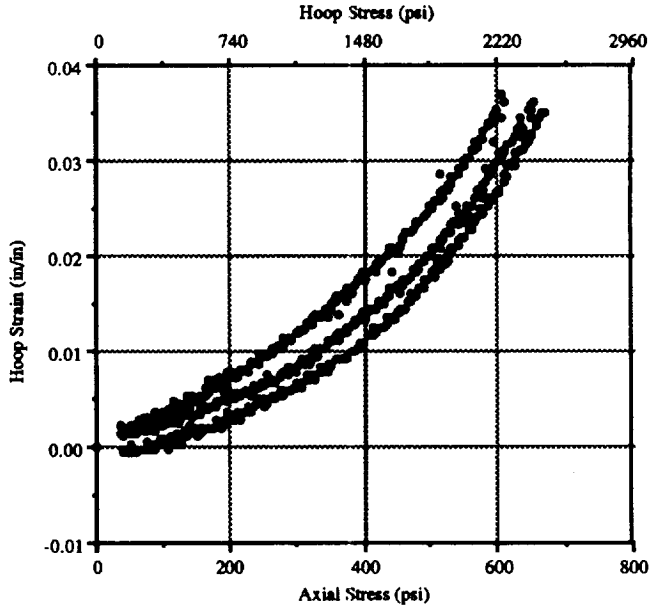

(b) Hoop Strain versus Axial Stress or Hoop Stress

Figure A.15 - Axial Strain and Hoop Strain versus Axial Stress or Hoop Stress for Load Path 16: Axial Load Rate = -230 lb/min, Pressure Rate = 56.5 psi/min, Octahedral Shear Stress Rate = 258 psi/min, and Hydrostatic Stress Rate = 260 psi/min.

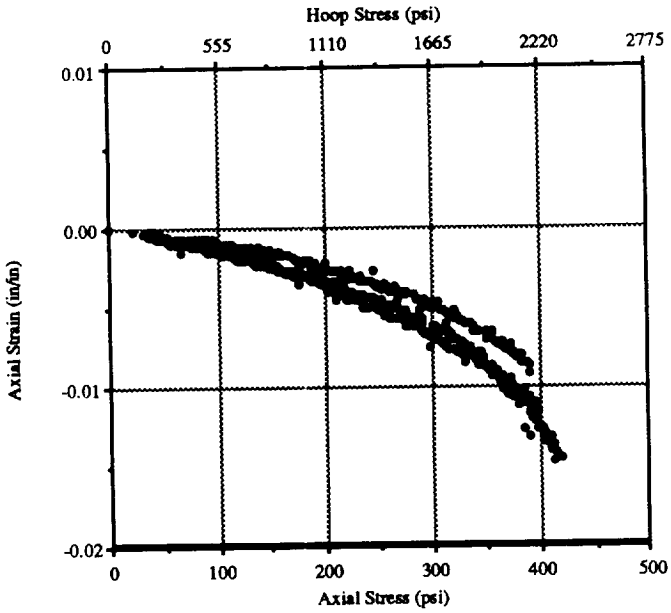

(a) Axial Strain versus Axial Stress or Hoop Stress

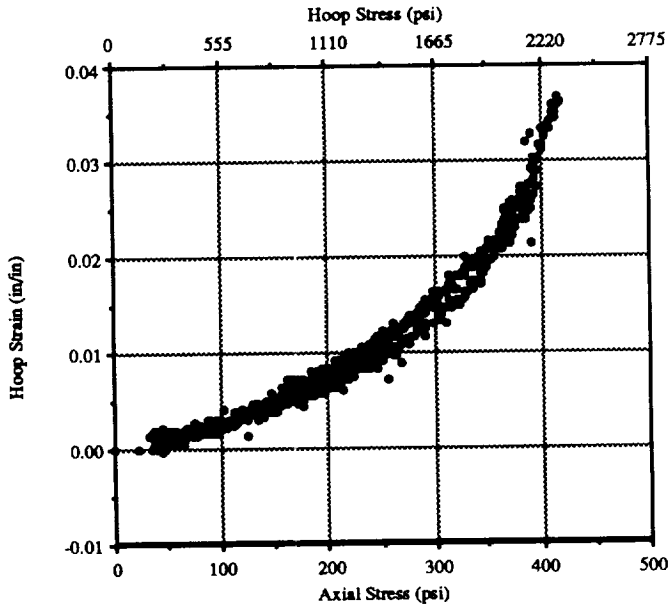

(b) Hoop Strain versus Axial Stress or Hoop Stress

Figure A.16 - Axial Strain and Hoop Strain versus Axial Stress or Hoop Stress for Load Path 17: Axial Load Rate = -311 lb/min, Pressure Rate = 55 psi/min, Octahedral Shear Stress Rate = 258 psi/min, and Hydrostatic Stress Rate = 236 psi/min.

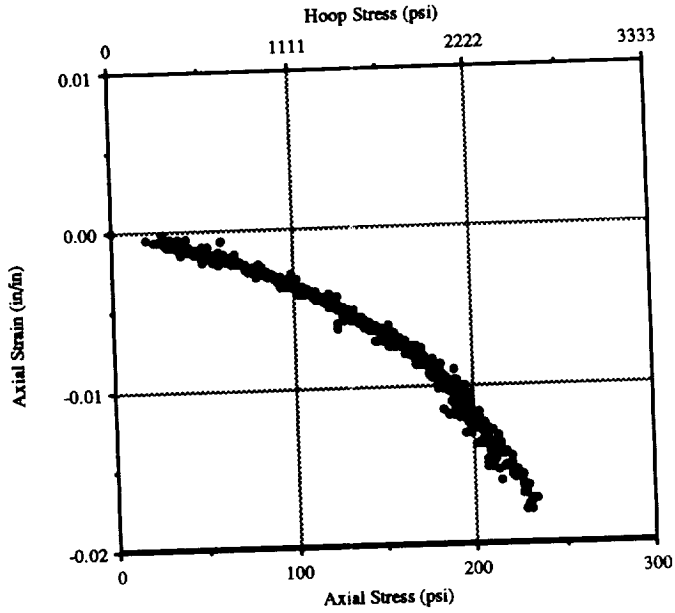

(a) Axial Strain versus Axial Stress or Hoop Stress

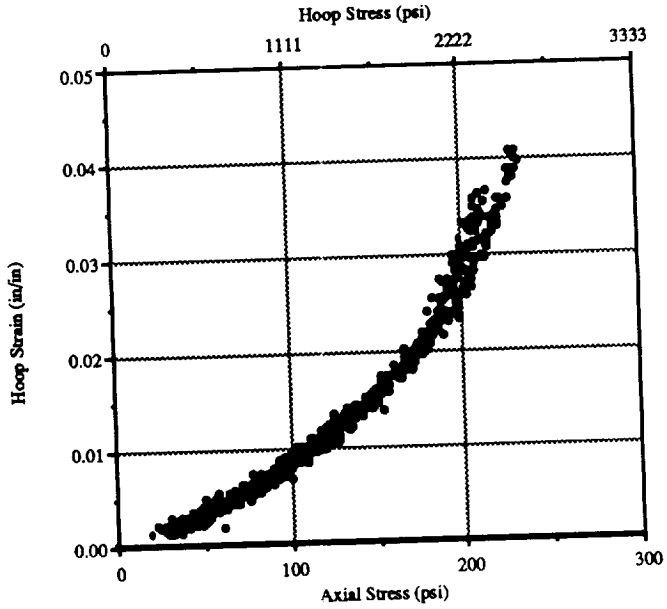

(b) Hoop Strain versus Axial Stress or Hoop Stress

Figure A.17 - Axial Strain and Hoop Strain versus Axial Stress or Hoop Stress for Load Path 18: Axial Load Rate = -384 lb/min, Pressure Rate = 53 psi/min, Octahedral Shear Stress Rate = 258 psi/min, and Hydrostatic Stress Rate = 210 psi/min.

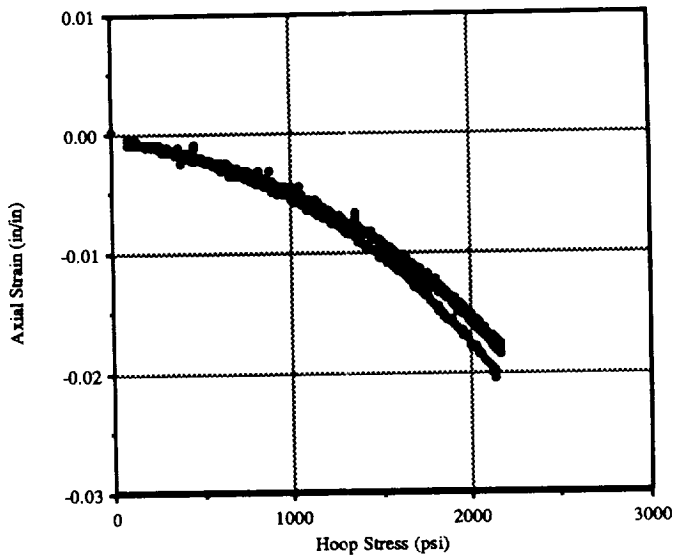

(a) Axial Strain versus Hoop Stress (Axial Stress ≈ 0)

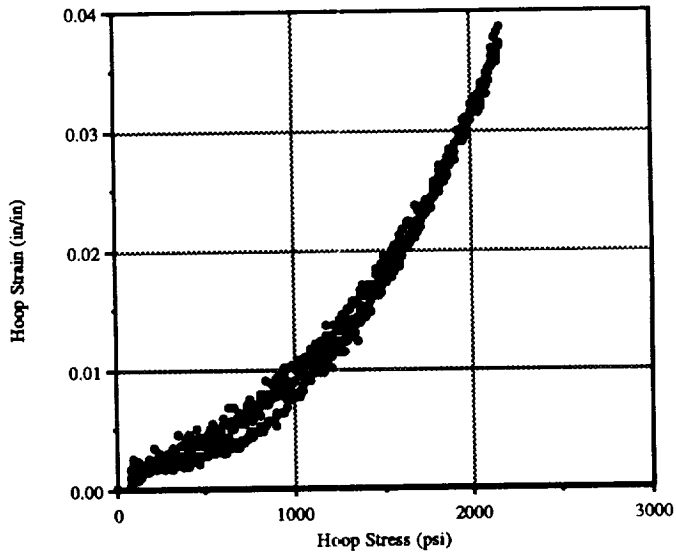

(b) Hoop Strain versus Hoop Stress (Axial Stress ≈ 0)

Figure A.18 - Axial Strain and Hoop Strain versus Axial Stress or Hoop Stress for Load Path 19: Axial Load Rate = -449 lb/min, Pressure Rate = 51 psi/min, Octahedral Shear Stress Rate = 258 psi/min, and Hydrostatic Stress Rate = 186 psi/min.

APPENDIX B - YIELD POINT DETERMINATION FOR ISOTROPIC AND TRANSVERSELY ISOTROPIC MODELS

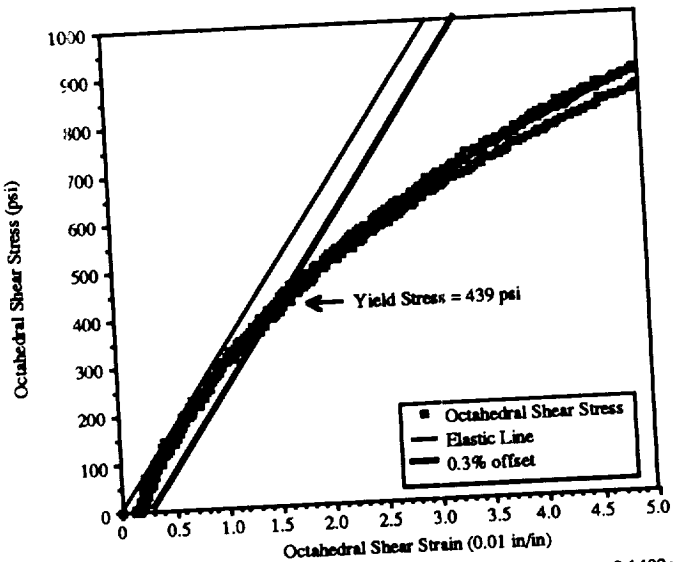

y = - 48.248 + 4.4059e+4x - 1.1832e+6x^2 + 2.2432e+7x^3 - 2.2119e+8x^4 + 8.1402e+8x^5 R^2 = 0.998

(a) Isotropic Model

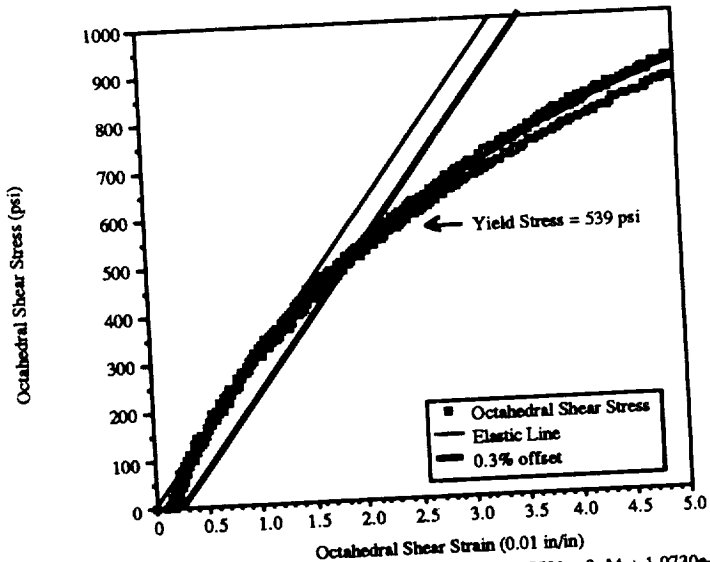

y = - 48.747 + 4.6382e+4x - 1.3165e+6x^2 + 2.6386e+7x^3 - 2.7521e+8x^4 + 1.0730e+9x^5 R^2 = 0.998

(b) Transversely Isotropic Model

Figure B.1 - Octahedral Shear Stress versus Octahedral Shear Strain for Load Path 1: Axial Load Rate = 900 lb/min, No Pressure, Octahedral Shear Stress Rate = 258 psi/min, and Hydrostatic Stress Rate = 186 psi/min.

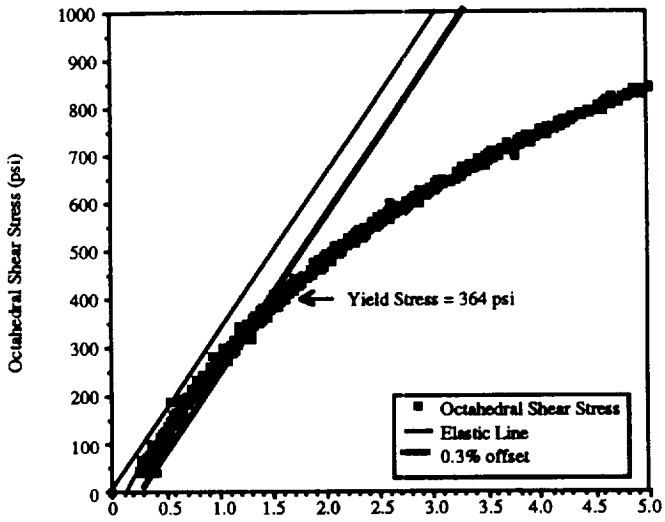

y = - 48.315 + 3.8660e+4x - 8.0732e+5x^2 + 1.1227e+7x^3 - 7.8266e+7x^4 + 1.8156e+8x^5 R^2 = 0.999

(a) Isotropic Model

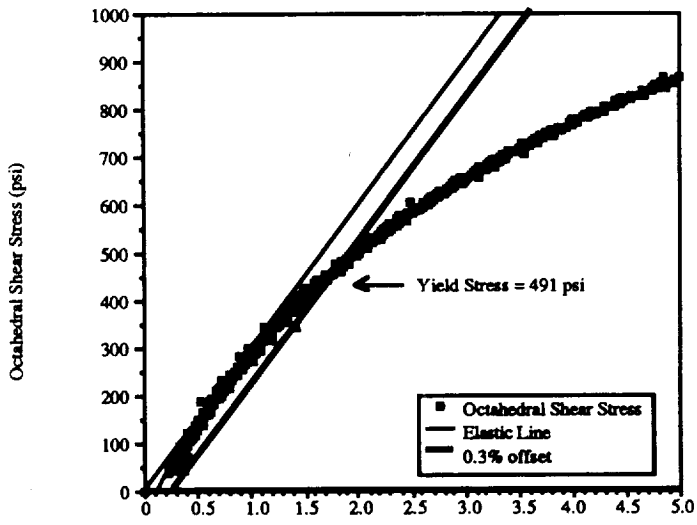

y = - 49.490 + 4.1457e+4x - 9.4777e+5x^2 + 1.4607e+7x^3 - 1.1553e+8x^4 + 3.2980e+8x^5 R^2 = 0.999

(b) Transversely Isotropic Model

Figure B.2 - Octahedral Shear Stress versus Octahedral Shear Strain for Load Path 3: Axial Load Rate = 885 lb/min, Pressure Rate = 10 psi/min, Octahedral Shear Stress Rate = 258 psi/min, and Hydrostatic Stress Rate = 236 psi/min.

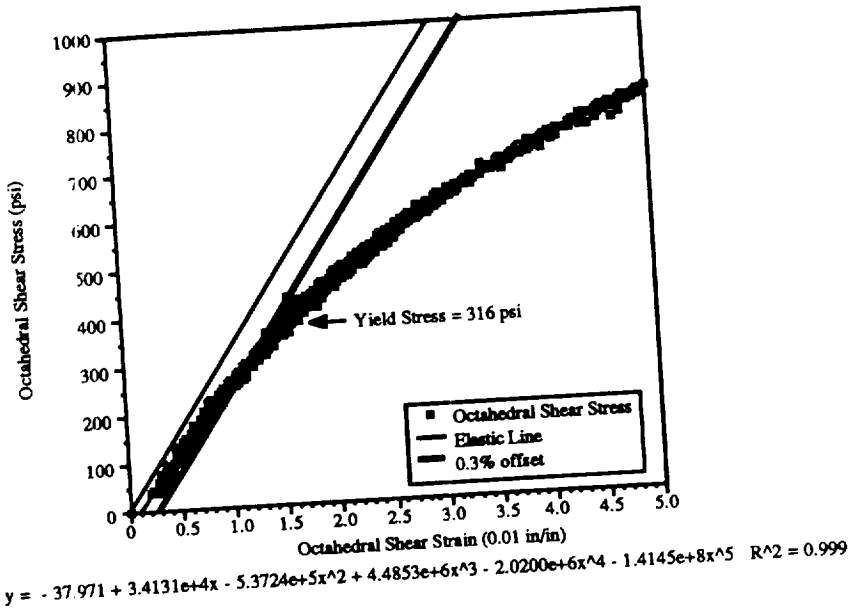

(a) Isotropic Model

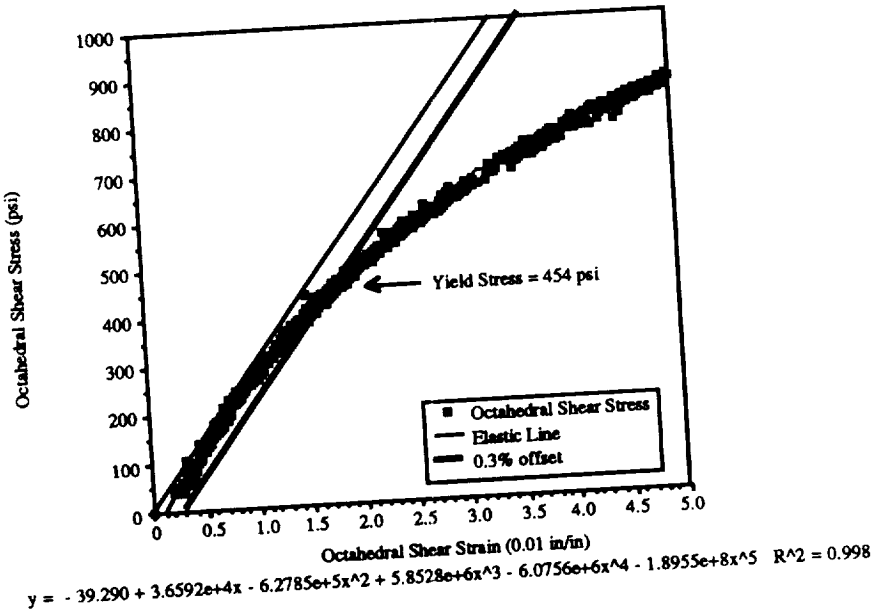

(b) Transversely Isotropic Model

Figure B.3 - Octahedral Shear Stress versus Octahedral Shear Strain for Load Path 4: Axial Load Rate = 867 lb/min, Pressure Rate = 15 psi/min, Octahedral Shear Stress Rate = 258 psi/min, and Hydrostatic Stress Rate = 260 psi/min.

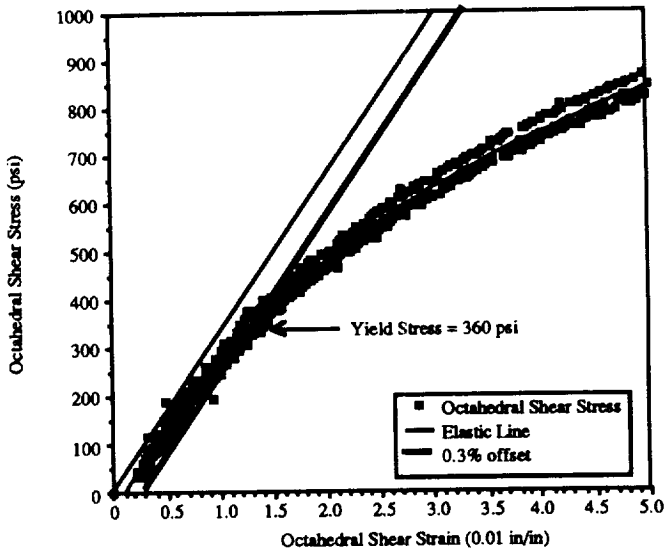

y = - 43.490 + 3.7845e+4x - 7.7524e+5x^2 + 1.0656e+7x^3 - 7.1793e+7x^4 + 1.3877e+8x^5 R^2 = 0.996

(a) Isotropic Model

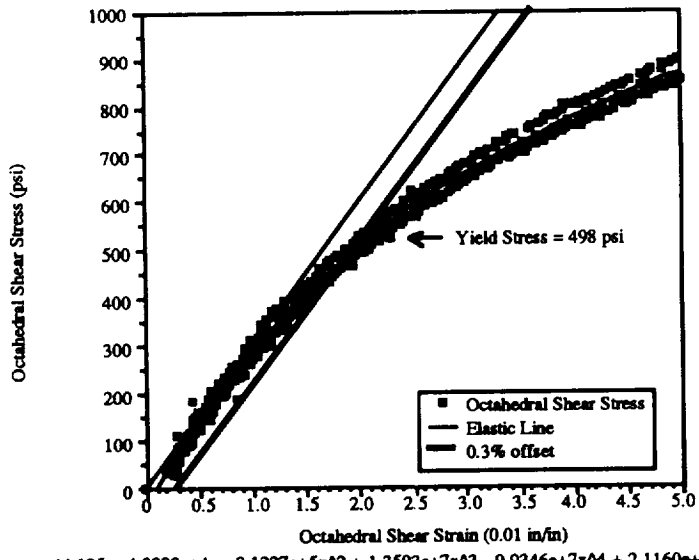

y = - 44.135 + 4.0990e+4x - 9.1227e+5x^2 + 1.3593e+7x^3 - 9.9346e+7x^4 + 2.1160e+8x^5 R^2 = 0.996

(b) Transversely Isotropic Model

Figure B.4 - Octahedral Shear Stress versus Octahedral Shear Strain for Load Path 5: Axial Load Rate = 838 lb/min, Pressure Rate = 21 psi/min, Octahedral Shear Stress Rate = 258 psi/min, and Hydrostatic Stress Rate = 284 psi/min.

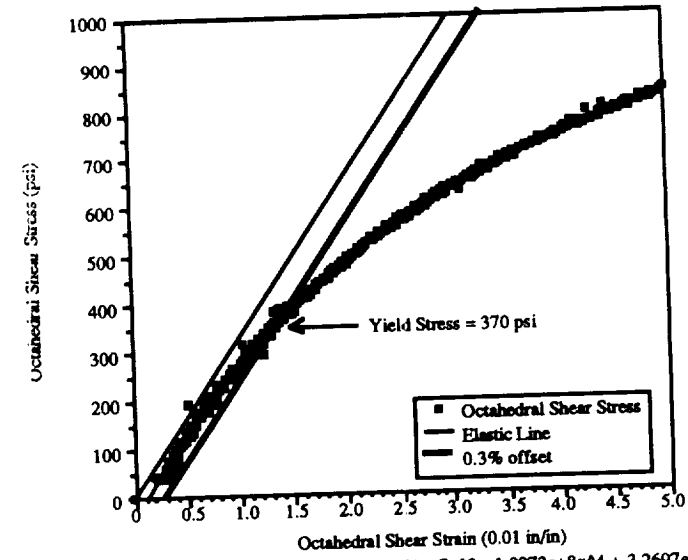

y = - 49.319 + 3.9849e+4x - 8.7268e+5x^2 + 1.2874e+7x^3 - 1.0273e+8x^4 + 3.2697e+8x^5 R^2 = 0.999

(a) Isotropic Model

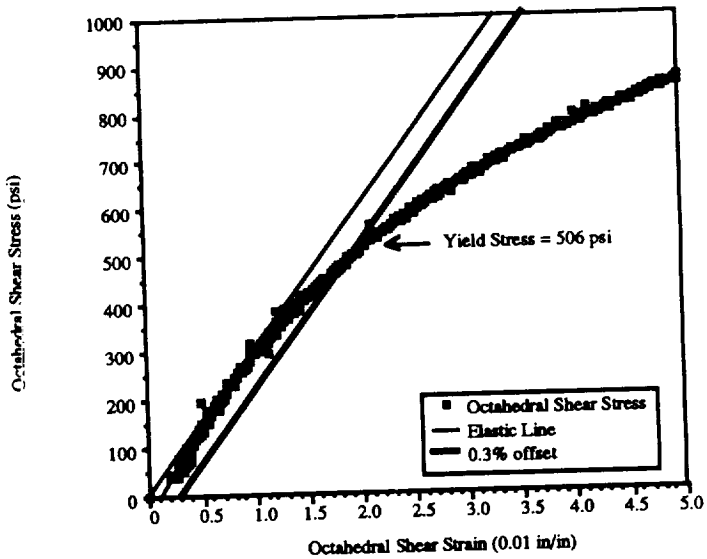

y = - 50.039 + 4.2889e+4x - 1.0196e+6x^2 + 1.6451e+7x^3 - 1.4411e+8x^4 + 5.0549e+8x^5 R^2 = 0.999

(b) Transversely Isotropic Model

Figure B.5 - Octahedral Shear Stress versus Octahedral Shear Strain for Load Path 6: Axial Load Rate = 795 lb/min, Pressure Rate = 27 psi/min, Octahedral Shear Stress Rate = 258 psi/min, and Hydrostatic Stress Rate = 310 psi/min.

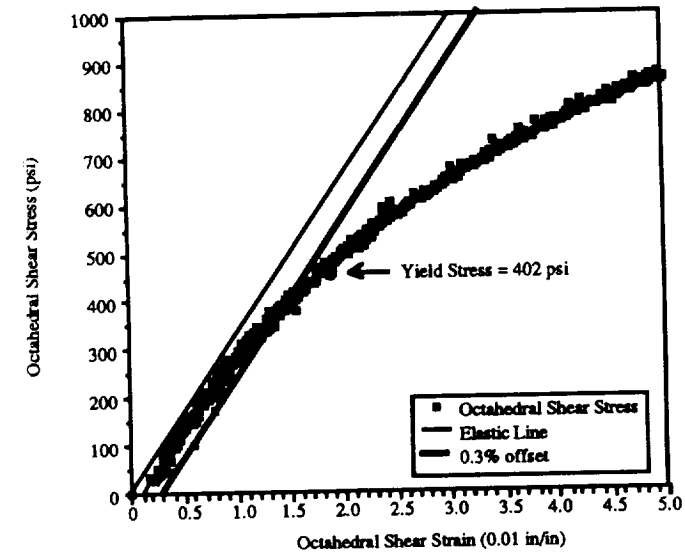

(a) Isotropic Model

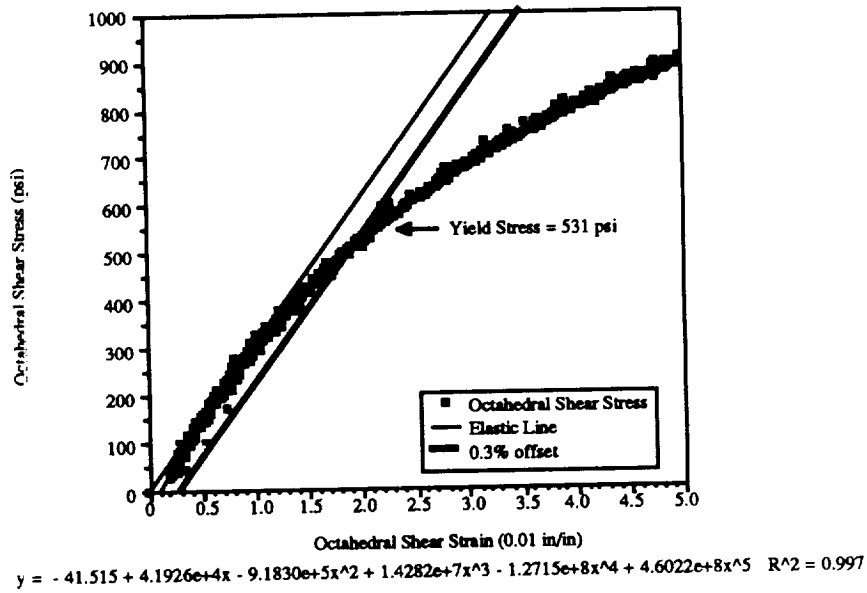

(b) Transversely Isotropic Model

Figure B.6 - Octahedral Shear Stress versus Octahedral Shear Strain for Load Path 7: Axial Load Rate = 734 lb/min, Pressure Rate = 34 psi/min, Octahedral Shear Stress Rate = 258 psi/min, and Hydrostatic Stress Rate = 331 psi/min.

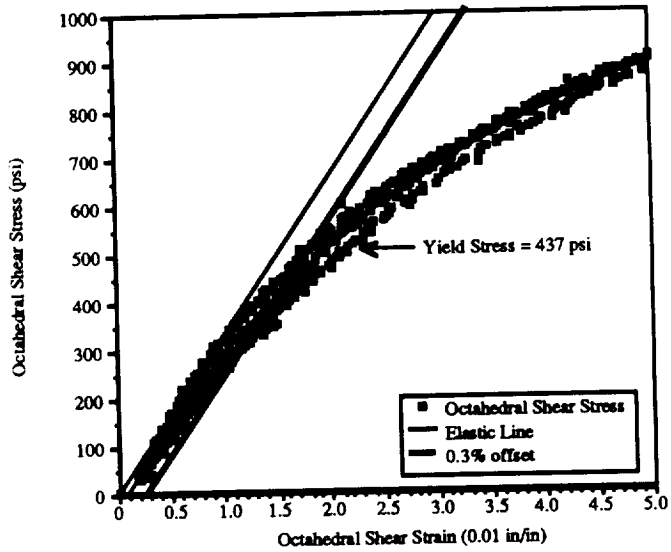

(a) Isotropic Model

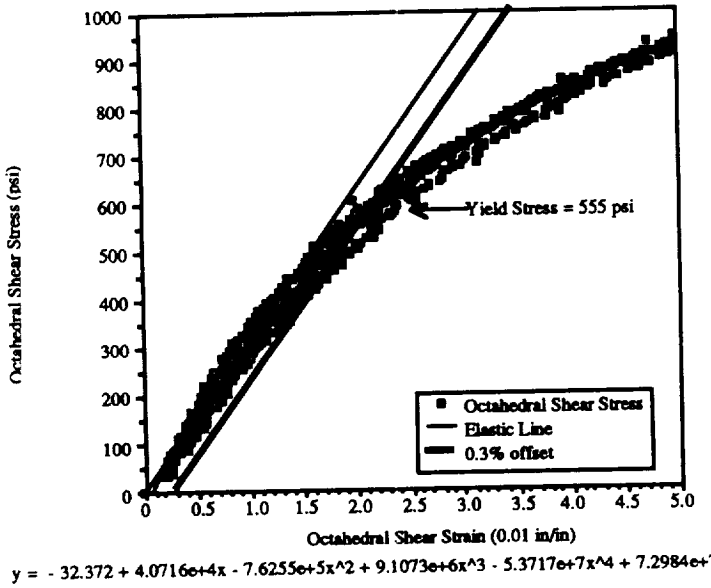

(b) Transversely Isotropic Model

Figure B.7 - Octahedral Shear Stress versus Octahedral Shear Strain for Load Path 8: Axial Load Rate = 657 lb/min, Pressure Rate = 40 psi/min, Octahedral Shear Stress Rate = 258 psi/min, and Hydrostatic Stress Rate = 348 psi/min.

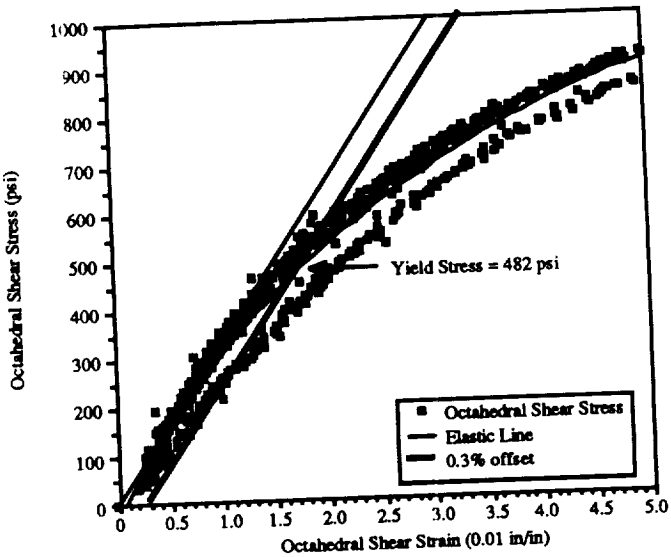

y = - 35.535 + 4.2683e+4x - 1.0492e+6x^2 + 2.0262e+7x^3 - 2.3068e+8x^4 + 1.0596e+9x^5 R^2 = 0.981

(a) Isotropic Model

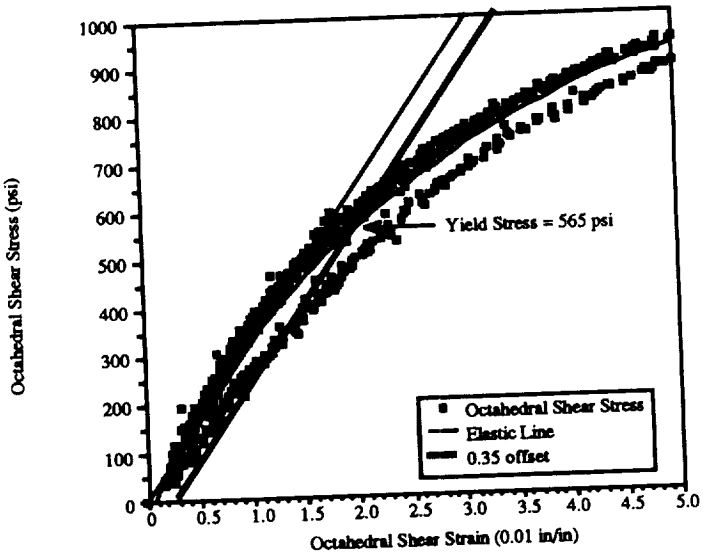

y = - 35.526 + 4.6169e+4x - 1.2353e+6x^2 + 2.6060e+7x^3 - 3.2326e+8x^4 + 1.6119e+9x^5 R^2 = 0.980

(b) Transversely Isotropic Model

Figure B.8 - Octahedral Shear Stress versus Octahedral Shear Strain for Load Path 9: Axial Load Rate = 560 lb/min, Pressure Rate = 46 psi/min, Octahedral Shear Stress Rate = 258 psi/min, and Hydrostatic Stress Rate = 357 psi/min.

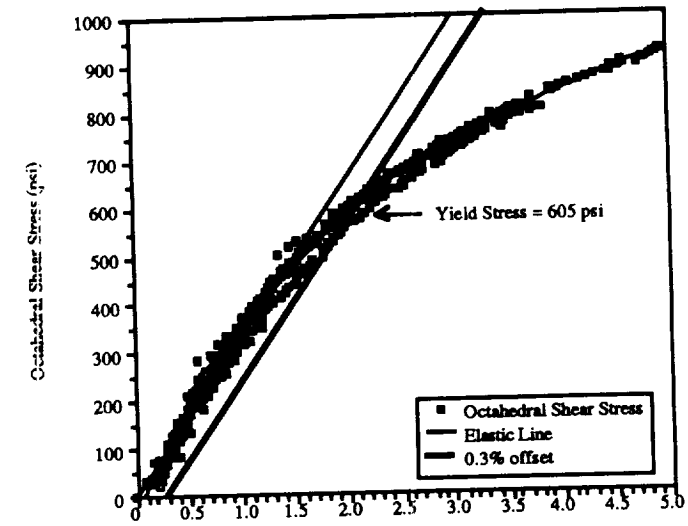

(a) Isotropic Model

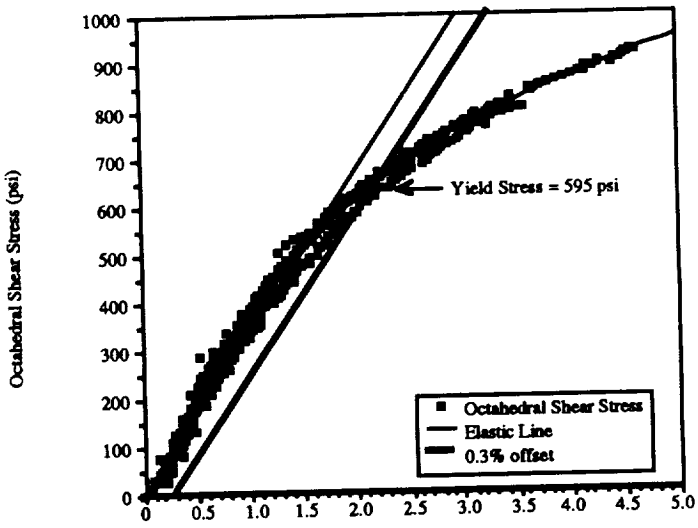

(b) Transversely Isotropic Model

Figure B.9 - Octahedral Shear Stress versus Octahedral Shear Strain for Load Path 10: Axial Load Rate = 449 lb/min, Pressure Rate = 51 psi/min, Octahedral Shear Stress Rate = 258 psi/min, and Hydrostatic Stress Rate = 365 psi/min.

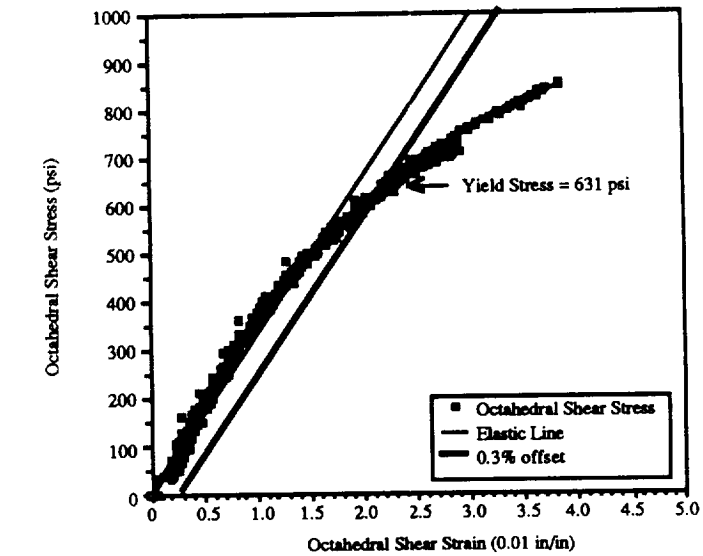

y = - 33.750 + 4.6357e+4x - 4.2335e+5x^2 - 4.6837e+7x^3 + 1.9874e+9x^4 - 2.3358e+10x^5 R^2 = 0.994

(a) Isotropic Model

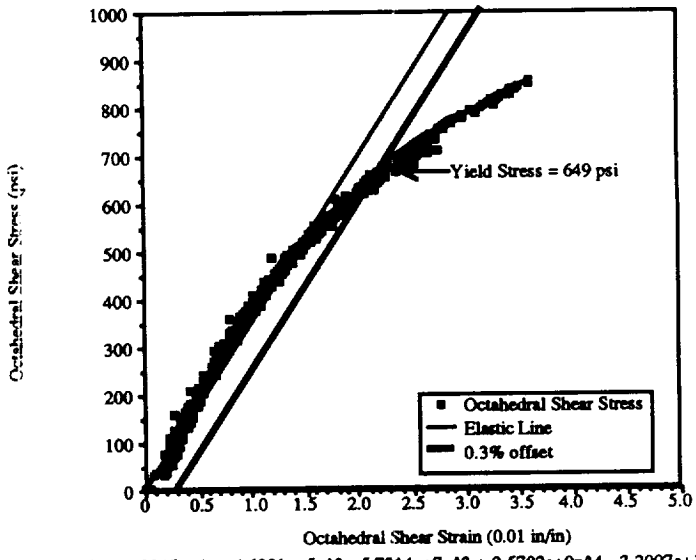

y = - 33.550 + 4.9345e+4x - 4.6981e+5x^2 - 5.7214e+7x^3 + 2.5702e+9x^4 - 3.2097e+10x^5 R^2 = 0.994

(b) Transversely Isotropic Model

Figure B.10 - Octahedral Shear Stress versus Octahedral Shear Strain for Load Path 11: Axial Load Rate = 328 lb/min, Pressure Rate = 54 psi/min, Octahedral Shear Stress Rate = 258 psi/min, and Hydrostatic Stress Rate = 357 psi/min.

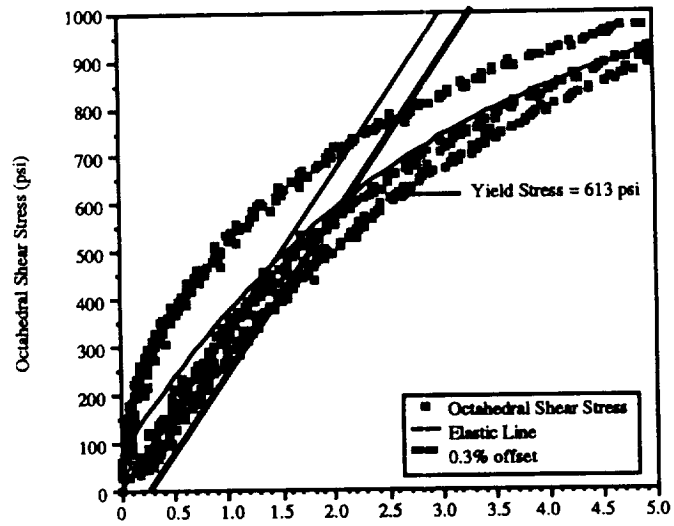

(a) Isotropic Model

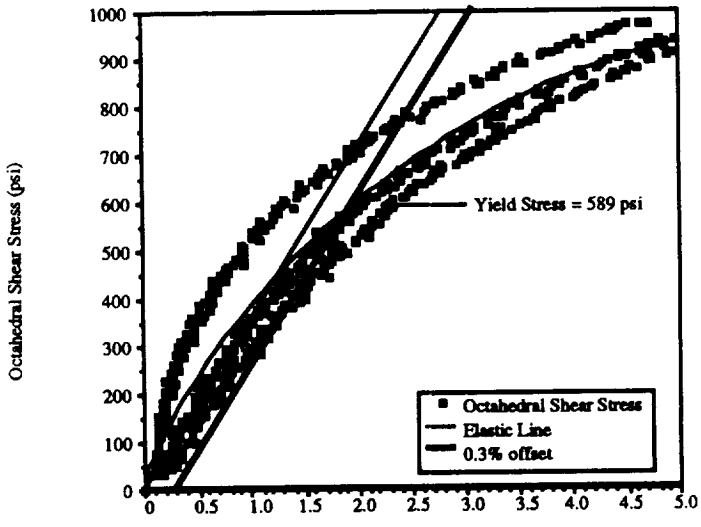

(b) Transversely Isotropic Model

Figure B.11 - Octahedral Shear Stress versus Octahedral Shear Strain for Load Path 12: Axial Load Rate = 202 lb/min, Pressure Rate = 57 psi/min, Octahedral Shear Stress Rate = 258 psi/min, and Hydrostatic Stress Rate = 348 psi/min.

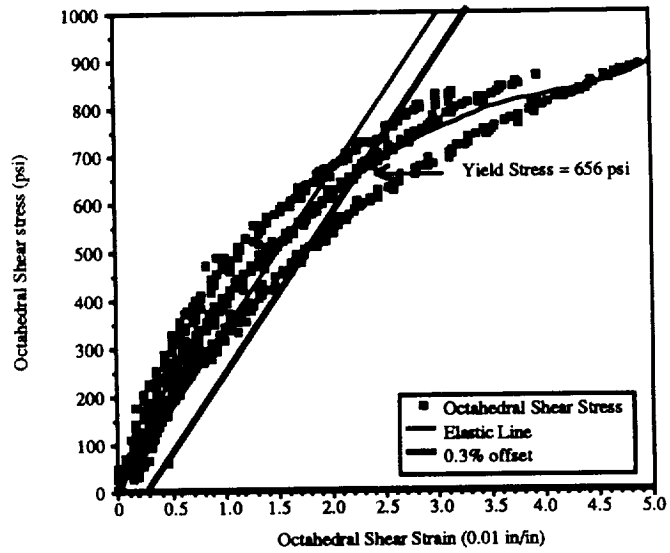

y = - 15.209 + 6.1243e+4x - 2.8852e+6x^2 + 1.0310e+8x^3 - 2.0099e+9x^4 + 1.5136e+10x^5 R^2 = 0.961

(a) Isotropic Model

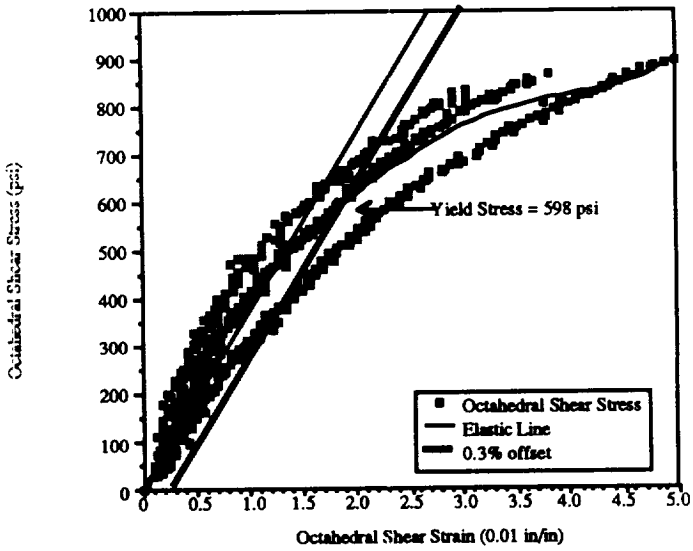

y = - 32.120 + 6.5249e+4x - 3.2993e+6x^2 + 1.2463e+8x^3 - 2.5209e+9x^4 + 1.9500e+10x^5 R^2 = 0.947

(b) Transversely Isotropic Model

Figure B.12 - Octahedral Shear Stress versus Octahedral Shear Strain for Load Path 13: Axial Load Rate = 83 lb/min, Pressure Rate = 58.2 psi/min, Octahedral Shear Stress Rate = 258 psi/min, and Hydrostatic Stress Rate = 331 psi/min.

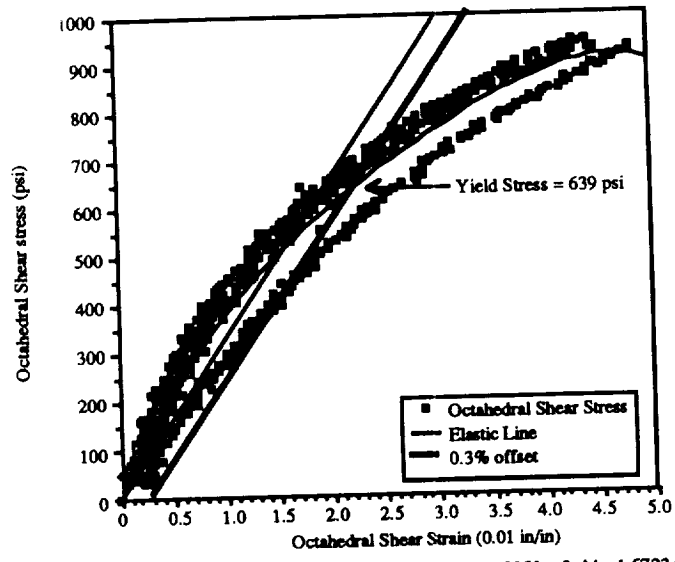

y = - 8.0947 + 5.0425e+4x - 1.4770e+6x^2 + 2.6568e+7x^3 - 1.2050e+8x^4 - 1.5723e+9x^5 R^2 = 0.962

(a) Isotropic Model

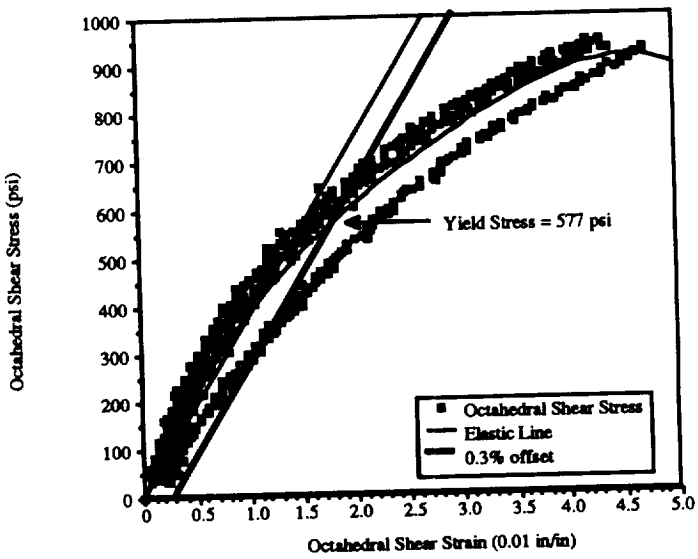

y = - 7.0159 + 5.1298e+4x - 1.5435e+6x^2 + 2.9044e+7x^3 - 1.5444e+8x^4 - 1.5222e+9x^5 R^2 = 0.961

(b) Transversely Isotropic Model

Figure B.13 - Octahedral Shear Stress versus Octahedral Shear Strain for Load Path 14: Axial Load Rate = -31 lb/min, Pressure Rate = 58.4 psi/min, Octahedral Shear Stress Rate = 258 psi/min, and Hydrostatic Stress Rate = 310 psi/min.

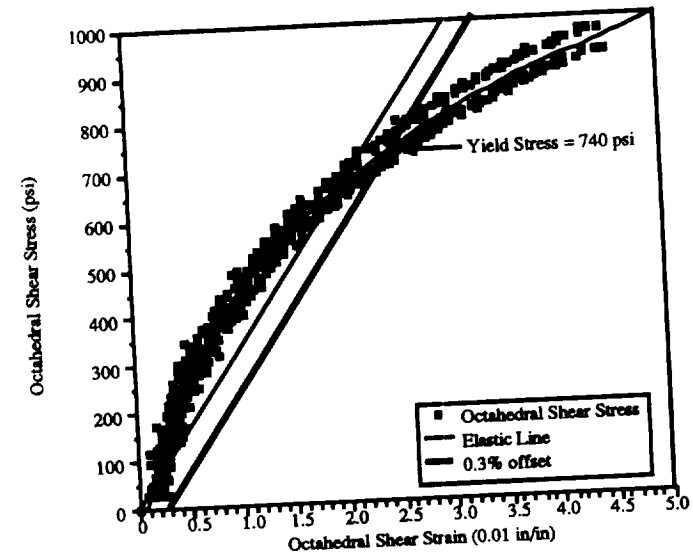

y = - 52.176 + 7.8122e+4x - 3.9504e+6x^2 + 1.2760e+8x^3 - 2.1199e+9x^4 + 1.3823e+10x^5 R^2 = 0.982

(a) Isotropic Model

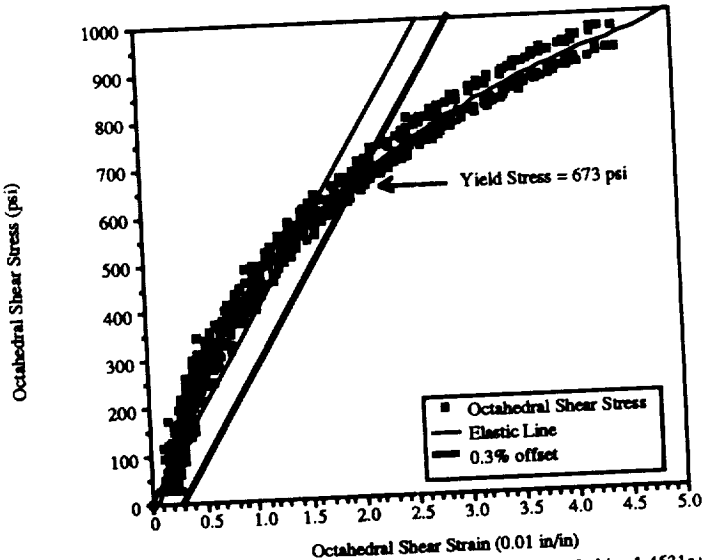

y = - 52.788 + 7.8802e+4x - 4.0288e+6x^2 + 1.3156e+8x^3 - 2.2078e+9x^4 + 1.4531e+10x^5 R^2 = 0.982

(b) Transversely Isotropic Model

Figure B.14 - Octahedral Shear Stress versus Octahedral Shear Strain for Load Path 15: Axial Load Rate = -143 lb/min, Pressure Rate = 57.7 psi/min, Octahedral Shear Stress Rate = 258 psi/min, and Hydrostatic Stress Rate = 284 psi/min.

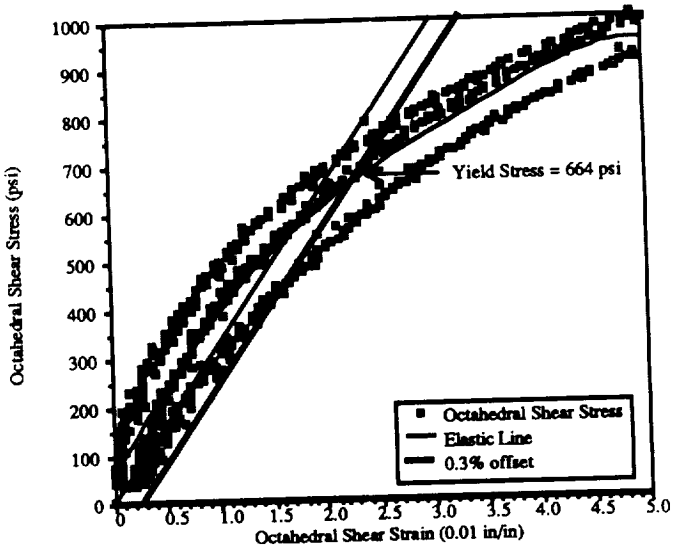

y = 56.055 + 3.6177e+4x - 3.4027e+4x^2 - 3.7491e+7x^3 + 1.1080e+9x^4 - 9.8166e+9x^5 R^2 = 0.942

(a) Isotropic Model

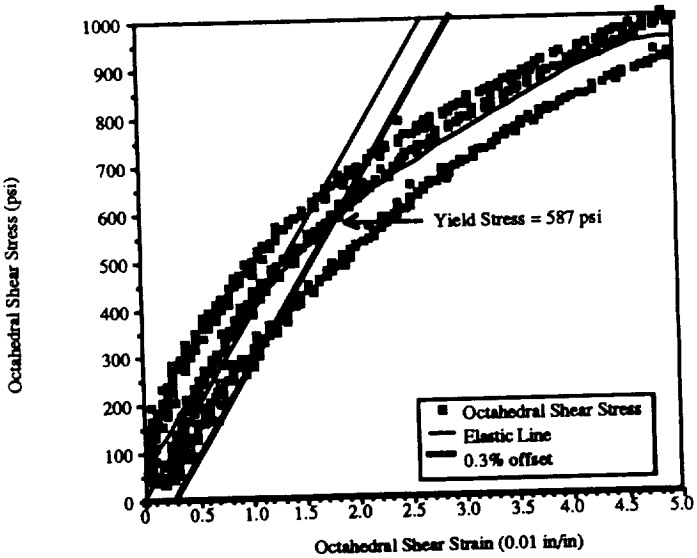

y = 56.334 + 3.5833e+4x - 3933.4x^2 - 3.8555e+7x^3 + 1.1238e+9x^4 - 9.8917e+9x^5 R^2 = 0.943

(b) Transversely Isotropic Model

Figure B.15 - Octahedral Shear Stress versus Octahedral Shear Strain for Load Path 16: Axial Load Rate = -230 lb/min, Pressure Rate = 56.5 psi/min, Octahedral Shear Stress Rate = 258 psi/min, and Hydrostatic Stress Rate = 260 psi/min.

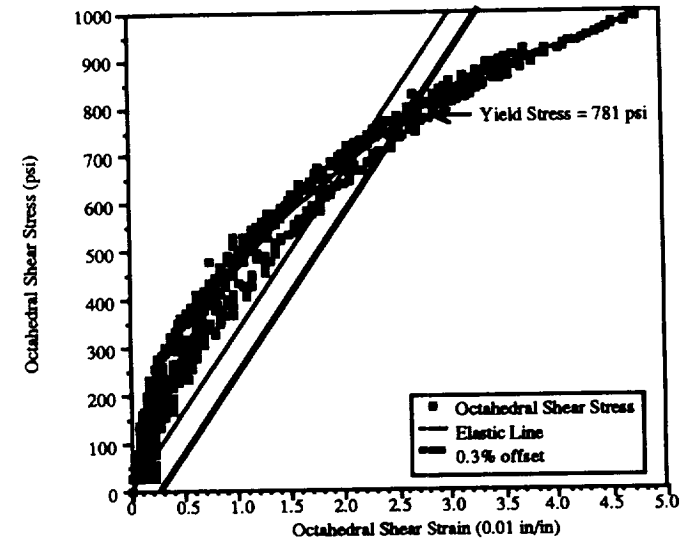

y = 23.745 + 6.8111e+4x - 3.5633e+6x^2 + 1.3294e+8x^3 - 2.5915e+9x^4 + 1.9514e+10x^5 R^2 = 0.981

(a) Isotropic Model

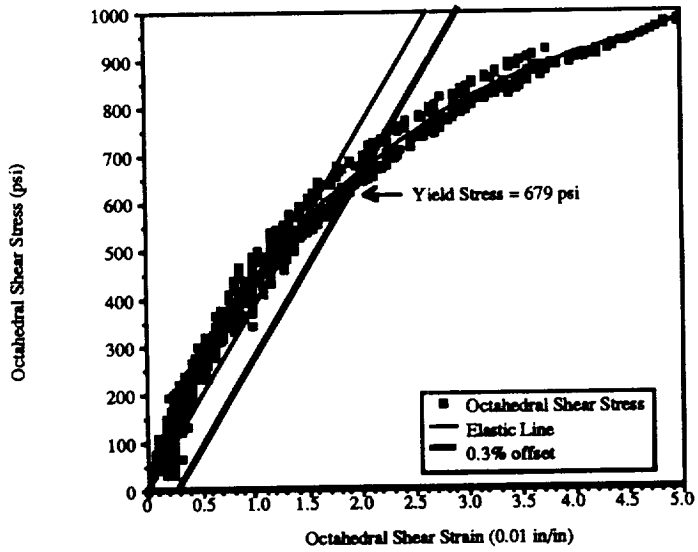

y = - 15.651 + 6.7685e+4x - 3.1416e+6x^2 + 1.0368e+8x^3 - 1.8344e+9x^4 + 1.2705e+10x^5 R^2 = 0.988

(b) Transversely Isotropic Model

Figure B.16 - Octahedral Shear Stress versus Octahedral Shear Strain for Load Path 17: Axial Load Rate = -311 lb/min, Pressure Rate = 55 psi/min, Octahedral Shear Stress Rate = 258 psi/min, and Hydrostatic Stress Rate = 236 psi/min.

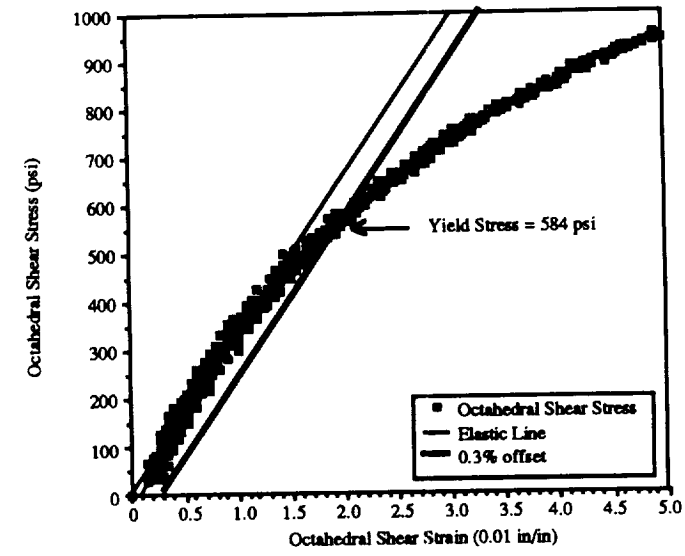

y = - 42.889 + 4.9166e+4x - 1.3483e+6x^2 + 2.6004e+7x^3 - 2.6410e+8x^4 + 9.7674e+8x^5 R^2 = 0.997

(a) Isotropic Model

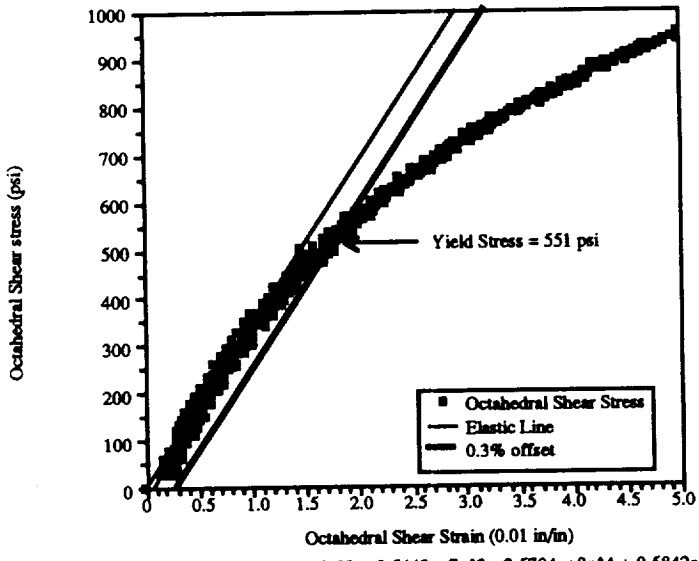

y = - 43.009 + 4.8704e+4x - 1.3261e+6x^2 + 2.5449e+7x^3 - 2.5794e+8x^4 + 9.5842e+8x^5 R^2 = 0.997

(b)Transversely Isotropic Model

Figure B.17 - Octahedral Shear Stress versus Octahedral Shear Strain for Load Path 18: Axial Load Rate = -384 lb/min, Pressure Rate = 53 psi/min, Octahedral Shear Stress Rate = 258 psi/min, and Hydrostatic Stress Rate = 210 psi/min.

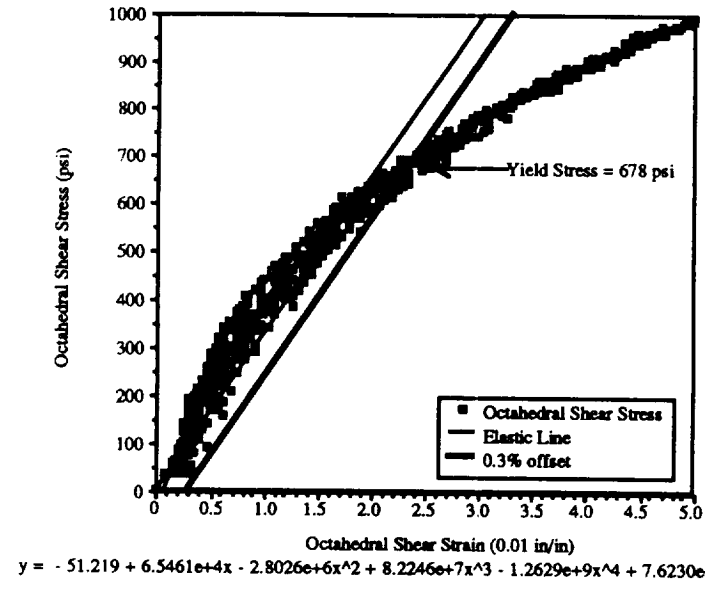

(a) Isotropic Model

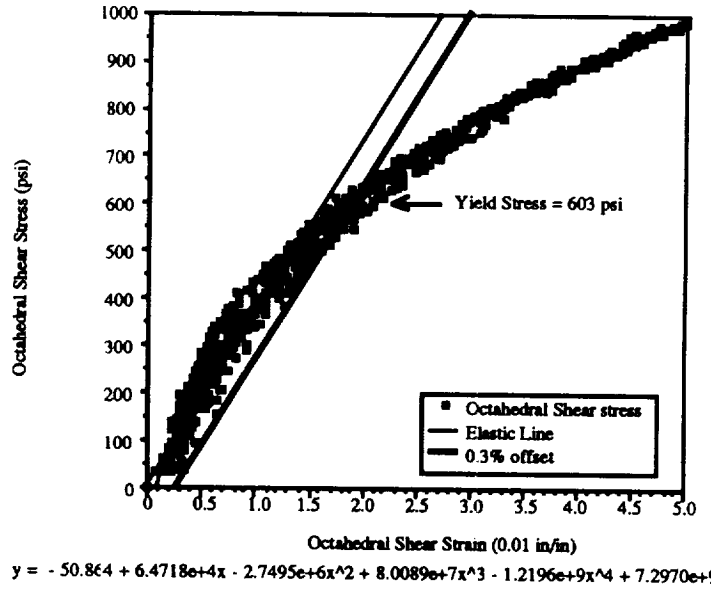

(b) Transversely Isotropic Model

Figure B.18 - Octahedral Shear Stress versus Octahedral Shear Strain for Load Path 19: Axial Load Rate = -449 lb/min, Pressure Rate = 51 psi/min, Octahedral Shear Stress Rate = 258 psi/min, and Hydrostatic Stress Rate = 186 psi/min.

APPENDIX C - STANDARD DEVIATION CALCULATION

The Pressure-modified Tsai-Hill is given by:

$$H(\sigma_1 - \sigma_2)^2 + F(\sigma_2 - \sigma_3)^2 + G(\sigma_3 - \sigma_1)^2 + K_1\sigma_1 + K_2\sigma_2 + K_3\sigma_3 = 1 \qquad (C.1)$$

with $H + G = \frac{1}{C_1T_1}$ $H + F = \frac{1}{C_2T_2}$ $G + F = \frac{1}{C_3T_3}$

$K_1 = \frac{C_1 - T_1}{C_1T_1}$ $K_2 = \frac{C_2 - T_2}{C_2T_2}$ $K_3 = \frac{C_3 - T_3}{C_3T_3}$

testing was completed under plane stress conditions, $\sigma_3 = 0$, therefore:

$$(H + G)\,\sigma_1^2 + (H + F)\,\sigma_2^2 - 2H\sigma_1\sigma_2 + K_1\sigma_1 + K_2\sigma_2 = 1 \qquad (C.2)$$

Substituting the coefficients defined in Equation (C.1) into Equation (C.2) results in:

$$\frac{\sigma_1^2}{C_1T_1} + \frac{\sigma_2^2}{C_2T_2} - \frac{\sigma_1\sigma_2}{C_1T_1} + \frac{C_1 - T_1}{C_1T_1}\sigma_1 + \frac{C_2 - T_2}{C_2T_2}\sigma_2 = 1 \qquad (C.3)$$

It is assumed that the material exhibits the same compressive strength to tensile strength ratio (S) in the 1- and 2- directions. That is, it is assumed that:

$$S = \frac{C_1}{T_1} = \frac{C_2}{T_2} \qquad (C.4)$$

Under this assumption, Equation (C.3) reduces to:

$$\frac{\sigma_1^2}{ST_1^2} + \frac{\sigma_2^2}{ST_2^2} - \frac{\sigma_1\sigma_2}{ST_1^2} + \frac{S-1}{S}\left(\frac{\sigma_1}{T_1} + \frac{\sigma_2}{T_2}\right) = 1 \qquad \text{(C.5)}$$

For a given load path of slope M, the following substitution can be made:

$$\sigma_1 = M\,\sigma_2 \qquad \text{(C.6)}$$

Therefore:

$$\frac{M^2\sigma_2^2}{ST_1^2} + \frac{\sigma_2^2}{ST_2^2} - \frac{M\sigma_2^2}{ST_1^2} + \frac{S-1}{S}\left(\frac{M\sigma_2}{T_1} + \frac{\sigma_2}{T_2}\right) = 1 \qquad \text{(C.7)}$$

Rearranging the previous equation results in the following:

$$\frac{\sigma_2^2}{S}\left(\frac{M^2}{T_1^2} + \frac{1}{T_2^2} - \frac{M}{T_1^2}\right) + \sigma_2\frac{S-1}{S}\left(\frac{M}{T_1} + \frac{1}{T_2}\right) = 1 \qquad \text{(C.8)}$$

If the C/T ratio (S) and slope of the load path (M) are given, one can use the quadratic equation to solve for the values of hoop stress (σ_2) which will satisfy the above relationship. The values of hoop stress which are the roots of the above equation correspond to the intersections of the Pressure-modified Tsai-Hill locus with a C/T ratio equal to S and the load path with the slope M. In other words, the roots of the above equation are the yield stresses for a given load path predicted by the Pressure-modified Tsai-Hill. Once the predicted hoop stress value (σ_2) is known, the predicted axial stress is equal to M times the hoop stress.

Example:

Given: (1) Consider Load Path 4. The slope of this load path is M = 3.73.

(2) Consider the Pressure-modified Tsai-Hill with a strength ratio of S = C/T = 1.08.

(3) The tensile yield strengths in the 1- and 2- directions are T_1 = 1143 psi, and T_2 = 1279 psi, as given in Table 2.

Substituting these values for M, S, T_1, and T_2 into Equation (C.8) results in the following expression:

$$7.783e^{-6}\,\sigma_2^2 + 2.996447e^{-4}\,\sigma_2 - 1 = 0 \qquad \text{(C.9)}$$

This results in a value for hoop stress at yield of 340 psi, and therefore the predicted axial stress at yield is 1268 psi.

The experimentally measured values at yield along Load Path 3 were 288 psi (σ_2) and 1074 psi (σ_1). The standard deviation was based on the radial distance from the origin to the point represented by the two stress values in principal stress space. The radius is defined as:

$$\text{Radius} = \sqrt{\sigma_1^2 + \sigma_2^2} \qquad \text{(C.10)}$$

Therefore the experimental radius and theoretical radius as predicted by the Pressure-modified Tsai-Hill with a C/T ratio equal to 1.08 are:

$$Radius_{exp} := 1112$$

$$Radius_{pred} = 1312$$

The deviation from experimental is then:

$$Deviation := \frac{Radius_{exp} - Radius_{pred}}{Radius_{exp}} \tag{C.11}$$

For this example, the deviation would be equal to -18%. The deviation of predicted from experimental yield stress was calculated for all 19 load paths. The standard deviation of the predicted yield locus based on the Pressure-modified Tsai-Hill from the experimental yield locus was calculated using the following relationship:

$$STD = \sqrt{\frac{\Sigma(Deviation^2)}{n - 1}} \tag{C.12}$$

where n is the number of load paths. The variation of the standard deviation with the C/T ratio is summarized in Figure 5.3.